TECHNISCHE UNIVERSITÄT MÜNCHEN

II. Medizinische Klinik und Poliklinik des

Klinikum rechts der Isar

Analysis of the function of Farnesoid X Receptor in a mouse model of Barrett's Esophagus and Adenocarcinoma

Andreas Hans Nuber

Vollständiger Abdruck der von der Fakultät für Medizin der Technischen Universität München zur Erlangung des akademischen Grades eines

Doktors der Naturwissenschaften (Dr. rer. nat.)

genehmigten Dissertation.

Vorsitzender: Univ.-Prof. Dr. R. R. Rad

Prüfer der Dissertation:

1. Univ.-Prof. Dr. R. M. Schmid

2. Univ.-Prof. Dr. M. W. Pfaffl

Die Dissertation wurde am 14.04.2016 bei der Technischen Universität

München eingereicht und durch die Fakultät für Medizin am 09.11.2016

angenommen.

meinen Kindern
meinen Eltern

Table of Content

List of abbreviations

BE	Barrett´s Esophagus
TNBS	2,4,6-Trinitrobenzenesulfonic acid
HEPES	4-(2-hydroxyethyl)-1-piperazineethanesulfonic acid
ASA	Acetyl salicylic acid
ANOVA	analysis of variance
ABC	Avidin-Biotin-Complex
BA	Bile acid
CDCA	Chenodeoxycholic acid
CGD	Cholesterol gallstone disease
CA	Cholic acid
cDNA	Complementary DNA
CSE	Cystathionine-γ-lyase
DCA	Deoxycholic acid
DNA	Deoxyribonucleic acid
DSS	Dextran sodium sulfate
DMSO	Dimethyl sulphoxide
DBD	DNA-binding domain
DSB	Double strand break
DPBS	Dulbecco's Phosphate buffered Saline
EMR	Endoscopic mucosal resection
EGF	Epidermal growth factor
EAC	Esophageal adenocarcinoma
ESCC	Esophageal squamous cell carcinoma
EGJ	esophagogastric junction
EGTA	Ethylene glycol tetraacetic acid
EDTA	Ethylenediaminetetraacetic acid
FBS	Fetal Bovine Serum
Fex	Fexaramine
FFPE	Formalin-fixed paraffin-embedded
GERD	Gastroesophageal reflux disease
GEMM	Genetically engineered mouse model
GSEA	Gene set enrichment analysis
H&E	Haematoxylin and eosin
HCC	Hepatocellular carcinoma
HFD	High fat diet

HGD	High grade dysplasia
HGNC	HUGO Gene Nomenclature Committee
IHC	Immunohistochemistry
k.o	Knock out
LCA	Lithocholic acid
LGD	Low grade dysplasia
LES	Lower esophageal sphincter
MIR	microRNA
NSAID	Non-steroidal anti-inflammatory drugs
OTC	Organotypic culture
PAS	Periodic acid Schiff
PCR	Polymerase chain reaction
PPI	Proton pump inhibitors
qRT-PCR	Quantitative real-time polymerase chain reaction
RFA	Radiofrequency ablation
ROS	Reactive oxygen species
RNA	Ribonucleic acid
shRNA	Small hairpin RNA
NaTC	Sodium taurocholate
SCJ	Squamocolumnar junction
SEM	standard error of the mean
UES	Upper esophageal sphincter
WAT	white adipose tissue
WT	Wild type

Summary

Barrett´s Esophagus (BE) is a disease of the esophagus in which squamous epithelium is replaced by columnar line epithelium caused by acid and bile in a gastroesophageal reflux disease. Especially bile acid can induce NfkB and DNA damage and maybe lead to transformation from BE to low grade dysplasia, to high grade dysplasia and finally to esophageal adenocarcinoma. A crucial player in this transformation could be the bile acid receptor FXR, a nuclear ligand activated receptor that has major functions in bile, glucose and lipid homeostasis.

In this project we aimed to analyze the effects of bile acids and FXR and its role during carcinogenesis by crossing our transgenic BE mouse model (pL2-IL-1 β) and FXR knock out mouse model ($FXR^{-/-}$). In our pL2-IL-1β mouse model, hIL1beta is over expressed in the esophageal and squamous forestomach mucosa and therefore imitates chronic inflammation. It provides us a model to study esophagitis as well as its progress from BE to adenocarcinoma. FXR is known to act as a protective factor in the liver and the gastrointestinal tract. We therefore hypothesized that a lack of FXR in pL2-IL-1β mice would increase BE development and accelerate its progression to EAC. pL2-IL-1β/$FXR^{-/-}$ mice were sacrificed at 6, 9, 12 and 15 months to monitor different stages of carcinogenesis. At any time point, histopathology, proliferation, differentiation and DNA damage were analyzed. Furthermore, we screen the gene profiles by microarray.

Our findings showed that pL2-IL-1β mice develop esophageal tumors, Barrett-Like Metaplasia, Neoplasia and dysplasia in cardia in 9 to 12 months. $FXR^{-/-}$ mice have disrupted homeostasis of bile acids, higher proliferating in the esophagus, esophagitis and show an increased carcinogenesis. pL2-IL-1β/$FXR^{-/-}$ mice showed a localized and stronger inflammation especially in 6 months old mice. pL2-IL-1β/$FXR^{-/-}$ mice at 9 months had an accelerated phenotype of metaplasia and dysplasia. Surprisingly, with an age of 15 months the two different genotypes showed almost no different phenotype anymore suggesting a role for FXR only in early carcinogenesis. We demonstrated that a lack of FXR resulted in more proliferation leading to less differentiation which was correlated with an increased metaplastic and dysplastic development. Only pL2-IL-1/$FXR^{-/-}$ mice show gH2AX staining indicating that loss of FXR would induce more DNA damage and therefor induce a more malignant phenotype during early carcinogenesis. Our findings in the mouse model correlated with the expression of FXR in human BE tissue as FXR expression was highest in BE tissue in both human and mouse and almost lost in cancer.

In conclusion we here provide evidence for the functional importance of FXR expression as a protective factor during esophageal carcinogenesis. Future studies should evaluate FXR as a potential biomarker for the progression to cancer.

1 Esophagus

The esophagus is a muscular tube that extends from the pharynx to the stomach. It has a rich blood supply and reaches a length of 25 cm in a human adult, with its main task being the transport of food into the stomach. The tube is subdivided in three different regions: cervical, thoracic and abdominal. The upper, cervical part consists of striated muscles which are under conscious control, while the lower part has smooth, involuntary muscles and the thoracic part exhibits a mixture of both muscle types. The upper and lower esophageal sphincter (UES and LES) close off the cervical and abdominal part of the esophagus. The UES is controlled consciously and helps to pass food through the esophagus into the stomach. In contrast the LES is not under voluntary control and prevents reflux of acid, bile and stomach contents. The histology of the esophagus is typical for the digestive tract with four different layers: Mucosa, Submucosa, Muscularis and Adventitia. The mucosa layer includes lamina ephithales, lamina propria and lamina muscularis. The submucosa layer contains glands that produce mucus to support the transport of food into the stomach; The same glands are found in the lamina propria. The muscularis propria actively contracts the esophagus to facilitate the food transport, while the last layer, the Adventitia, contains connective tissue to increase the firmness (Schünke, Schulte, & Schumacher, 2012). In the gestation of a human, the esophagus begins to grow from the foregut by the tenth week. From the fourth month, the ciliated epithelium is gradually replaced by squamous epithelium (Henning, 1986). The clinical significance of the esophagus is widely varied: Diseases can derive from congenital conditions or be acquired later in life. Some diseases that can affect the esophagus are, esophagitis, reflux, hiatus hernia or Barrett's esophagus.

2 Gastroesophageal Reflux Disease (GERD)

“Gastroesophageal reflux disease (GERD) is a condition which develops when the reflux of stomach contents causes troublesome symptoms or complications.” (Vakil et al., 2006), (Kahrilas, 2008) It is the most common gastrointestinal disease, which affects up to 20 % of adults in the United States. Several factors support the reflux, such as lower esophageal sphincter hypotension, abdominal obesity, loss of esophageal peristaltic function or hernia (“Increased Frequency of Transient Lower Esophageal Sphincter Relaxation Induced by Gastric Distention in Reflux Patients With Hiatal Hernia,” 2015), (de Vries, van Herwaarden, Smout, & Samsom, 2008), (Corley et al., 2007), (Kahrilas, 2008). GERD is paradoxical in that not all patients with heartburn develop esophagitis, and not every patient with esophagitis reported heartburn symptoms, but gastroesophageal reflux is nevertheless the most common cause of heartburn - although other disorders (like achalasia and eosinophilic esophagitis) may also cause or contribute to heartburn. (Vakil et al., 2006), (Kahrilas, 2008) If GERD symptoms are typical and the patient reacts to therapy, no further diagnostic tests are necessary to verify the diagnosis (DeVault & Castell, 2005), (Armstrong et al., 2005), (Kahrilas, Shaheen, & Vaezi, 2008b), (Kahrilas, 2008). If not, endoscopy with biopsy can help detect alternative causes, such as esophagitis or Helicobacter pylori infection (Kahrilas, Shaheen, & Vaezi, 2008a), (Kahrilas, 2008). Suggested therapy options for GERD are lifestyle changes that lead to the reduction of body weight and the avoidance of foods that support acid production or reflux symptoms. Proton pump inhibitors (PPI) can be used as reflux medication to reduce acid production in the stomach and ease heartburn symptoms. GERD can lead to further symptoms and diseases like esophagitis, Barrett’s esophagus or adenocarcinoma. The progression to BE and cancer are poorly understood. Biomarker or the analyze of the pathogenesis could help to understand the disease better. If lifestyle changes and the treatment with PPI are not successful in reducing heartburn symptoms, surgery can be another option for the patient. The Nissen fundoplication is the most common surgery method, wherein the proximal stomach is be wrapped around the distal esophagus. The new created esophagus operates as an anti-reflux barrier (Finks, Wei, & Birkmeyer, 2006), (Kahrilas, 2008).

3 Barrett`s Esophagus (BE)

Barrett´s esophagus (BE) is a disease of the distal esophagus, which transforms normal squamous epithelium into columnar line epithelium (Spechler, Fitzgerald, Prasad, & Wang, 2010), (Quante, Abrams, Lee, & Wang, 2012a), (Spechler & Souza, 2014). (Figure 1) In 1976, three different types of BE were described in the literature: cardia type, gastric fundic type and the intestinal type which is most common of the columnar epithelial (Paull et al., 1976), (Quante, Abrams, Lee, & Wang, 2012a). For the last decades, intestinal metaplasia (IM) with goblet cells was essential for the diagnosis of BE, while recently, data in the mouse model and clinical studies suggest IM without goblet cells might show a higher risk for esophageal adenocarcinoma (EAC) than classical goblet cell metaplasia (Quante, Abrams, Lee, & Wang, 2012a). Notch inhibition results in decreased proliferation both in mice and humans, which leads to a rebuild into a goblet cell-rich phenotype and reduced progression to EAC (Menke et al., 2010), (Quante, Bhagat, Abrams, Marache, Good, et al., 2012b), (Quante, Abrams, Lee, & Wang, 2012a). A commonly accepted cause of BE is hiatus hernia and gastroesophageal reflux disease. Hiatus hernia is a protrusion of the upper part of the stomach into the thorax caused by a tear or weakness in the diaphragm (Sontag, 1999). The resulting reflux in the esophagus contains not only acid from the stomach, but also bile acids (BAs). The average bile acid concentration of the reflux in patients with Barrett's esophagus was 181 µmol/l – compared to 124 µmol/l for esophagitis or 14 µmol/l in patients with minimal injury. Controls had a bile salt concentration of 0 µmol/l (Nehra, Howell, Williams, Pye, & Beynon, 1999). The reflux episodes have a duration of about 3 min. with a pH of 2 (Dvorak et al., 2006), (Coenraad et al., 1998). The paradox of Barrett's Esophagus is that not every patient with reflux develops BE, and not every BE patient reported reflux symptoms before. Additional risk factors for BE are smoking, obesity, white race, older age and male sex. BE can transform from low grade dysplasia (LGD) to high grade dysplasia (HGD) and finally to esophageal adenocarcinoma (shown in Figure 2), through factors that are unknown at the time.

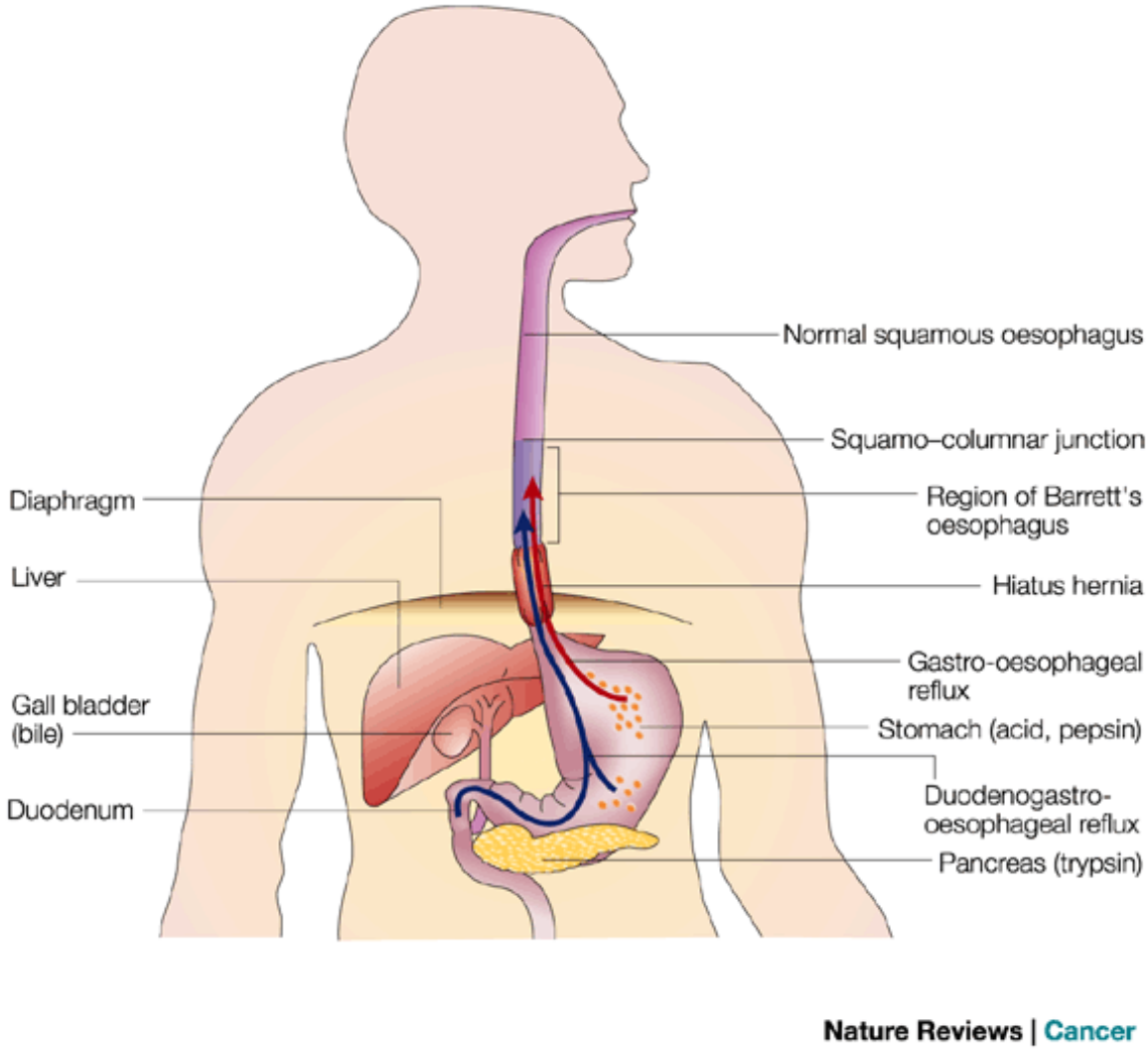

Figure 1: Barrett's Esophagus occurring in the distal esophagus. There, normal squamous epithelium is replaced with columnar line epithelium. Common causes are hiatus hernia and reflux in BE patients. The gastro-esophageal reflux (red arrow) contains gastric acids and the duodenogastro-esophageal reflux (blue arrow) contains additional bile components such as bile acids. Adapted from: Wild and Hardie 2003 (Wild & Hardie, 2003)

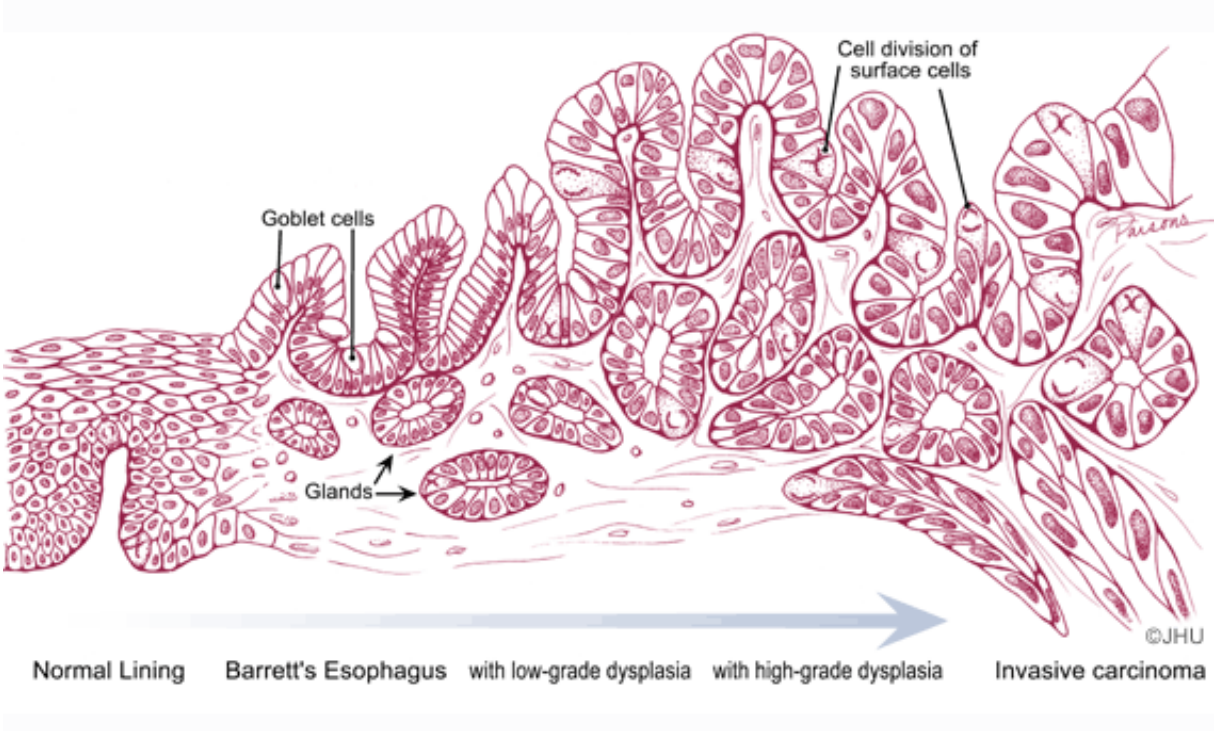

Figure 2: Barrett`s Esophagus (BE) progression. BE occurring in the distal esophagus. There, normal squamous epithelium is replaced with columnar line epithelium. Common causes are hiatus hernia and reflux in BE patients. The gastro-esophageal reflux (red arrow) contains gastric acids and the duodenogastro-esophageal reflux (blue arrow) contains additional bile components such as bile acids. Adapted from: Wild and Hardie 2003 (Wild & Hardie, 2003)

This progression occurs in only 0,5 % of BE patients per year (Shaheen, Crosby, Bozymski, & Sandler, 2000). However, two large population-based studies reported progression rates of only 0.10 % per year (Hvid-Jensen, Pedersen, Drewes, Sørensen, & Funch-Jensen, 2011), (Bhat et al., 2011), (Quante, Abrams, Lee, & Wang, 2012a). In the last decades, the BE incidence rate has risen over 500 % in Western Countries, while people from Asia or Africa are rarely associated with BE (Everhart & Ruhl, 2009), (Corley et al., 2009). The mechanism behind the progression is still unknown, but factors like GERD or obesity are actively discussed. Proton-pump inhibitors (PPIs) are used for the treatment of GERD, but even long term PPI treatment does not reduce the length of the BE segment. Surgical approaches like endoscopic mucosal resection (EMR) and radiofrequency ablation (RFA) have failed to reduce EAC incidence (Fitzgerald et al., 2002), (Quante, Abrams, Lee, & Wang, 2012a) (see Figure 3). EAC belongs to the most common causes of cancer related deaths worldwide. Until recently, examination of the disease has been lacking because suitable models were not available. Only a rat surgical model was used, in which an esophagojejunostomy was performed to induce gastroduodenal reflux. The success of this method highly depended on the quality of the surgeon (Fein et al., 1998), (Quante, Abrams, Lee, & Wang, 2012a). Quante et al. created the first transgenic mouse model for BE and EAC; With this model, new

insights into the early pathogenesis of BE are possible. The EBV-L2- IL-1β transgene in the mouse line leads to an overexpression of human IL-1β in the esophageal and squamous forestomach mucosa. The mice display esophagitis and progress to BE in the first year. These mice eventually developed spontaneous adenocarcinoma in older age. The addition of 0.2 % deoxycholic acid (DCA) to the drinking water of the mice led to an accelerated BE phenotype and earlier tumor development. Furthermore, the combination of DCA and nitrosamine N-methyl-N-nitrosourea (NMU) in the drinking water induced a markedly accelerated BE and tumor phenotype in the mice (Quante, Bhagat, Abrams, Marache, Good, et al., 2012b), (Quante, Abrams, Lee, & Wang, 2012a).

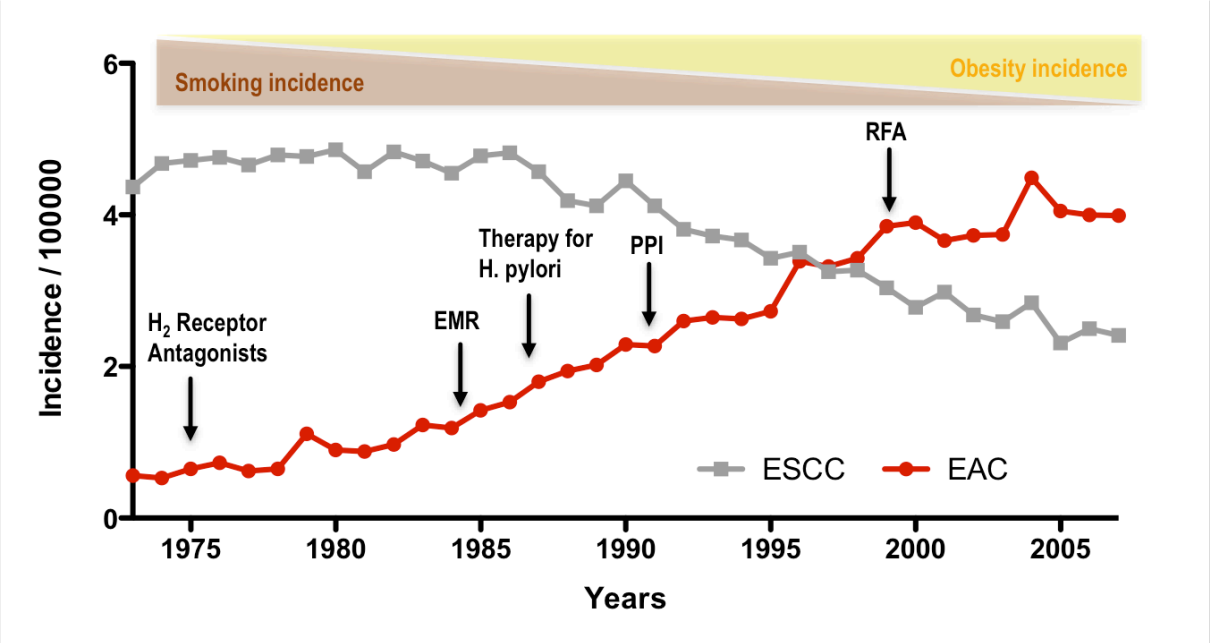

Figure 3: The rise of the EAC incidence rate between 1975 and 2005. During this time period, the incidence rate of esophageal squamous cell carcinoma (ESCC) has declined together with tobacco use as a risk factor. Notably, obesity rates increased in the same time as EAC. Despite medical improvements like EMR, RFA, treatments of heartburn and H. pylori, the rising trend of EAC was not stopped. Adapted from: Quante et al 2012 (Quante, Abrams, Lee, & Wang, 2012a)

Through treatment of human BE cell lines with bile acid, it was shown that BA generates DNA damage and leads to activation of apoptosis pathways (Huo et al., 2011). Reflux in BE patients can trigger progression from IM to BE and to cancer. The nuclear farnesoid X receptor (FXR) could be a viable candidate to protect the tissue from reflux complication. The expression level of FXR varies between normal tissue and BE over EAC. The highest expression of FXR is in Barrett tissue, while in EAC, the expression of the receptor is completely lost (De Gottardi et al., 2006).

Cancer is associated with six different features, and inflammation is an important characteristic that is still not completely understood (Hanahan & Weinberg, 2000), (Hanahan & Weinberg, 2011). Cells of the immune system release many different factors that create an inflammatory and pro-carcinogenic microenvironment (Karin, Lawrence, & Nizet, 2006), (Mantovani, Allavena, Sica, & Balkwill, 2008). Chronic inflammation supports the survival and proliferation of malignant cells likely caused by acid reflux (gastric and bile acid), impeding the innate and adaptive immune system responses and causing an altered reaction to hormones and chemotherapeutic agents (Quante, Abrams, Lee, & Wang, 2012a). Furthermore, reflux compounds and subsequent esophagitis can induce reactive-oxygen species, deplete antioxidants (for example, glutathione) and increase the expression of oxidative-stress-related genes (H. Bernstein et al., 1999), (Lechner et al., 2002), (Oh et al., 2001), (X. Chen et al., 2000), (Wild & Hardie, 2003). BE patients display reduced levels of glutathione and vitamin C in the metaplastic epithelium (Wetscher et al., 1997), (Wild & Hardie, 2003). Nitric oxide synthase, cyclooxygenase-2 (COX2) and myeloperoxidase are upregulated during the development of BE and EAC. This indicates increased levels of nitric oxide, reactive lipid and hypochlorite species (Sihvo et al., 2002), (Ferguson et al., 2008), (Wild & Hardie, 2003). Free radicals like reactive oxygen species (ROS) have several biological effects, especially inducing DNA damage and supporting carcinogenesis. Increased strand breaks and the presence of the pro-mutagenic oxidative DNA lesion 8-hydroxy-deoxyguanosine have been observed in BE cells (Olliver, Wild, Sahay, Dexter, & Hardie, 2003), (Carlson et al., 2002), (Wild & Hardie, 2003). (Figure 4)

The NFκB downstream target IL-6 was identified as a relevant mediator of tumorigenesis for colon and liver cancer in mouse models. IL-6 could be a possible explanation for gender disparities in BE (Naugler et al., 2007), (Grivennikov & Karin, 2008). It has been shown that IL-1β and IL-8 are upregulated in BE, especially at the junction (Fitzgerald et al., 2002)

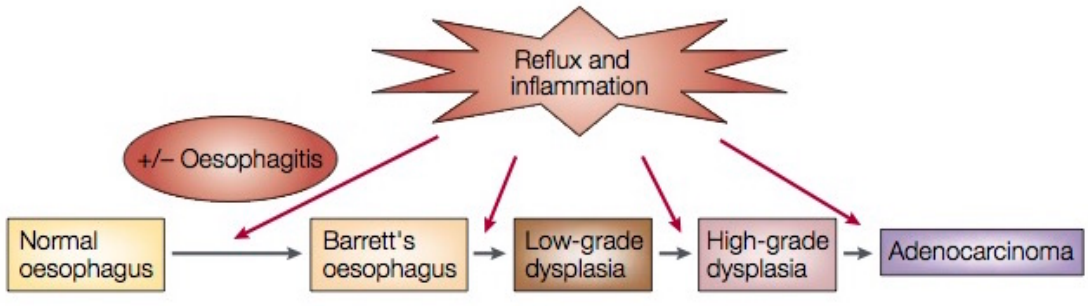

Figure 4: Reflux and inflammation are associated with the development of Barrett's esophagus (BE) and its progression to cancer. The mechanism behind is poorly understood. Reflux and inflammation might act individually or together and could have a key role in disease development. Adapted from: Wild and Hardie 2003 (Wild & Hardie, 2003)

The cellular origin of the columnar cells in Barrett's metaplasia is currently unknown. At least three possible sources of cells have been proposed: esophageal stem cells that are reprogrammed into intestinal epithelial stem cells, stem cells present in the submucosal gland and stem cells located in the gastric cardia adjacent to the gastroesophageal junction (Barbera & Fitzgerald, 2010), (Burke & Tosh, 2012). Quante demonstrated the likely origin of the metaplastic BE tissue through lineage tracing studies. The cells from the gastric cardia are Lgr5+ and serve as both progenitor and stem cell. The fact that Barrett heterogeneity results from multiple independent stem clones is an argument against a transdifferentiation (Leedham et al., 2008), (Quante, Abrams, Lee, & Wang, 2012a), (Quante, Bhagat, Abrams, Marache, Good, et al., 2012b).

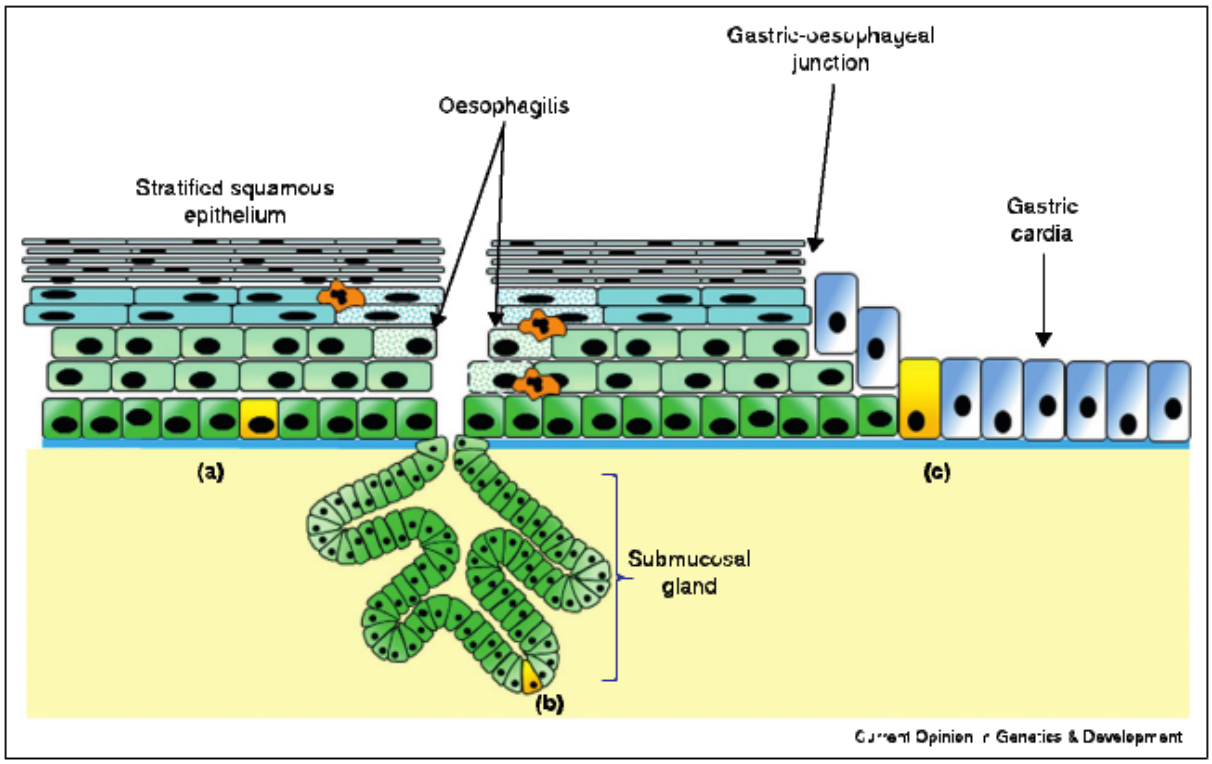

Figure 5: The cellular origin of Barrett's metaplasia is still unknown. Three sources have been proposed (yellow): (a) esophageal stem cells, (b) stem cells present in the submucosal gland and (c) stem cells located in the gastric cardia adjacent to the gastroesophageal junction. Adapted from: Burke and Tosh 2012 (Burke & Tosh, 2012)

4 Farnesoid X Receptor (FXR) in BE and EAC

4.1 Farnesoid X Receptor

A member of ligand-activated transcription nuclear receptors is FXR, also known as bile acid receptor (BAR). It was originally called retinoid X receptor interacting protein 14 (RIP14). The official name is nuclear receptor subfamily 1, group H, member 4 (NR1H4), as provided by HUGO Gene Nomenclature Committee (HGNC) (Modica, Gadaleta, & Moschetta, 2010). In 1999, it was shown that bile acids are natural ligands of FXR (Makishima, 1999), (Parks et al., 1999), (H. Wang, Chen, Hollister, Sowers, & Forman, 1999), (Modica et al., 2010). Activated by a ligand, FXR forms a heteromer with the retinoid X receptor (RXR), translocates to the nucleus and binds to the DNA-binding domain (DBD), which regulates the expression of certain genes (Modica et al., 2010).

4.2 Bile Acid

Bile acids are a steroid end product of cholesterol catabolism. They can be produced in a classical or in an alternative pathway: The classical pathway is a multiple enzymatic process in hepatic cells via cytochrome P450, whereas the alternative pathway is a bacterial process in the colon. BAs are classified in primary – cholic acid (CA) and chenodeoxycholic acid (CDCA) – or secondary BAs – lithocholic acid (LCA) and deoxycholic acid. Primary BAs are synthesized in the liver via the classical pathway, while secondary BAs are produced from primary BAs by intestinal bacteria (Chiang, 2002), (Modica et al., 2010) (see Figure 6) Mice present muricholic acids, a derivative of chenodeoxycholic acid, which is more hydrophobic and less toxic for cells than CDCA (Baptissart et al., 2013). In the liver, most of the circulating BAs are conjugated in the C24 carboxyl group with taurine or glycine (Falany, Johnson, Barnes, & Diasio, 1994), (Modica et al., 2010). The hydrophobicity of a BA rises proportionally to its conjugations. More hydrophobic acids are easier to dispose. In humans, 7-alpha-hydroxylase (CYP7A1) is the enzyme for de novo synthesis of bile acids. Together with cholesterol, phospholipids and bilirubin, BAs are the main components of bile (Baptissart et al., 2013)

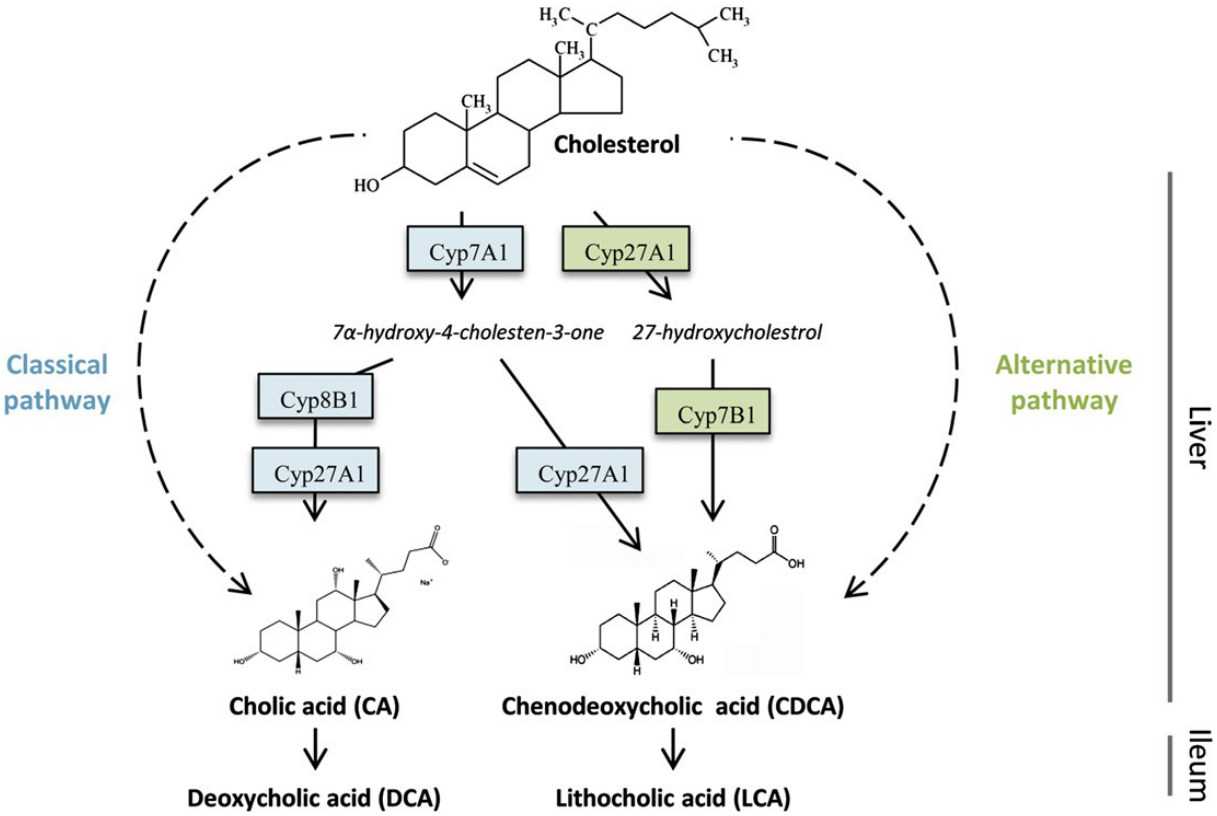

Figure 6.: Schematic representation of pathways of bile acid (BA) synthesis. BA synthesis takes place in the liver. They are made from cholesterol. The classical pathway and alternative pathways involve different cytochromes. Primary BAs, like chenodeoxycholic (CDCA), are converted into secondary BAs, like deoxycholic acid, by the bacteria. Adapted from: Basptissart et al 2013 (Baptissart et al., 2013)

4.3 Gene and Protein

FXR is a conserved gene with 11 exons and 10 introns. It is suggested that FXR plays a crucial role in the organism. Its expression is high in the liver, the intestine, the adrenal glands and the kidneys. The gene is mapped to chromosome 10c.2 in humans and chromosome 12 q23.1 in mice, and encodes four different isoforms – FXR 1, FXR 2, FXR 3 and FXR 4 – as a result of different splicing variants of exon 5 and two distinct promoters (Huber et al., 2002), (Zhang, 2002), (Modica et al., 2010).

4.4 Bile Acid Metabolism

A postprandial stimulus is necessary to release the gall bladder into the duodenum. The absorption of lipophilic nutrients is supported by bile in the intestine. Lipophilic nutrients are, among others, lipids and lipophilic vitamins like vitamin E. About 95 % of BAs are actively absorbed and only 500 mg of BAs are lost on average per day via defecation. BAs are not expelled into urine under normal conditions. This recycling process is called enterohepatic circulation (Love & Dawson, 1998), (Modica et al., 2010). The small heterodimer partner (SHP) is upregulated in the liver by activation of FXR. The receptor suppresses the de novo synthesis of BAs (Goodwin et al., 2000), (Y.-K. Lee & Moore, 2008), (Lu et al., 2000), (Modica et al., 2010). At the same time, FXR activation induces fibroblast growth factor 19 (FGF19) (FGF15 in mice) in the intestine. FGF19 circulates to the liver through the portal vein and binds to the growth factor receptor 4 (FGFR4) which blocks cholesterol 7-alpha-hydroxylase (CYP7A1) (Kim, Morimura, et al., 2007b), (Modica et al., 2010). The conjugation of BA from CoA thioesters is regulated with the BA CoA synthase (BACS) and BA-CoA amino acid N-acetyltransferase (BAAT) (Solaas, Ulvestad, Söreide, & Kase, 2000), (Modica et al., 2010). The active secretion of conjugated BAs is controlled by the bile salt export pump (BSEP), multidrug related protein 2 (MRP2/ABCC2) and multidrug protein 3/2 (MDR3/Mdr2, ABCB4/Abcb4). Conjugated BAs are stored in the gall bladder (Modica, Bellafante, & Moschetta, 2009), (Modica et al., 2010). They can be actively absorbed through the Apical sodium-dependent bile acid transporter (ASBT) in the enterocyte brush border membrane (Dawson et al., 2003), (Oelkers, Kirby, Heubi, & Dawson, 1997), (Modica et al., 2010). After they are taken up by ASBT, BAs are shuttled from the apical to the basolateral membrane by the intestinal bile acid-binding protein (IBABP) (Gong, Everett, Schwartz, Norris, & Wilson, 1994), (Tochtrop, DeKoster, Covey, & Cistola, 2004), (Toke et al., 2006), (Modica et al., 2010). Finally, they are secreted into the portal blood by the heterodimeric organic solute transporter α/β (OSTα/β) (Dawson et al., 2005), (Modica et al., 2010). Two phases of BA biotransformation occur mainly in the liver. Oxidation reactions are characteristic for phase I. CYP3A4/Cyp3a11 catalyze more polar products (Araya & Wikvall, 1999), (Bodin, Lindbom, & Diczfalusy, 2005), (Modica et al., 2010). In phase II, enzymes are responsible for the conjugation of phase I products. The conjugation with endogenous molecules is necessary to further increase their water solubility. Sulfotransferase 2A1 (SULT2A1) plays an important role in the biotransformation (Song et al., 2001), (Modica et al., 2010). At the end of phase II, conjugated BAs are polar enough to be easily expelled from the organism. However, they cannot be delivered from the liver into the bile by passive diffusion. Therefore, a phase III is required. An active secretion of BAs into the bile can be managed by MDR3/Mdr2 and BSEP (Modica et al., 2010). For illustration see Figure 7.

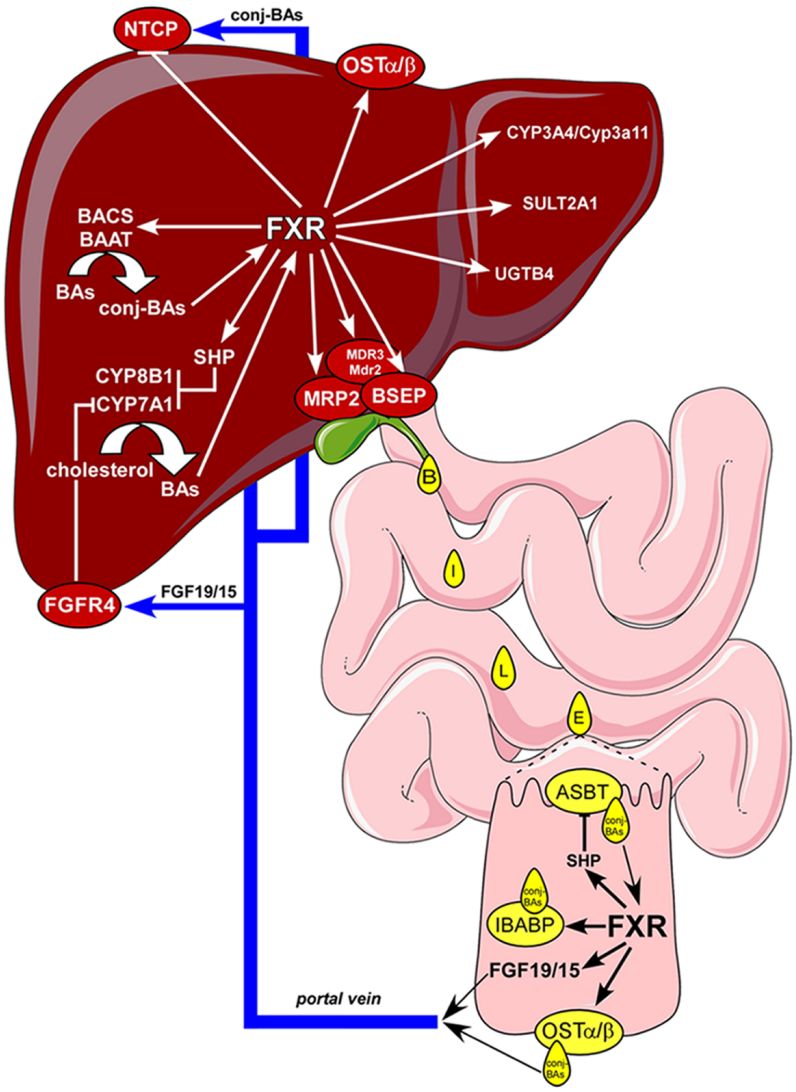

Figure 7: Bile acids activate hepatic and intestinal FXR to regulate important genes for bile acid (BA) metabolism. Hepatic FXR activates SHP and suppresses BA synthesis by reducing several cytochromes, and furthermore promotes BA conjugation. FXR controls BA secretion in the small intestine by upregulating the expression of several transporters. BA are passively reabsorbed in the distal ileum, while conjugated BAs are actively taken up at the ileal luminal membrane, shuttled to the basolateral membrane and secreted into the portal blood to travel back to the liver. There BAs can be taken up, completing the enterohepatic circulation. In addition, FXR induces expression of a hormone (FGF19/15) and suppresses BA synthesis through FGFR4. Adapted from: Modica et al 2010 (Modica et al., 2010).

4.5 Diseases associated with FXR

Bile acids have important roles for liver maintenance, inducing liver regeneration and hepatocyte proliferation (Barone et al., 1996), (Modica et al., 2010). Blocking of the enterohepatic BA circulation leads to an inhibition of liver regeneration (Ueda, Chijiiwa, Nakano, Zhao, & Tanaka, 2002), (Modica et al., 2010). Cholesterol gallstone disease (CGD) is associated with a high cholesterol of the bile and leads to precipitation of cholesterol crystals and gallstone formation (Sasso, Petruzzelli, & Moschetta, 2008), (Portincasa, Moschetta, & Palasciano, 2006), (Modica et al., 2010). However, a high BA and phospholipid concentration protects from gallstone formation (Modica et al., 2010). A reduction or impairment of bile flow is characterized by Cholestasis. This pathological condition is a result of defects in the process of bile formation in hepatocytes or cholangiocytes (intrahepatic cholestasis). An extrahepatic cholestasis results from physical obstructions in bile ducts due to tumors or stones (Modica et al., 2010). The levels of bile acids in the intestine are tightly regulated; A reduced intestinal BA concentration leads to bacterial overgrowth and translocation across the mucosal barrier. This way, bile flow obstruction can cause a systemic infection. Bile acids have surfactant properties and can control intestinal bacterial proliferation. This property is partially controlled by FXR (Inagaki et al., 2006). A high level of BAs in the intestine due to defects in BA reabsorption results in inflammatory bowel disease, chronic diarrhea and promotion of intestinal tumorigenesis (Modica et al., 2010). A hyperproliferation of intestinal bacteria can be seen in mice with FXR knock-out. The mice also show evidence of a compromised epithelial barrier. Bacteria can easily infiltrate the epithelium and recruit of activated macrophages/neutrophils, which leads to inflammation (Inagaki et al., 2006), (Modica, Murzilli, Salvatore, Schmidt, & Moschetta, 2008), (Modica et al., 2010). FXR-/- mice have chronically high levels of circulating BAs. The cytotoxic effects of BA lead to the spontaneous development of hepatocellular carcinoma (HCC) in the age of 12-15 months (Kim, Ahn, et al., 2007a), (F. Yang et al., 2007), (Modica et al., 2010).

5 FXR and Carcinogenesis

FXR shows several protective features in the gastrointestinal (GI) tract. Activated FXR prevents dextran sodium sulfate (DSS)- and 2,4,6-trinitrobenzenesulfonic acid (TNBS)-induced intestinal inflammation in wild type (WT) mice. Furthermore, mice show improvement of colitis symptoms, reduced goblet cell loss and inhibition of epithelial permeability. Proinflammatory cytokine in the mouse colonic mucosa are inhibited by FXR activation, and the inhibition is reproducible even in different cell culture immune cell populations (Gadaleta et al., 2011). This prevention of chemically induced intestinal inflammation is triggered by the toll-like receptor 9 (TLR9) (Renga et al., 2013). The gastric and intestinal mucosal barrier maintenance is FXR regulated (Fiorucci et al., 2011), (Gadaleta et al., 2011). FXR agonists can protect against gastric injury caused by different drugs like acetyl salicylic acid (ASA) and non-steroidal anti-inflammatory drugs (NSAIDs). This protection is mediated by generation of hydrogen sulphide through the enzyme cystathionine-γ-lyase (CSE) (Fiorucci et al., 2011). FXR can activate differentiation processes in different tissues and stem cells. In the intestinal and the gastric epithelium, mucin 2 (MUC2) and caudal type homeobox 2 (CDX2) were unregulated during CDCA treatment in rat gastric epithelial cells (RGM-1) (Y. Xu et al., 2010). However, proteasome degradation of CDX2 is FXR regulated, too. Exposure of esophageal cells to BAs leads to increased levels of microRNAs (MIRs) 221 and 222 and reduced levels of cyclin-dependent kinase inhibitor 1B (p27Kip1) (Matsuzaki et al., 2013). It was shown that the antioxidant tempol remodels the gut microbiome and leads to inhibition of FXR, which decreases obesity in mice (F. Li et al., 2013). The adipocyte fates are controlled by FXR. Their differentiation is regulated by the peroxisome proliferator-activated receptor gamma (PPARγ) and wnt/β-catenin pathways. The adipocyte function is under FXR control, as well (Abdelkarim et al., 2010). In bone marrow, the balance of osteoblast/adipocyte is mediated by runt-related transcription factor 2 (RUNX2) under assistance of FXR. FXR activation supports osteoblastic differentiation of human bone marrow stromal cells (BMSC) by RUNX2, while its inhibition shows an adipocyte-like phenotype (Boufker et al., 2011). Apoptosis activation and removal of genetically altered cells is mediated by FXR in the intestine and in colon cancer cells, which may stop the transformation of these cells to cancer (Modica et al., 2008). Adenoma reduction in APCmin mice was demonstrated with sodium taurocholate (NaTC) treatment. NaTC is an FXR agonist which promotes the

expression of SHP, FGF15, cyclin D1 and IBABP. However, additional FXR k/o in APCmin mice shows an increased size of small intestine adenocarcinomas. This suggests that activation of FXR by non-bile acid ligands may protect against intestinal carcinogenesis (Maran et al., 2009). The tumor cell viability was suppressed by FXR inhibition by FXR shRNA or guggulsterone. The tumor formation and growth was reduced in a nude mouse xenograft model (Guan, Li, Yang, Hoque, & Xu, 2012). FXR deficiency promotes cell proliferation such as cyclin D1, inflammation such IL6, and tumorigenesis in vivo and in vitro (Maran et al., 2009), (Guan et al., 2012). A summary of gene regulation is in Table 1.

Table 1: Gene Regulation of FXR

Gene/Pathway	Regulation	Paper
IL-1β, interferon y, IL-6, wnt-pathway	down	(Kim et al., 2007), (Yang et al., 2007), (Maran et al., 2009)
SHP, FGF15 /19, cyclin D1, IBABP	up	(Smith, Keshavan, Avissar, Ahmed, & Zucker, 2010)
microRNA 221&222, p27Kip1, MUC2	down	(Matsuzaki et al., 2013)
IL18, iNOS, CAR12 (intestinal mucosa defense), SHP, PPAR	up	(Modica, Gadaleta, & Moschetta, 2010)
NfkB, CYP7A1, ASBT	down	(Modica, Gadaleta, & Moschetta, 2010)
MUC2, CDX2	up	(Xu et al., 2010)

6 The Role of FXR in BE and EAC

FXR k/o mice display disrupted bile acid homeostasis, intestinal and liver inflammation and liver tumor progression. The loss of FXR also promotes carcinogenesis (Kim, Ahn, et al., 2007a), (F. Yang et al., 2007), (Modica et al., 2010)] and leads to hyperkeratosis, increased proliferation in the esophagus and esophagitis (Lian et al., 2011). However, an activated FXR protects against hepatocarcinoma development during the life span. The nuclear FXR is over-expressed in BE patients and in specialized intestinal BE cells, while almost no FXRα was found in a healthy squamous epithelium. With the progression from normal conditions to BE, the expression of FXR is at the highest level, whereas in EAC, the FXR expression is completely lost (De Gottardi et al., 2006), (Capello et al., 2008).

7 Hypothesis and Aim

We hypothesized that during early steps in the development of BE the expression of FXR is upregulated as a protective defense against irritation from bile in the reflux. This may result in tissue homogenization to maintain and protect the differentiation state of intestinalized metaplasia in BE. FXR is a factor discussed to inhibit inflammation and tissue damage, two important mediators of carcinogenesis in BE. In the mouse model cardia stem cells migrate into the esophagus and give rise to BE and dysplasia and therefore FXR mediated reduced inflammation might inhibit attracting the immune system and recruiting cardia stem cells towards the lower esophagus. In the late state of progression to EAC, the expression of FXR seems to be silenced. We thus further hypothesized that in an established tumor FXR, with its anti-inflammatory and prodifferentiation properties, would inhibit its rapid growth and FXR knockdown would therefore lead to an accelerated carcinogenesis.

In order to test our hypotheses, we crossed the pL2-IL-1β mouse model to a complete FXR knockout mouse model as in the mouse model pL2-IL-1β mice with FXR knockdown should show increased inflammation and accelerated procession to BE and EAC. The aim of this thesis was to analyze the loss of FXR during BE formation and progression to cancer, and to decipher the influence of bile acid using a genetically engineered mouse model (GEMM). Our data will hopefully result in a better understanding of BE biology and therefore enable us to improve the early discovery of relevant precursor lesions and the assessment of putative therapeutic targets.

8 Material

8.1 Chemicals and Kits

8.1.1 Immunohistochemistry (IHC)

Antigen unmasking solution H-3300	Vector Labs, Burlingame USA
Biotinylated Goat Anti-Rabbit IgG Antibody BA-1000	Vector Labs, Burlingame USA
DAB Peroxidase (HRP) Substrate Kit, SK-4100	Vector Labs, Burlingame USA
Dako Pen	Vector Labs, Burlingame USA
Ethanol (100%, 96%, 70%)	Pharmacy of Klinikum rechts der Isar, Munich
Hemalaun according to Mayer	Pharmacy of Klinikum rechts der Isar, Munich
Isoflorane CP	CP-Pharma, Burgdorf
Isopropanol	Pharmacy of Klinikum rechts der Isar, Munich
Normal Goat Serum Blocking Solution S-1000	Vector Labs, Burlingame USA
Protinase K	Qiagen, Hilden
Streptavidin/Biotin Blocking Kit SP-2002	Vector Labs, Burlingame USA
Pertex® mounting medium for coverslipping	Medite, Burgdorf
VECTASTAIN Elite ABC Kit (Standard) PK-6100	Vector Labs, Burlingame USA
Xylol	Hedinger, Stuttgart
Zinc Formalin Fixative	Polyscience, Warrington USA

8.1.2 Kits

AllPrep DNA/RNA/Protein Mini Kit	Qiagen, Hilden
QuantiTect Reverse Transcription Kit	Qiagen, Hilden
QuantiTect SYBR Green PCR Kit	Qiagen, Hilden
QuantiTect Whole Transcriptome Kit	Qiagen, Hilden
REDTaq® ReadyMix™ PCR Reaction Mix	Sigma-Aldrich, Stammheim

8.1.3 Others

Phosphate buffered saline (Dulbecco's PBS)	Applichem, Darmstadt
β-Mercaptoethanol	Sigma-Aldrich, Stammheim

8.2 Antibodies

Table 2: List of Antibodies for Immunohistochemistry

Antibody	company	concentration	Host	application	product code	Type
Dclk1	Abgent	unknown	rabbit	1:500	AP7219b	unknown
FXR	Abcam	1 mg/ mL	rabbit	1:400	ab28676	IgG
γH2AX	Millipore	200 µg	mouse	1:1000	05-636	IgG

8.3 Consumables

1 mL Sub-Q	BD, Franklin Lakes USA
CellStar Culture Flasks 75 cm^2	greine bio-one, Kremsmünster Austria
Cell strainer 40 µm	BD, Franklin Lakes USA
Cell strainer 70 µm	BD, Franklin Lakes USA
Cell strainer 100 µm	BD, Franklin Lakes USA
Histosette, embedding cassettes	Simport, Beloeil Canada
Microvette 500 Z-Gel	Sarstedt, Nümbrecht
Sponges for embedding cassettes	Simport, Beloeil Canada
Syringe filters, diameter 25 mm and pore size 0.2 µm	Schleicher & Schuell, Dassel
Six-well multiwell plate	Sarstedt, Nümbrecht
Six-well transwell carrier	Organogenesis, Reinach Switzerland
Tissue-culture dish 10 cm	Sarstedt, Nümbrecht
Transwell insert 24 mm with 3.0 µm pore	Corning, Amsterdam The Netherlands
Whatman paper	Schleicher & Schuell, Dassel

8.4 Devices

Axio Lab.A1 microscope	Zeiss, Jena
Axio Imager.A1 microscope; AxioCam HRc	Zeiss, Jena
Lenses:	
10x: EC-Plan NEOFLUAR 10x/0,3	
40x: Plan-APOCHROMAT 40x/0,95	
Axiovert 40 CFL microscope	Zeiss, Jena
Centrifuge 5702R	Eppendorf, Hamburg
Centrifuge 5415D	Eppendorf, Hamburg
LightCycler® 480	Roche, Penzberg
Maxwell® 16 Research Instrument	Promega GmbH, Mannheim
Mini-Transblot Cell	Bio-Rad, Munich
Nanodrop 2000 Spectrophotometer	Thermo Scientific, Dreieich
S300 tissue processing unit	Leica Biosystems, Wetzlar
T100 Thermal Cycler	Bio-Rad, Munich
Ricoh CX6	Ricoh, Tokyo, Japan

8.5 Software

AxioVision Rel. 4.8	Zeiss, Jena
GSEA software	Broad institute Cambridge, USA
ImageJ (Freeware)	National Institute of Health (NIH)
Image Scope	Leica Biosystem, Wetzlar
InkSccape (Freeware)	Martin Owens
LightCycler 4.0	Roche, Penzberg
Prism 6	GraphPad Software Inc., La Jolla USA

8.6 Cell culture Media and Groth Factors

Adenine	Sigma-Aldrich, Stammheim
B27 Supplements 100x	gibco© by life technologiesTM
Bovine collagen type I	Organogenesis, Reinach Switzerland
Bovine pituitary extract	gibco© by life technologiesTM
Calcium chloride	Sigma-Aldrich, Stammheim
Deoxycholic acid	Sigma-Aldrich, Stammheim
Dimethyl sulphoxide (DMSO) ≥99,5 %	Roth, Karlsruhe
Dulbecco's Phosphate buffered Saline (DPBS)	gibco© by life technologiesTM
EDTA	Sigma-Aldrich, Stammheim
Eagle's minimum essential medium	Lonza, Cologne
EGTA	Sigma-Aldrich, Stammheim
EGF human	gibco© by life technologiesTM
EGF murine	Peprotech, Hamburg
Fetal Bovine Serum, Heat inactivated	gibco© by life technologiesTM
FGF-10 murin	Peprotech, Hamburg
Gentamicin sulfate	gibco© by life technologiesTM
GlutaMax 100x	gibco© by life technologiesTM
Ham's F12	gibco© by life technologiesTM
Hanks' balanced salt solution	gibco© by life technologiesTM
HEPES	gibco© by life technologiesTM
Insulin, transferrin, ethanolamine and selenium	Lonza, Cologne
Keratinocyte–serum-free medium (KSFM)	gibco© by life technologiesTM
L-Glutamine	gibco© by life technologiesTM
Matrigel	BD, Franklin Lakes USA
N2 Supplements 50x	gibco© by life technologiesTM
N-Acetylcysteine	Sigma-Aldrich, Stammheim
Noggin murine	Peprotech, Hamburg
O-Phosphorylethanolamine	Sigma-Aldrich, Stammheim
Penicillin – Streptomycin, 10.000 U/ mL	gibco© by life technologiesTM
Progesterone	Sigma-Aldrich, Stammheim
RPMI 1640 + L-Glutamine medium	gibco© by life technologiesTM
R-Spondin-1 human	Peprotech, Hamburg
Sodium bicarbonate	Sigma-Aldrich, Stammheim
Triiodothyronine	Sigma-Aldrich, Stammheim
Trypsin-EDTA (0.05 %), phenol red	gibco© by life technologiesTM
Trypsin-EDTA (0.25 %), phenol red	gibco© by life technologiesTM

8.7 Prepared Media

Cardia medium:

- DMEM with 10 % FBS and 1x P/S (ground medium)
- B27 1x
- N2 1x
- n-Acetylcysteine 1mM
- mEGF 50 ng/ mL
- mNoggin 100 ng/ mL
- mFGF-10 100 ng/ mL
- R-Spondin 1 µg/ mL

8.8 Cell Lines

hTERT	Human Immortalized esophageal cell line
FEF	Human fetal embryonic fibroblast
OE19	Human esophageal adenocarcinoma cell line
OE21	Human esophageal squamous-cell carcinoma cell line
OE33	Human esophageal adenocarcinoma cell line

9 Methods

9.1 Mice

pL2-IL-1β and FXR$^{-/-}$ strains have been described previously (Quante, Bhagat, Abrams, Marache, Good, et al., 2012b), (Sinal et al., 2000). Experiments were carried out in accordance with the German Federal Animal Protection Laws and approved by the Institutional Animal Care and Use Committees of the Technische Universität München. Mice were intercrossed to obtain pL2-IL-1β/FXR$^{-/-}$ type. For genotyping, mouse tail tissue was taken between three and four weeks of age. DNA was isolated and PCR was performed as described in DNA isolation from mouse tissue and Genotyping PCR. Littermates without pL2-IL-1β and FXR WT allele served as wild type. Controls are WT, pL2-IL-1β and FXR$^{-/-}$. Mice were killed by an overdose of isoflurane anesthesia, either upon indicated time points or notable symptoms of disease met euthanization criteria.

9.2 Cell Culture

9.2.1 Cardia Crypt Culture

The stomach was opened along the large curvature and put flat on a hard surface like petri dish with the inside up. It was cut 1 mm at each side of the squamocolumnar junction. The rest of the stomach was discarded. With a razor blade the squamocolumnar junction tissue was disrupted in very small pieces, transferred in 15-20 mL PBSO/EDTA-EGTA buffer and incubated for 45 minutes on a shaker at 4 °C. After this the small pieces were allowed to settle down and the supernatant was removed. 10 mL PBSO with 10 % FBS was added. The mix was between three to five times pipetted up and down and collected the supernatant passing a 100 µm strainer. This was repeated once with a new strainer. The crypts were spun down at 800 g for 5 min. Most of the supernatant was removed and the pellet was gently re-suspended in 100 - 150 µL of Matrigel. A preheated 24 wells plate from an incubator at 37 ˚C was used to seed crypts in 50 µL Matrigel drops. Plate was incubated 2 min. at room temperature and 5 min at 37 °C. Finally, 500 µL cardia medium was added. (PAPER!!!)

9.2.2 9.2.2 Culture and Passaging of 3D-Crypt-Culture

Culture medium was changed at least two times per week, usually Monday and Friday. Pre-wetted pipettes were used to avoid the crypts sticking inside the pipette tips. Medium was replaced through 1 mL cold culture medium. Matrigel was broke up by a 1000 µL tip and transferred to a 15 mL tube at ice. Another 1 mL cold medium was added to wash the well. The hole volume was transferred the medium to a 15 mL tube. The medium was then pipetted up and down a few times to break up the crypts in smaller pieces. 2 mL cold medium was added and spun down for 5 min at 600 g. The supernatant was removed and three times more Matrigel per well was added. 50 µL Matrigel drops were again seeded in a pre-heated 24 wells plate at 37 ˚C. Plate was incubated 2 min. at room temperature and 5 min at 37 °C. Finally, 500 µL cardia medium was added.

9.3 3D organotypic culture (OTC)

The organotypic culture was performed as previously described (Kalabis et al., 2012). Acellular matrices were prepared as previously published, but each cellular matrix contained 800.00 fibroblast per well. After the solidification of the matrixes, at day 0 cells (OE19, 21, 33 or hTERTs) were seeded. 7,5 mL of the grow medium of the seeded cells were added per well. Cells were treated with 50 µM or 200 µM DCA twice a day for 10 or 60 min. for 14 days Finally the cells were fixed in formalin, dehydrated, and embedded in paraffin. On the cut slides H&E, PAS, Ki-67and Dclk1 staining were performed.

9.4 Macroscopic scoring

The stomach was opened along the greater curvature and spread out after sacrifice. Macroscopic pictures were taken by a digital camera in macro mode. The size of tumor at the SCJ was determined with ImageJ according the ruler – pixel ratio of the picture The tumor size score was determined according to the Table 3. The total length of the cardia was measured with ImageJ and the percent which is influenced of tumors was determine.

Table 3: Tumor Size Score at the Cardia Regions

Tumor Size Score at cardia regions	Tumor Size
0	No abnormalities
1	< 0,5 mm
2	< 1,0 mm
3	< 2,0 mm
4	> 3,0 mm

9.5 Histological Analysis

9.5.1 Formaldehyde Fixation and Conservation

Tissue of sacrificed mice was rapidly removed and immediately incubated over night at room temperature in formalin for fixation. Tissue was either stored for up to 3 days or directly dehydrated and paraffinized with increasing concentrations of ethanol followed by xylol ensued by paraffin using a Leica S300 tissue processing unit. Tissue was embedded in liquid paraffin and cooled for hardening. Formalin-fixed, paraffin-embedded (FFPE) blocks were stored at room temperature. For analysis, blocks were cut on a microtome to 1,5 µm slices, transferred to a 50 °C water bath for stretching and collected on microscopy slides. Sections were allowed to dry 20 min at 65 °C. For stainings, Hematoxylin & Eosin (H&E), periodic acid–Schiff (PAS) and Immunohistochemistry (IHC) slides were deparaffinized with two times of 10 min. xylol and rehydrated in distilled water after decreasing alcohol row (twice 100 % isopropanol, twice 96 % ethanol and twice 70 % ethanol 3 minutes each). The staining was performed according protocol (see below). For conservation, sections were dehydrated in an inverted row and embedded in Pertex.

9.5.2 Hematoxylin & Eosin (H&E)

Hematoxylin & Eosin (H&E) is a two-compound staining. The first stains acidic structures in blue, the second basic structures in red. Slides were stained with hematoxylin for 2 min followed by 3 min raising tap water to wash. Counterstaining with eosin was performed like the hematoxylin part. A specialized pathologist evaluated the slides and created a metaplasia and dysplasia score.

9.5.3 Periodic acid-Schiff (PAS)

Periodic acid–Schiff (PAS) is a staining method for detection of polysaccharides, mucosubstances and mucins in tissue. The reaction is based on the oxidation of the vicinal diols to aldehydes. Tissue were oxidized 5 min. in periodic acid and 3 min rinsed in tap water. Slides were placed in Schiff reagent for 15 minutes and 5 min in lukewarm tap water to turn tissue in pink color. Counterstaining was performed 2 min. in hematoxylin followed by 3 min raising tap water. Five fields of view at 40x magnification were used to quantify the percent of PAS+ cells. Additionally, the PAS slides ware used from pathologist to create metaplasia and dysplasia score.

9.5.4 Immunohistochemistry (IHC)

The antigen was unmasked through boiling slides for 20 min in a pressure cooker with citrate buffer of pH 6.0. Boiling was followed by a 20 min cool down period. After unmasking endogenous peroxidases were quenched within 10 min by 3 % hydrogen peroxide (H_2O_2). After three changes of puffer (PBS or TBST) 5 % goat serum for blocking was used for 30 min. at room temperature. The first antibody was used and incubated as indicated in Table x* in a wet chamber. Followed by three washing steps secondary biotinylated antibody was applied in a 1:500 dilution for 30 min. An Avidin-Biotin Complex was generated using the ABC-Kit. After discarding of secondary antibody ABC solution was put on the slide for 30 min. at room temperature. After five washing steps DAB reaction was followed for max of 1 min. DAB reaction was stopped in distilled water and slides were counterstained with hematoxylin for 1 min. followed by 3 min. raising tap water. For quantification representative slides of each mouse were chosen and several pictures per slide were taken. Calculations were performed using the AxioVision 4.8 software and ImageJ of at least three mice per group. All nuclei of the cardia region were counted to calculate the ratio of positive cells for PAS staining. The score of Ki67 and Dclk1 was determined according Table 4 and Table 5.

Table 4: Ki67 Score of the Cardia Regions

Ki67 Score	Number of positive cells
0	< 10
1	< 50
2	< 100
3	< 200
4	> 200

Table 5: Dclk1 Score of the Cardia Regions

Dclk1 Score	Number of positive cells
0	< 3
1	< 15
2	< 30
3	< 50
4	> 50

9.6 DNA/RNA Analyses

9.6.1 DNA isolation from mouse tissue

DNA was isolated from tail tips. Tissue was incubated in 200 µL 1x PCR Tail direct Lysis Buffer containing 600 mAU mL of Proteinase K over night at 400 rpm and 55 °C. Afterwards Proteinase K was heat-inactivated at 95 °C for 45 min. Samples were shortly spun down and 0,5 µL of supernatant was directly used as template for genotyping PCR.

9.6.2 Genotyping PCR

For genotyping 2,5 µL REDTaq® ReadyMix™ PCR Reaction Mix was mixed with 1 µL of primer mix (respective primers each in a concentration of 10 pmol/ µL, see Table 6). Then 0,5 µL of isolated DNA was added and 35x PCR cycles were performed at 95 °C denaturation for 30 seconds, 57 °C for pL2-IL-1β or 60 °C for $FXR^{-/-}$, annealing for 15 seconds and 72 °C elongation for 30 seconds, followed by a final elongation step for 5 min. Genotyping results were visualized in a 2 % (w/v) TAE agarose gel containing 3 µM ethidium bromide.

Table 6: Overview of Genotyping Primers

Gene	Primer sequence (5'-3')	Amplicon size
pL2-IL-1β		277 bp
Forward	CTT CCT GTT CCA TTC AGA GAC GAT	
Reverse	CTC CAG CTG TAG AGT GGG CTT ATC	
$FXR^{-/-}$		WT 250 bp Mut 291 bp
Forward	TCT CTT TAA GTG ATG ACG GGA ATC T	
Mutant Forward	GCT CTA AGG AGA GTC ACT TGT GCA	
Reverse	GCA TGC TCT GTT CAT AAA CGC CAT	

9.6.3 RNA isolation / extraction

For RT-PCR and array experiments tissues were immediately shock frozen in liquid nitrogen. The tissue was homogenized with disperser. Total RNA, DNA and Protein was isolated according to the manufacturer's protocol. RNA and DNA concentration was evaluated on a Nanodrop2000 spectrophotometer and quality was checked on a 1 % (w/v) TAE agarose gel.

9.6.4 cDNA Synthesis

For cDNA synthesis 100 ng of RNA was used and processed according to the manufacturer's instructions. RNA was incubated for 2 min at 42 °C with gDNA Wipeout Buffer and water to degenerate gDNA. Afterwords reverse transcriptase buffer and primer mix were added and for 20 min. at 42 °C incubated. The enzyme was inactivate at 95 °C for 3 min. The generated cDNA was directly used for RT-PCR.

9.6.5 Microarray

The microarray was performed from KFB Regensburg on an Affymetrix GeneChip. The final concentration of the RNA was greater than 50 ng/ µL. Analyzes and comparisons was done from Friedmann Richard at the Cancer Center Colombia

9.6.6 Statistical Analysis

Statistical analysis was performed with GraphPad Prism version 6.0. Multiple t test was used to determined significance and ordinary analysis of variance (ANAVA) with Tukey's multiple comparisons test was used for gammaH2AX staining. Error bars show standard error of the mean (SEM).

10 Results

10.1 The influence of DCA in a 3D cell culture system

hTERT, OE19, OE21 and OE33 were used for an OTC assay. The cells were seeded and treated 14 days twice a day with 50 µM or 200 µM DCA for 10 min. (Figure 8) The bile acid had no effect on the migration and invasion of tumor cells. To test the effect on non-cancer cells, hTERT was used in the OTC system. These cells were treated twice a day with 50 µM or 200 µM DCA for 10 min (Figure 8) or 1 h (data not shown). Esophageal cell started dying after the third day of treatment. After 14 days all cells in all conditions were dead whereas the cells in the control group that where not treated with DCA, survived.

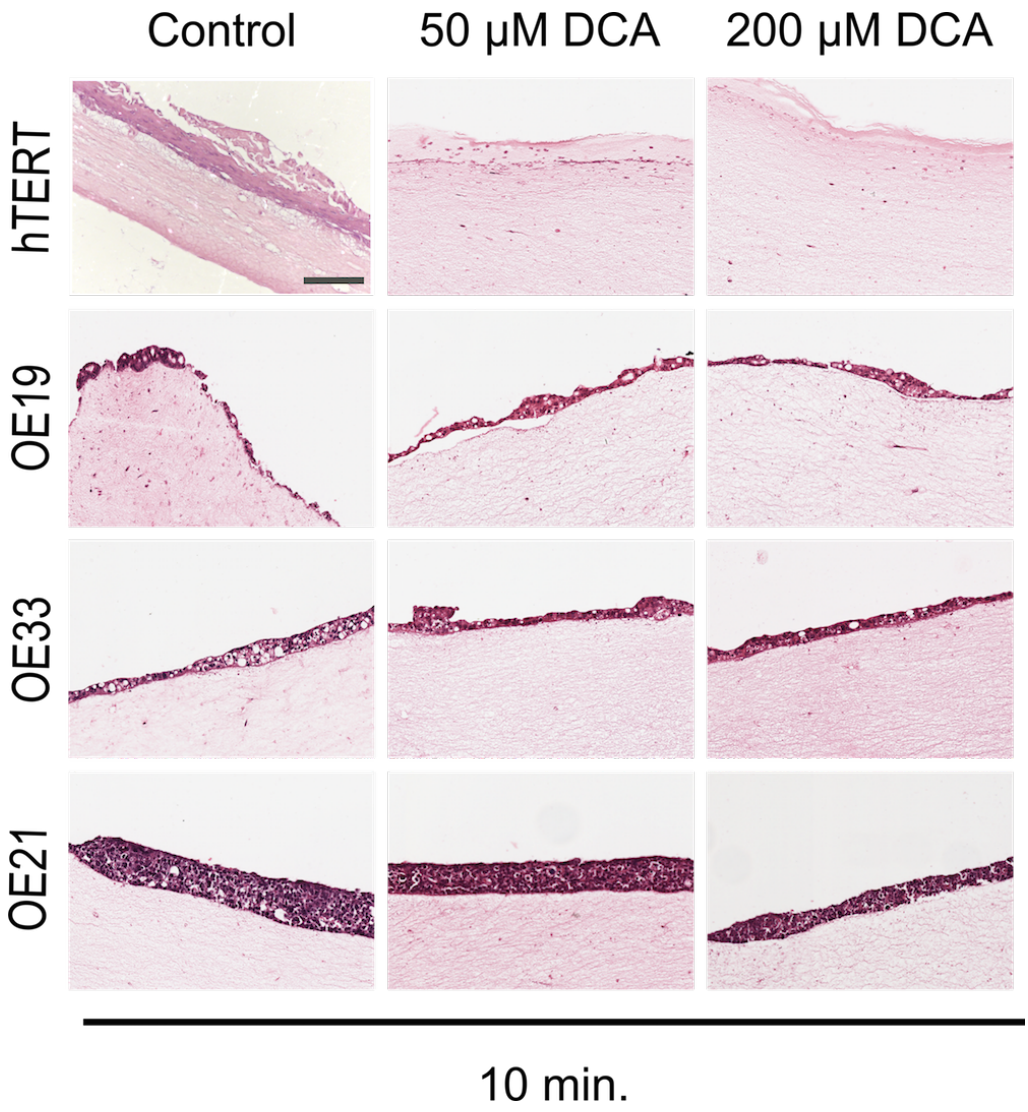

Figure 8: Deoxycholic acid treatment of hTERTS and OE cells in OTC system. All cells were treated with 50 or 200 µM DCA for 10 min. and afterwards stained H&E. Scale bar: 200 µm.

10.2 FXR level in human and mouse tissue

In order to understand the expression level of FXR through tumor progression, first, we checked the expression of FXR level in human and mouse cardia samples by immunohistochemistry. Only low expression of FXR was in normal human and pL2-IL-1β mouse squamous epithelium was detected (Figure 9). Immunohistochemistry shows that high FXR expression level was found in BE tissue of mouse and human while the level of FXR was not detectable in epithelium cells in dysplasia or cancer stage in human and mouse (Figure 9). FXR expression was only detected in stromal cells and immune cells in dysplasia stage

(Figure 9). Additionally, microarray data from our group (Quante, Bhagat, Abrams, Marache, Good, et al., 2012b) shows that from BE mice have high mRNA expression of FXR while EAC mice have low mRNA expression of FXR (Figure 10). When mice were treated with bile acid, FXR mRNA expression decreased. Both immunohistochemistry and microarray issue show that FXR increases in BE stage and decreases in EAC stage

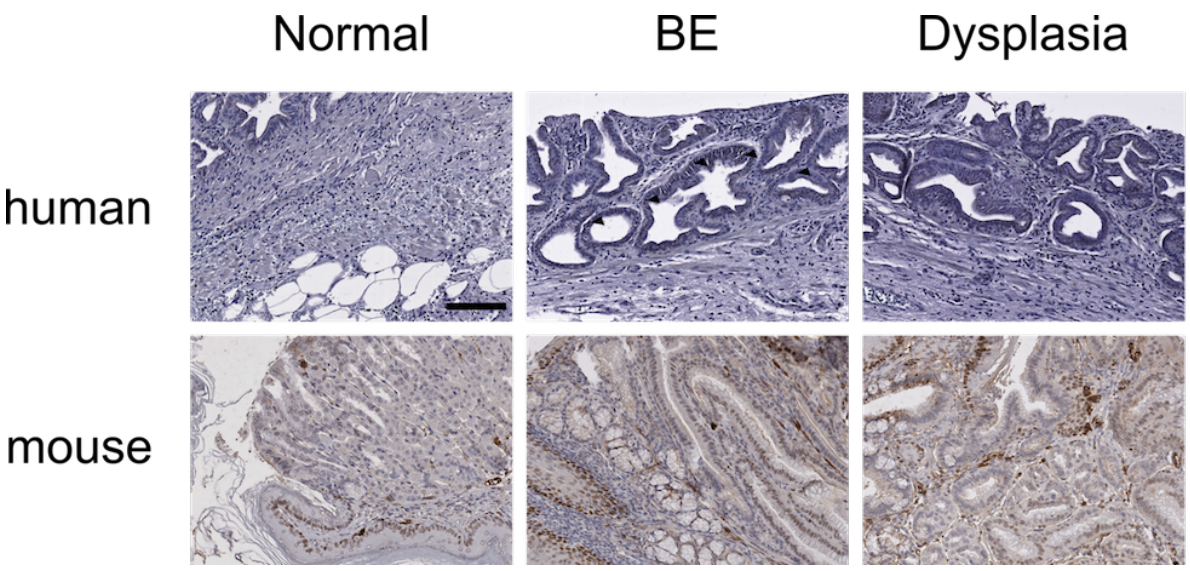

Figure 9: Immunohistochemistry of FXR in human and mouse. The level in humans and mice rises until BE is distinct, after this the level goes down. Arrows show positive cells in Barrett tissue of human. Stromal cells are positive for FX, too. Scale bar: 200 µm

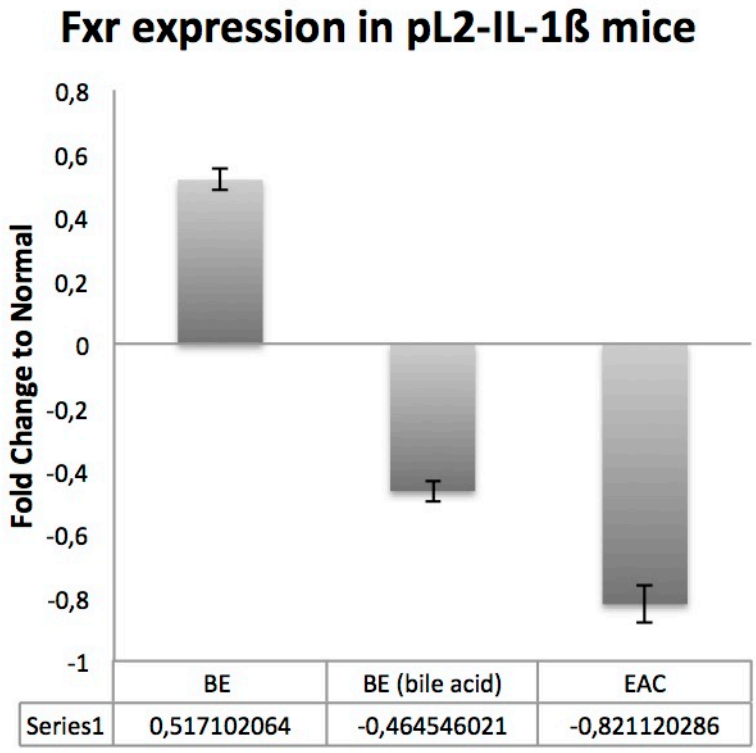

Figure 10: mRNA level of FXR in mouse in microarray. Barrett tissue has high mRNA expression of FXR. With the progression to cancer the level goes down. Bile acids treatment decrease FXR expression. Data from Quante et al 2012 (Quante, Bhagat, Abrams, Marache, Good, et al., 2012b)

10.3 Evaluation of pL2-IL-1β compared to pL2-IL-1β/FXR$^{-/-}$ mice

10.3.1 Macroscopic and histological analyzes

When pL2-IL-1β mice cross with FXR whole body knock out mice, double knockout mice show less fertility. Double knockout mice (pL2-IL-1β /FXR$^{-/-}$) show sickness phenotype at 9 months time. Mice with only pL2-IL-1β show sickness with 12 months. Mice were sacrificed at 6, 9, 12 and 15 months for histology (n>=4). Mice from the control cohort have a constant body weight about 25 g and with age older age about 30 g (Figure 12). The control mice didn't show any alterations in the SCJ of the stomach and no body weight lost. WT body weight increase with time. The treatment with 200 ppm of DCA in drinking water shows a dramatically toxic effect on the health of the pL2-IL-1β/FXR$^{-/-}$ mice so that further experiments couldn't go ahead and the addition of DCA in the drinking water was canceled. Only mice with the pL2-IL-1β transgene show tumors in the SCJ. Mice that develop metaplasia start to loose body weight between 9 and 12 months instead FXR$^{-/-}$ mice with or without transgene (pL2-IL-1β) have lower weight start with 12 months compared to WT. (Figure 12). In all time points more percent of pL2-IL-1β/FXR$^{-/-}$ cardia is covered with tumors. At time point 12 months, more percentage of cardias in pL2-IL-1β/FXR$^{-/-}$ mice are covered with tumors when compare to pL2-IL-1β mice. ($p<0,0025$) (Figure 13). The tumor size score was created according Table 3. pL2-IL-1β/FXR$^{-/-}$ mice have larger tumors from 6 to 12 months. At 15 months, there is no difference in tumor size between pL2-IL-1β mice and pL2-IL-1β/FXR$^{-/-}$.(Figure 13) (tumor size score pL2-IL-1β versus pL2-IL-1β/FXR$^{-/-}$: 6 months 0.75 to 1.25, 9 months 0.67 to 2.00, 12 months 1.86 to 3.00, 15 months 3.00 to 3.00). Figure 11 show that Mice with pL2-IL-1β transgene develop with an age of about 6 months metaplasia. The pathologic score for metaplasia of pL2-IL-1β is slightly lower than pL2-IL-1β mice with additional FXR$^{-/-}$ (metaplasia score pL2-IL-1β versus pL2-IL-1β/FXR$^{-/-}$: 6 months 1,25 to 2,00, 9 months 2,00 to 2,22, 12 months 1,56 to 2,33, 15 months 2,20 to 2,50) ($p>0.05$) (Figure 14). The score for dysplasia (pL2-IL-1β versus pL2-IL-1β/FXR$^{-/-}$) is: 6 months 1,0 to 2,00, 9 months 1,83 to 2,20, 12 months 1,88 to 2,17, 15 months 1,8 to 2,50) (Figure 14).

In summary, pL2-IL-1β/FXR$^{-/-}$ mice have larger tumors in the SCJ than pL2-IL-1β mice. They show more local and slightly stronger inflammation compared to mice with wild type FXR mice, especially in younger age. At age of 6 to12 months, slightly more metaplasia occurs in pL2-IL-1β/FXR$^{-/-}$ mice when compared to pL2-IL-1β mice whereas there is almost no difference between these mice in the age of 15 months.

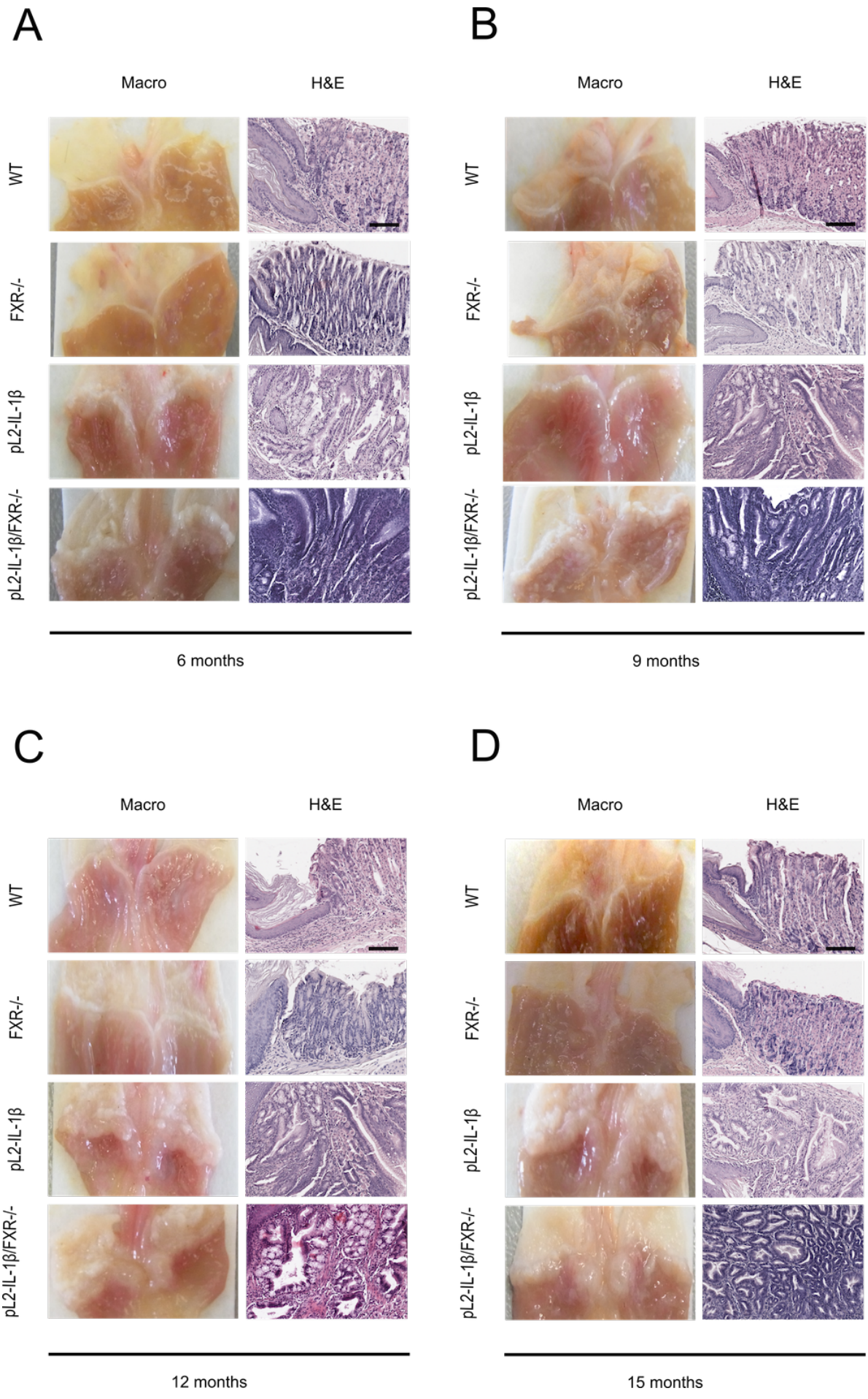
A
Macro
H&E
WT
FXR-/-
pL2-IL-1β
pL2-IL-1β/FXR-/-
6 months
B
Macro
H&E
WT
FXR-/-
pL2-IL-1β
pL2-IL-1β/FXR-/-
9 months
C
Macro
H&E
WT
FXR-/-
pL2-IL-1β
pL2-IL-1β/FXR-/-
12 months
D
Macro
H&E
WT
FXR-/-
pL2-IL-1β
pL2-IL-1β/FXR-/-
15 months

Figure 11: Macroscopic and H&E staining overview of WT, FXR$^{-/-}$, pL2-IL-1β and pL2-IL-1β/FXR$^{-/-}$ mice with 6, 9, 12 and 15 months. The representative cardia and H&E staining A) Shows mice with an age of 6 months and B) shows mice with an age of 9 months. C) shows mice with an age of 12 months. D) shows mice with an age of 15 months. Scale bar: 200 µM

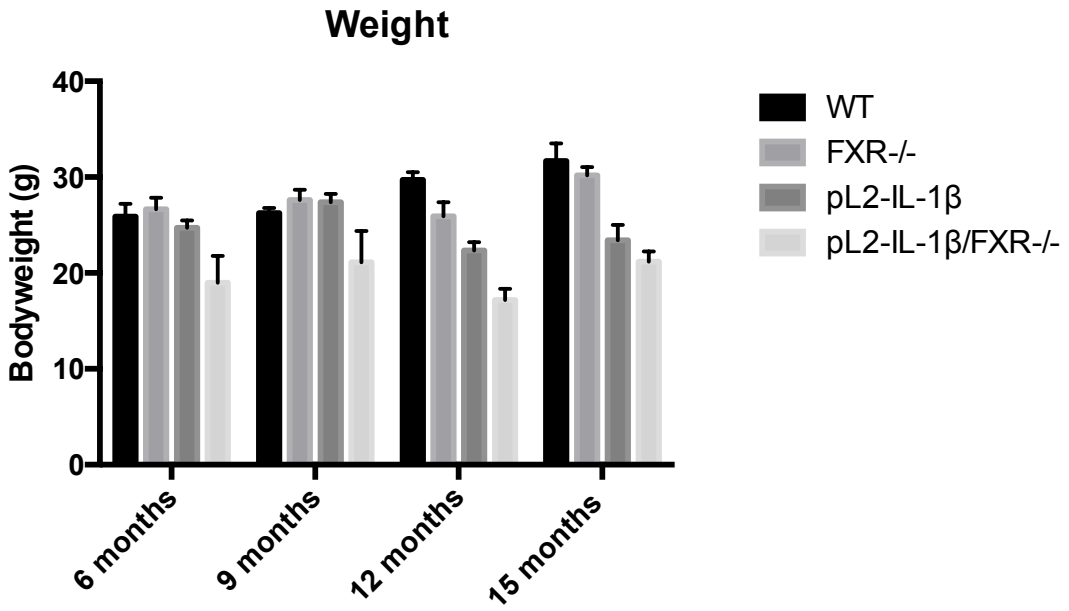

Figure 12: Bodyweight of WT, FXR$^{-/-}$, pL2-IL-1β and pL2-IL-1β/FXR$^{-/-}$ mice. Bodyweight was measured at day of death. Data are presented as mean with SEM.

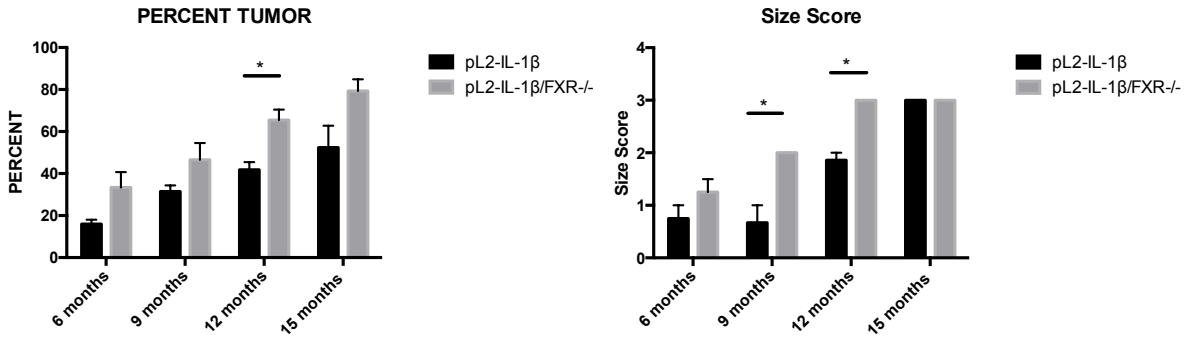

Figure 13: Overview of macroscopic evaluation of WT, FXR$^{-/-}$, pL2-IL-1β and pL2-IL-1β/FXR$^{-/-}$ mice stomach. Cardia tumors were counted and scored according to 9.4. Data are presented as mean with SEM.

.

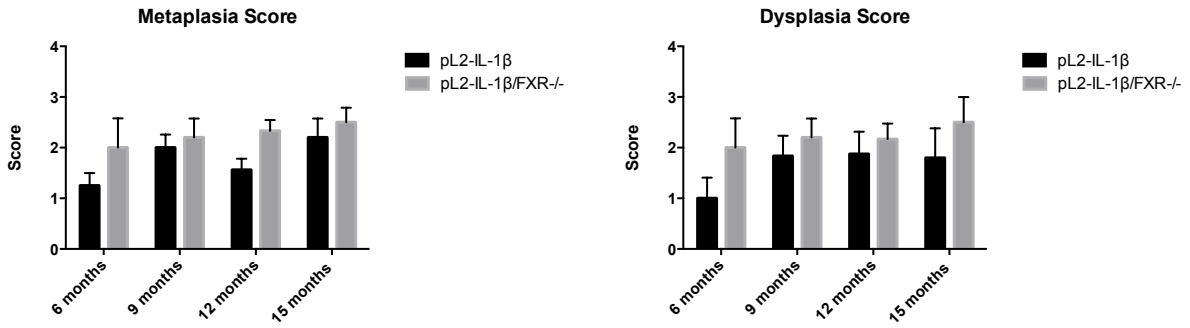

Figure 14: Metaplasia and dysplasia score of pL2-IL-1β and pL2-IL-1β/FXR$^{-/-}$ mice. H&E and PAS slides were used to calculate score. Data are evaluated by a specialized pathologist by specialized pathologic. Data are presented as mean with SEM.

10.3.2 Quantification of differentiation

PAS staining was used to visualize differentiated mucus producing cells in the cardia region. The control group (WT and FXR$^{-/-}$ mice) does not show PAS staining (Figure 15). pL2-IL-1β mice with an age of 6, 9 and 12 months showed about 50-60 % PAS+ cells. With 15 months the number of PAS+ cells slightly decreased. pL2-IL-1β mice with additional FXR$^{-/-}$ have only between 30-40 % stained PAS+ cells at all time points (Figure 15 and Figure 16).

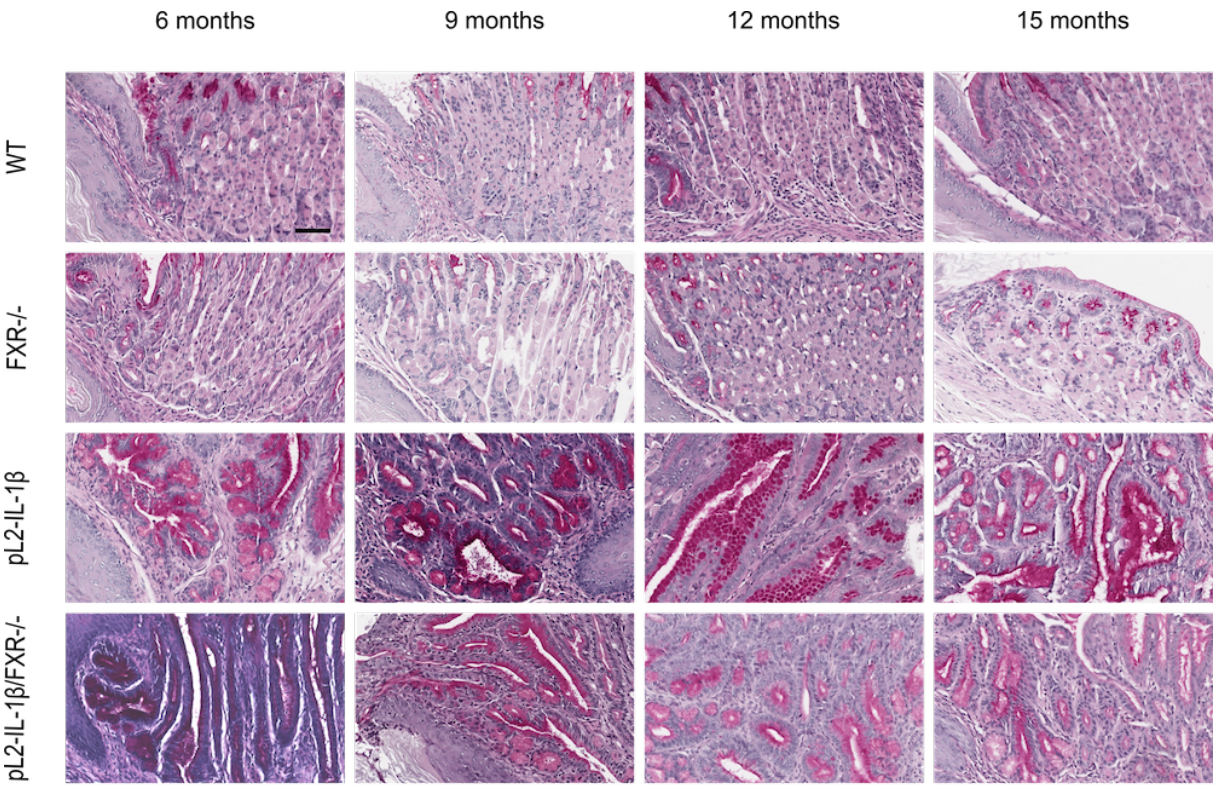

Figure 15: Representative PAS staining of WT, FXR$^{-/-}$, pL2-IL-1β and pL2-IL-1β/FXR$^{-/-}$ mice with 6, 9, 12 and 15 months. Scale bar: 100 µm

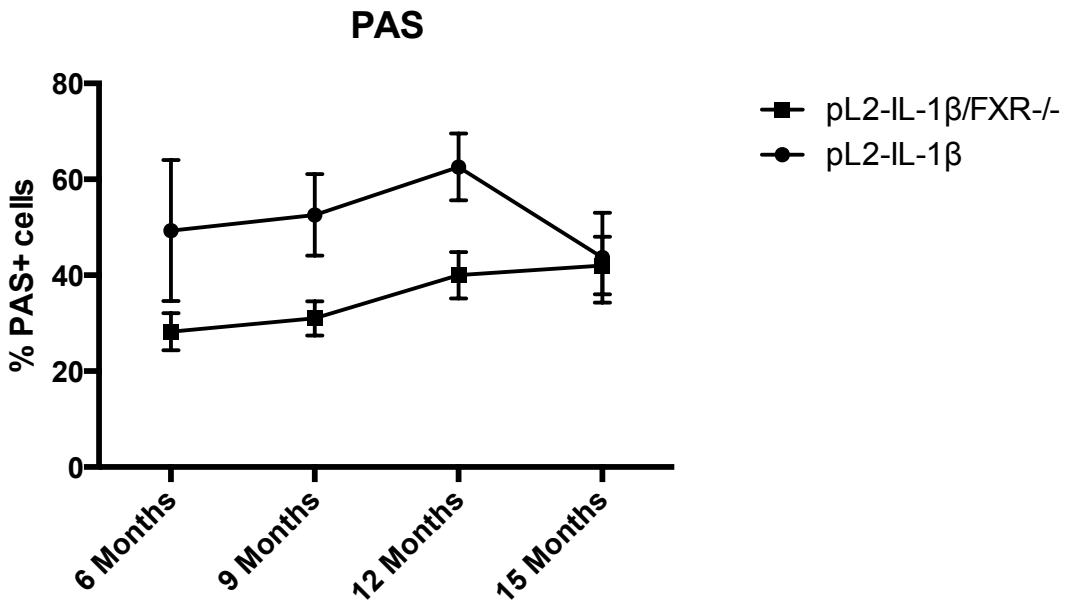

Figure 16: Quantification of PAS+ cells in pL2-IL-1β and pL2-IL-1β/FXR$^{-/-}$ mice. 5 fields of view of PAS+ cells were counted at age of 6, 9, 12 and 15 months. WT and FXR$^{-/-}$ mice don´t show PAS staining. At least 3 mice per group were used. Data are presented as mean with SEM

10.3.3 Quantification of proliferating

Ki67 staining was used as proliferation marker. The control group, WT and FXR$^{-/-}$ mice, have a similar amount of proliferating cells of lower then 10 (Figure 17). Their score is at all time points 0. BE mice (pL2-IL-1β and pL2-IL-1β/FXR$^{-/-}$ mice) showed raising amount of proliferating cells from 6 – 12 months. The highest score is at 12 months time point. The score decreases between 12 and 15 months. pL2-IL-1β/FXR$^{-/-}$ mice have a higher score until 9 months as mice with FXR WT allele. At 12 months time point, Mice with pL2-IL-1β have a higher score than pL2-IL-1β/FXR$^{-/-}$ mice with 15 months of age the score of pL2-IL-1β/FXR$^{-/-}$ mice is decreased (Figure 18).

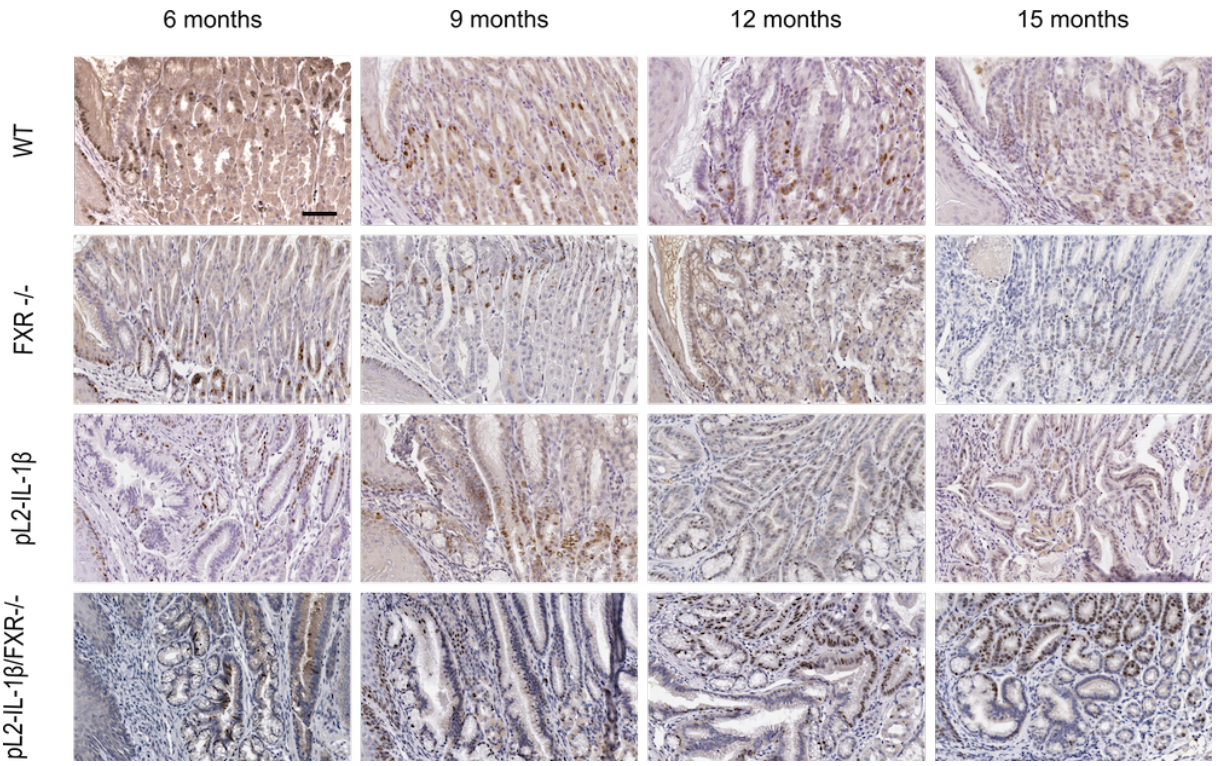

Figure 17: Representative Ki67 staining of WT, FXR$^{-/-}$, pL2-IL-1β and pL2-IL-1β/FXR$^{-/-}$ mice with 6, 9, 12 and 15 months. Scale bar: 100 µm

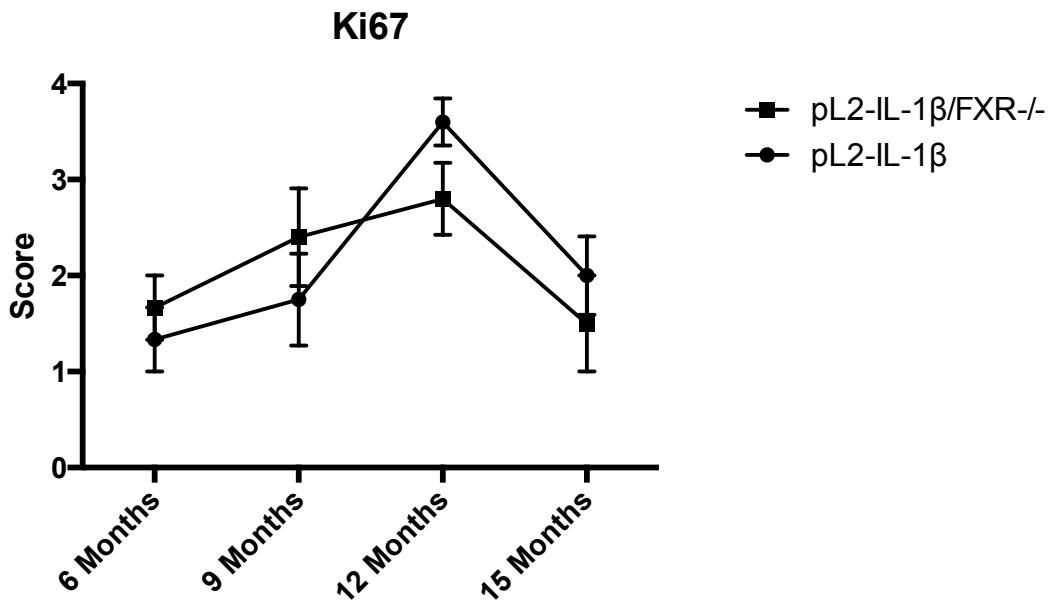

Figure 18: Quantification of Ki67+ cells in pL2-IL-1β and pL2-IL-1β/FXR$^{-/-}$. mice with an age of 6, 9, 12 and 15 months. Graph shows Ki67 score determined according Table 4. At least 3 mice per group were used. Data are presented as mean with SEM

10.3.4 Quantification of Dclk1+ cells

Doublecortin-like kinase 1 protein (DCLK1) is a gastrointestinal tuft cell marker. This cells proposed to be quiescent and tumor growth-sustaining stem cells. They are increased in carcinogenesis especially in BE. However, the role of these cells are poorly understood (Westphalen et al., 2014), (May et al., 2009), (May et al., 2008).

To analyze this cell population in the cardia Dclk1 was stained. The control mice display a weak expression of Dclk1+ cells of lower then 10 (Figure 19). Their score is at all time points 0. pL2-IL-1β and pL2-IL-1β/FXR$^{-/-}$. mice have similar scores until time point 12 months. At 15 months the number of Dclk1+ cells in pL2-IL-1β mice is significant higher than in pL2-IL-1β/FXR$^{-/-}$. mice ($p<0,0019$). The score of mice with pL2-IL-1β/FXR$^{-/-}$. decreased with 15 months (Figure 20).

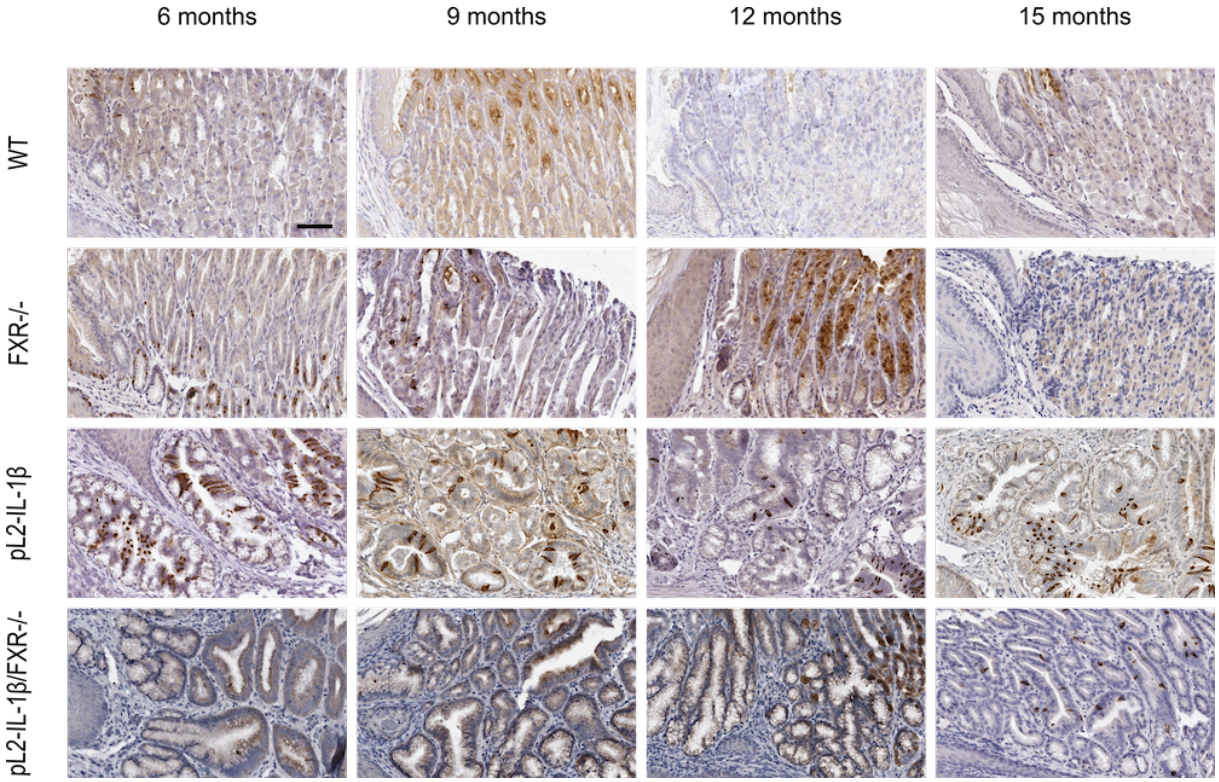

Figure 19: Representative Dclk1 staining of WT, FXR$^{-/-}$, pL2-IL-1β and pL2-IL-1β/FXR$^{-/-}$ mice with 6, 9, 12 and 15 months. Scale bar: 100 µM

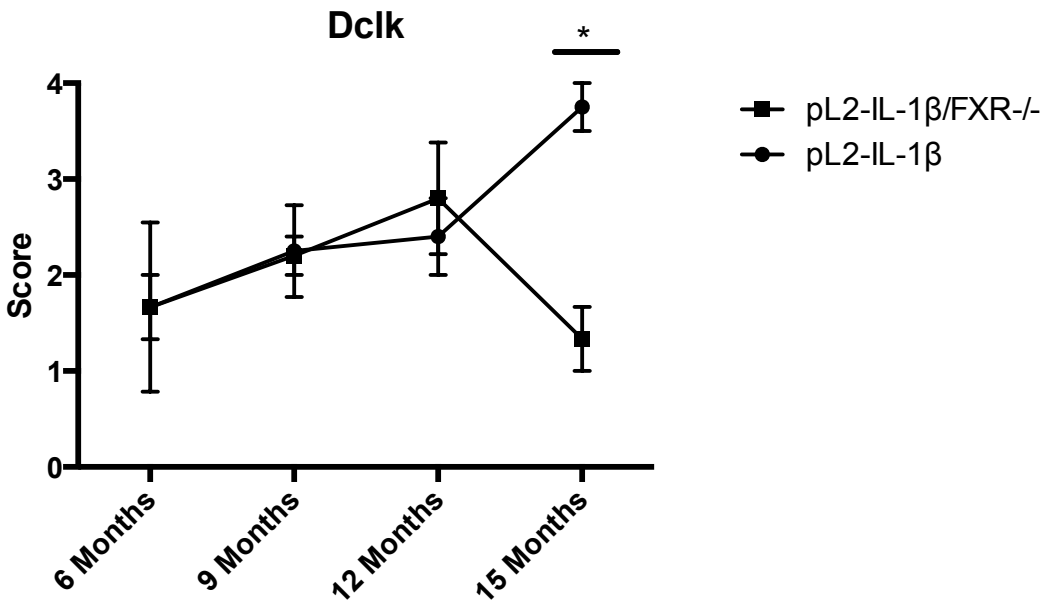

Figure 20: Quantification of Dclk1+ cells in pL2-IL-1β and pL2-IL-1β/FXR$^{-/-}$. mice with an age of 6, 9, 12 and 15 months. Graph shows Dclk1 score determined according Table 5. At least 3 mice per group were used. Data are presented as mean with SEM

10.3.5 DNA double strain brake

FXR knockout leads to DNA damage in cells occurs from bile acid accumulation in the cells. DNA damage is a major cause of cancer. To analyze DNA double strand breaks in the cardia gH2AX, a biomarker for DNA double-strand breaks, staining was performed. As the histon H2AX becomes phosphorylated, then called gamma-H2AX (Kuo & Yang, 2008), (C. Bernstein, R, Nfonsam, & Bernstei, 2013).

The control groups do not show any DNA breaks in the cardia region. pL2-IL-1β mice display a very weak staining of gammaH2AX staining. However, pL2-IL-1β with FXR knock out have clear positive stained cells (Figure 21). The number of gammaH2AX+ cells rises with the age from 1,25 % with 6 months to 14,50 % with 15 months. The comparisons 6 months vs. 15 months, 9 months vs. 15 months and 12 months vs. 15 months are significant (p<0,0001) (Figure 22).

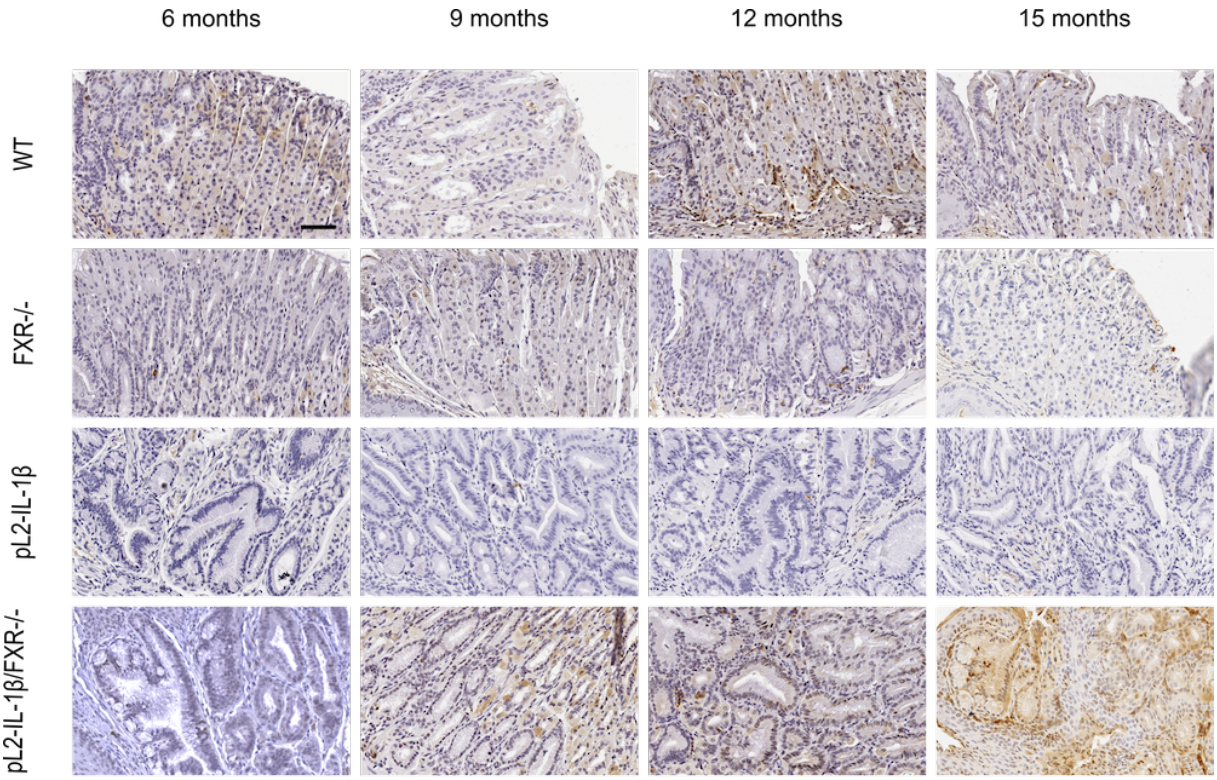

Figure 21: Representative gH2AX staining of WT, FXR$^{-/-}$, pL2-IL-1β and pL2-IL-1β/FXR$^{-/-}$ mice with 6, 9, 12 and 15 months. Scale bar: 100 µM

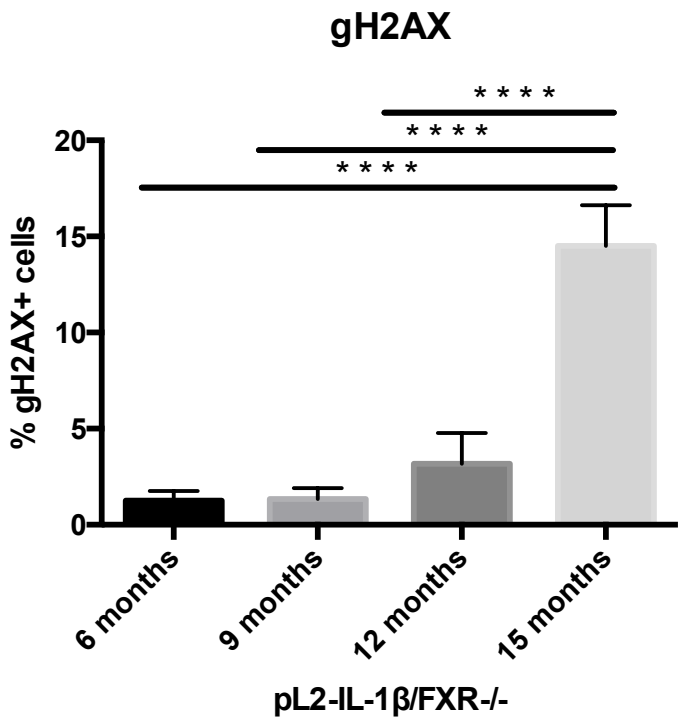

Figure 22: Quantification of gH2AX+ cells of pL2-IL-1β/FX$^{-/-}$ mice. Graphs show counted cells of the hole cardia region with an age of 6, 9, 12 and 15 months. At least 3 mice per group were used. Data are presented as mean with SEM

10.4 RNA analysis

10.4.1 Microarray

RNA from carida was isolated from 12 months WT, FXR$^{-/-}$, pL2-IL-1β and pL2-IL-1β/FXR$^{-/-}$ mice for microarray analysis. Selected FXR regulated genes (fold changed >1.5 or <0.67 pL2-IL-1β/FXR v.s pL2-IL-1β) are presented in Appendices 13.1. Selected pL2-IL-1β regulated genes (fold changed >1.5 or <0.67 pL2-IL-1β v.s WT) are presented in in Appendices 13.2. The gene function of the selected genes are presented in Appendices 13.3. Genes mark with asterisk are genes FXR upregulated but pL2-IL-1β downregulated or FXR downregulated but pL2-IL-1β upregulated. These genes may play potential roles that are responsible for FXR accelerating tumor size phenotype. Microarray results were further analyzed by gene enrichment analysis (GSEA) online (http://software.broadinstitute.org/gsea/index.jsp). Figure 23 shows the heat map representing the level of expression of many differential genes across pL2-IL-1β mice and pL2-IL-1β/FXR mice. The differentiated gene set of pL2-IL-1β v.s pL2-IL-1β/FXR$^{-/-}$ is further compared with the BIOCARTA data set. Appendices 13.5 shows the overview of pathways analysis. Appendices 2.2 shows the detail pL2-IL-1β regulated genes in top 14 pathways and detail pL2-IL-1β/FXR$^{-/-}$ regulated genes in top 12 pathways

The microarray data were used for several pathway analyses, including GESA like apoptosis, stress or the NFkB pathway. The results did unfortunately not show any significant differences between pL2-IL-1β and pL2-IL-1β/FXR$^{-/-}$ mice at age of 12 months. Our data show that mice with 12 months begin to adjust to the same phenotype. The analysis of tissue from 12 months old mice did not reveal significant alterations in the pathways of the mice groups. To get a deeper insight into the progression to BE and identify significant differences younger mice, for example with 6 months of age, should be used for microarray analyses

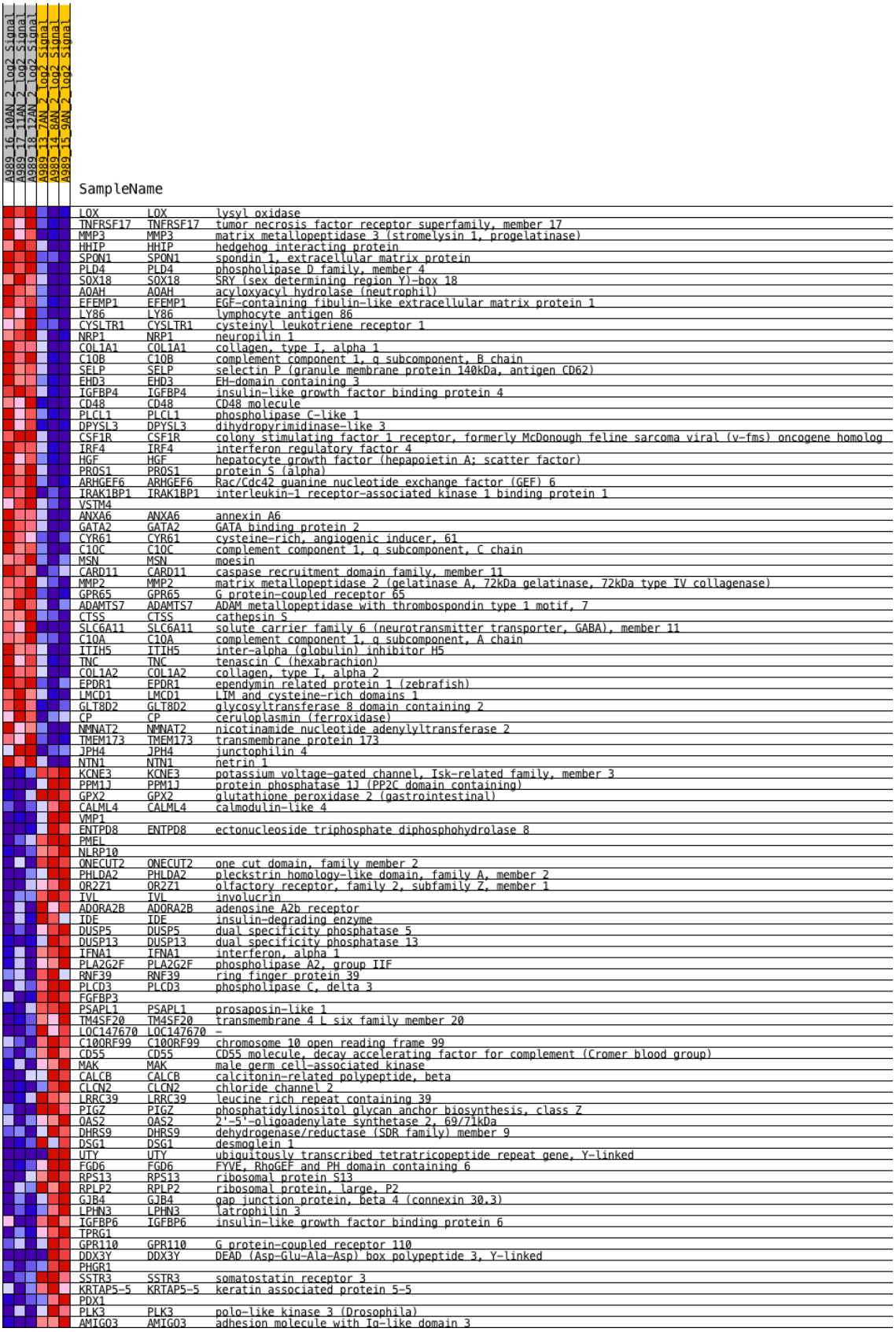

Figure 23: Heat map of microarray analysis. RNA from cardia was isolated from 12 months old WT, FXR$^{-/-}$, pL2-IL-1β and pL2-IL-1β/FXR$^{-/-}$ mice. Picture generated by Hsin-Yu Fang, member of our lab. (7AN pL2_12moths_mouse 1, 8AN pL2_12months_mouse 2, 9AN pL2_12months_mouse 3, 10AN pL2FXR_12months_mouse1, 11AN pL2FXR_12months_mouse2, 12AN pL2FXR_12mothns_mouse 3)

10.5 Cardia culture from pL2-IL-1β and pL2-IL-1β/FXR$^{-/-}$ mice

It was first able to culture carida organoids from 12 months old pL2-IL-1β mice at least for 12 months in vitro. pL2-IL-1β/FXR$^{-/-}$ mice with an age of 12 and 15 months were used to culture cells in vitro with the same conditions as cells from pL2-IL-1β mice. Organoids of pL2-IL-1β/FXR$^{-/-}$ mice did not survived more than 2 weeks in culture while organoids of pL2-IL-1β mice remain alive. The number of organoids from pL2-IL-1β mice were higher and larger then from pL2-IL-1β/FXR$^{-/-}$ mice (Figure 24 and Figure 25). Organoids were used to prepare FFPE slides and stained with HE, PAS, Ki67 and Dclk1 (Figure 25). PAS+ cells was only noticed in later passage. Ki67 staining showed no different. Dclk1 staining was never observed in carida culture system (data not sown).

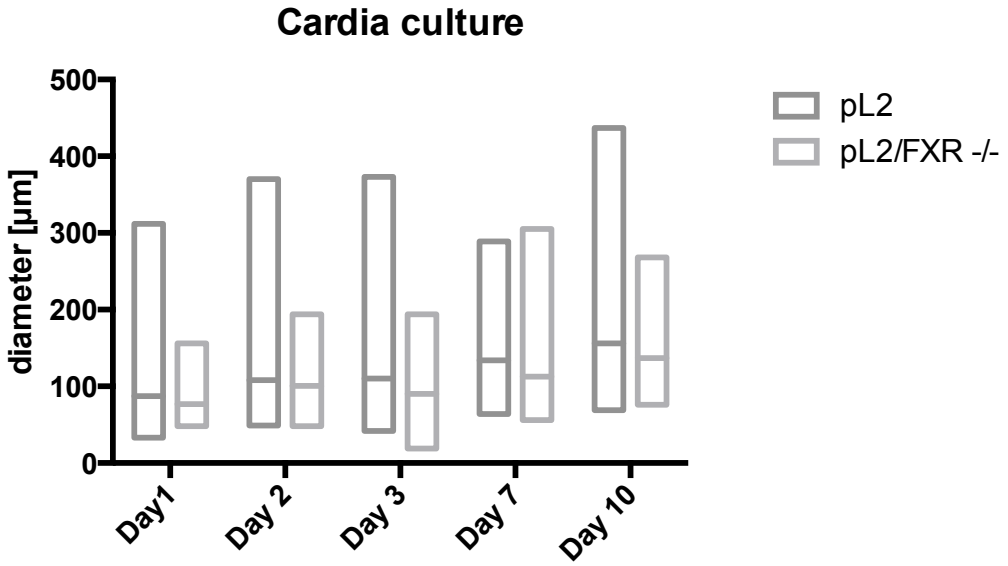

Figure 24: Organoids from pL2-IL-1β and pL2-IL-1β/FXR$^{-/-}$. mouse cardia. Diameter was measured at day 1, 2, 3, 7 and 10. pL2-IL-1β/FXR$^{-/-}$. organoids start dying after 1 week in culture.

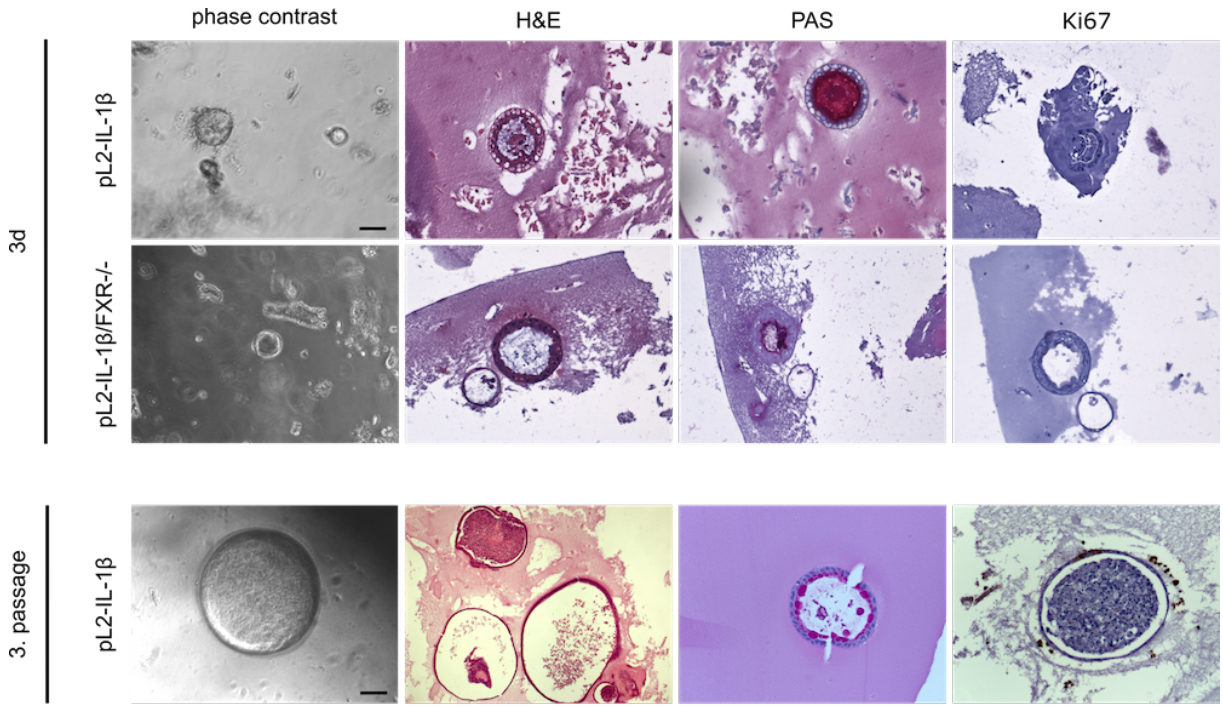

Figure 25: Overview of cardia culture. Cardia was used for FFPE slides to stain H&E, PAS and Ki67. pL2-IL-1β and pL2-IL-1β/FXR$^{-/-}$.carida after 3 day in culture. Only pL2-IL-1β carida survived longer than 2 weeks in culture. Scale bar: 100 µM

11 Discussion

Esophageal Adenocarcinoma is among the types of cancer with the most rapidly rising prevalence. Over the last decades the incident rates increased more than fivefold. EAC has an overall survival rate of less than 16 % (Everhart & Ruhl, 2009), (Corley et al., 2009). Thus, significant effort has been placed on early detection and surveillance of high-risk patients. It is agreed on that novel surveillance strategies are needed. Currently, the greatest risk factors for EAC are Barrett's Esophagus, a metaplastic change in the esophageal epithelium that results from gastroesophageal reflux disease, continued exposure of the BE epithelium to gastric contents (e.g. acid and bile) during neoplastic progression, and obesity with its associated metabolic effects including increased bile acid production. The pathogenesis of BE-associated EAC involves histologic progression of disease from benign metaplasia to high-grade dysplasia followed by invasive carcinoma. The risk of developing EAC in patients with metaplastic BE is 0.5% per year, while this risk increases to 6% per year in BE patients with HGD. Due to the increased risk of EAC in BE, current treatment guidelines focus on endoscopic surveillance for HGD at 1-3 year intervals and endoscopic ablation (cryo/radiofrequency ablation [RFA]) of dysplastic BE lesions or surgical esophagectomy to prevent progression to EAC.

Pharmacologic approaches that are well-tolerated have the potential for high impact in the management of non-dysplastic BE providing a non-invasive therapy to control progression of BE to BE-HGD and reducing the number of patients that develop EAC. This would be particularly attractive in the context of a prevention paradigm that targeted other metabolic disturbances underlying cancer risk in the older population and in the obese and sedentary population. Although the pathogenetic mechanisms of EAC are still unknown, one hypothesis suggests lifestyle and dietary changes like an increased fat intake as potentially relevant factors. Bile acids are known to serve as several different signal molecules in the body. They can influence lipid and glucose metabolism and also the immune system. Moreover, the bile acid profile is tightly regulated and altered in patients of higher age or in a diseased state (Joyce & Gahan, 2015). We previously treated pL2-IL-1β mice with DCA in drinking water and demonstrated an accelerated BE and EAC phenotype (Quante, Bhagat, Abrams, Marache, Good, et al., 2012b), indicating that bile acid would contribute to esophageal carcinogenesis.

Current chemoprevention research efforts for inhibiting BE progression to EAC have largely focused on the efficacy of non-steroidal anti-inflammatory drugs (NSAIDs) and high-dose proton pump inhibitors. These studies are focused on chronic exposure to gastric contents that promote inflammation and acidic damage. While there is strong evidence for inflammation in the carcinogenic process in the esophagus, neither of these strategies addresses bile acids as a critical co-factor. This is despite significant evidence that bile,

particularly secondary bile acids such as deoxcycholic acid, have substantial carcinogenic properties in the esophagus. Obesity leads to increases in the bile pool and bile secretion, and delay in gastric emptying, suggesting that obesity may contribute to BE progression by increasing or prolonging esophageal exposure to the gastric content that includes bile acids. In rodent surgical models of BE/EAC increased body weight and a diet rich in animal fat increased both the incidence of EAC and the amount of secondary bile acids present in the bile pool (data not shown). Thus, chemopreventive strategies targeted toward reducing/controlling the contribution of bile in BE progression to EAC would address a primary factor in disease initiation rather than the consequences of chronic inflammation (e.g., NSAIDs). A compound with both an anti-inflammatory and anti-bile acid effect in the esophagus would be an ideal modality for this disease.

An interesting candidate gene of the progression to BE and EAC is FXR. Farnesoid X Receptor is a nuclear hormone receptor involved in regulating bile acid, lipid, and glucose metabolism. FXR was classified originally as an orphan receptor until it was discovered that bile acids were the endogenous ligands for FXR. Functioning in adsorption of dietary lipids and lipid soluble vitamins, bile acids are synthesized from cholesterol in the liver and stored in the gall bladder. Studies in animal models and in humans have been integral in elucidating the metabolic functions of FXR. FXR knock-out mice revealed the role of FXR in regulating bile acid homeostasis. $FXR^{-/-}$ mice display an enlarged pool of bile acids, a result of increased synthesis of bile acids from cholesterol. Interestingly, FXR has been found to have considerable anti-tumor function. FXR knock-out mice develop spontaneous liver tumors, while loss of FXR accelerates tumorigenesis in both the Apc^{Min} transgenic and chemically-induced mouse models of intestinal cancer (Lian et al., 2011), (Prade et al., 2012), (Modica et al., 2008), (D. L. H. Smith, Keshavan, Avissar, Ahmed, & Zucker, 2010). Analyses of human intestinal tumors reveal reduced expression of FXR whereas re-expression of FXR in human colorectal cancer cells inhibits in vivo tumor growth in xenograft models. Similarly, treatment with FXR agonists reduced growth and metastasis of liver cancer cells in orthotopic xenograft models. Together, these findings suggest that FXR may act as a tumor suppressor, and the existence of FXR agonists has garnered interest in FXR as a potential therapeutic target for controlling cancer. FXR-knockout mice show alterations in the stomach and esophagus but no transformation to stomach cancer (Lian et al., 2011). Moreover, these mice show an increased proliferation in the esophagus, hyperkeratosis, esophagitis and enhanced carcinogenesis (Modica et al., 2010). Our assumption was that pL2-IL-1β/$FXR^{-/-}$ mice have an increased inflammation and effects of BAs with an accelerate procession to BE and EAC. In humans, the expression of FXR varies in normal tissue, BE or EAC. (De Gottardi et al., 2006) (Van de Winkel et al., 2011). We present here within the esophagus, FXR is present at low levels in the normal squamous tissue, highly expressed in metaplastic

BE, then reduced during progression to HGD. Collectively, these and other observations have led to numerous clinical efforts to develop FXR agonists to treat diseases related to metabolic syndrome and dysfunction of bile secretion and flow.

In this project we utilized a novel mouse model of BE and EAC the pL2-IL-1β model and crossed it to $FXR^{-/-}$ mice in order to analyze the protective effect of FXR or the impact of a loss of FXR on esophageal carcinogenesis. Our work should serve as a functional assessment of FXR expression during BE carcinogenesis as a basis for potential chemoprevention studies in the future. We demonstrated that during early carcinogenesis the lack of FXR leads to an accelerated esophageal phenotype with increased dydplasia and tumor growths indicating that FXR seems to have a protective function. Nevertheless during late carcinogenesis the accelerating effect of the loss of FXR could not be further observed.

Initially we planned to analyze the effect of bile acids in an accelerated phenotype in our BE mouse model of esophageal carcinogenesis, unfortunately pL2-IL-1β/$FXR^{-/-}$ mice which were given DCA-containing water did not tolerate this treatment well. BA-treated drinking water had a toxic effect on pL2-IL-1β/$FXR^{-/-}$ mice which first stopped drinking and began to dehydrate. These mice also were in a reduced general condition. Despite using a gentler rotating regime of one week BA-treated and one week normal drinking water the effect on the mice was too strong. Hence, we stopped adding BAs to drinking water. Previously diet supplemented with 1 % cholic acid in $FXR^{-/-}$ mice already resulted in a decrease in body weight and increased mortality within seven days (Sinal et al., 2000). Despite of less BA concentration and treated water instead of supplemented food the treatment of our mice showed similar toxicity. Therefore, a direct analysis of the effect of bile acids on the BE phenotype in $FXR^{-/-}$ mice could not be analyzed due to animal conditions.

As the in vivo treatment did not reveal any results we moved on to an in vitro system. The mechanisms underlying the epithelial-stromal interactions can be investigated using organotypic cell culture methods which mimicks an in-vivo situation of the esophagus. Previously the esophageal model helped to understand the progression of metaplasia in an in-vitro system (Pastuła et al., 2016). In our experiments bile acid showed no influence in wild type epithelium and had no effect on cells or tissue without any inflammation. We further couldn't find an accelerating effect on the growth and migration of tumor cells. Our immortalized human esophageal keratinocytes (hTERT cells) didn't survive the treatment with 50 or 200 µM DCA indicating that tumor cells were resistant to BA but keratinocytes were not. Secondary bile acids are known to cause DNA damage in in-vitro experiments (Huo et al., 2011). Subsequent treatment of the cells with a lower concentration of DCA or a less toxic primary bile acid like LCA could lead to extended survival of the cell to enable the investigation of carcinogenesis. Nevertheless, since we postulate that BE originates from cardia stem cells and not keratinocytes these experiments are in line with the hypothesis that

BA induce cell damage in the squamous esophagus but not on the developed tumor cells. Therefore, BAs may be important during early carcinogenesis and bile acid receptors such as FXR which is upregulated in early BE metaplasia might be one of the factors that play an important role here.

In order to test the function and role of FXR during esophageal carcinogenesis we crossed our BE and EAC mouse model with pL2-IL-1β mice to $FXR^{-/-}$ mice and aged these mice to analyze the effect of loss of FXR on carcinogenesis. The generated BE mouse model for esophageal inflammation metaplasia and dysplasia in combination with the $FXR^{-/-}$ mice demonstrated that the bile receptor acts as a protective factor against the progression of Barrett`s Esophagus and the development to EAC. Compared to FXR expressing mice those with $FXR^{-/-}$ had a stronger and more local inflammation metaplasia and dysplasia. The inflammation occurred at younger age and the switch to metaplasia also occurred earlier. However, at age of 12 months the phenotype of the mice got similar and was almost the same at 15 months of age. For the first nine months pL2-IL-1β/$FXR^{-/-}$ mice had significantly higher proliferation rate as pL2-IL-1β mice with wild type FXR. This correlated with increased tumor growth, metaplasia and dysplasia scores. They also showed less differentiation of mucus producing cells and the same score for Dclk1 as pL2-IL-1β mice. Less cell differentiation was associated with reduced dysplasia formation and especially with increased goblet cell differentiation. These data correlate with data from patients with high goblet cell differentiations being associated with a reduced risk of progression to dysplasia and cancer. (Quante, Bhagat, Abrams, Marache, Good, et al., 2012b), (Quante, Abrams, Lee, & Wang, 2012a). At the age of 12 months, pL2-IL-1β mice without FXR had decreasing proliferation and Dclk1 score. Loss of FXR leads to an increase in proliferation in the cardia at early age in our mouse model. This resulted in a reduced differentiation and reduced mucus producing cells. Moreover, with the increasing proliferative and malignant phenotype we observed a loss of Dclk1+ cells in the cardia at later ages. This again correlated with increased dysplasia scores and more tumors.

Dclk1 was proposed as a quiescent and tumor growth-sustaining stem cell marker (Westphalen et al., 2014), (May et al., 2009), (May et al., 2008). Nakanishi and colleagues demonstrated that Dclk1+ cells did not act as functional stem cells under pathologic conditions but they display cancer stem cell properties in established tumors. (Nakanishi et al., 2012). We and others correlated Dclk1 cell number with pre-malignant development whereas Dclk1 cells decrease in tumor tissue. The decreasing number of Dclk1 cells would therefore point to a tumor development as suggested in other cancers such as colon or pancreatic cancer. From the pL-IL-1b mouse model it is known that with decreased number of Dclk1 cells Lgr5 cells are increasing, which have been shown to give rise to metaplasia and dysplasia (Quante, Bhagat, Abrams, Marache, Good, et al., 2012b). An explanation for

the decreasing number of Dclk1 cells in late carcinogenesis could thus be that a different stem cell population such as Lgr5 is upregulated instead. This would explain the earlier decrease of Dclk1 in pL2-IL-1β/FXR$^{-/-}$ mice compared to pL2-IL-1β mice. Therefore, possibly, FXR has only a beneficial effect on the progression to cancer during early stages where it protects against DNA damage but becomes less conducive in later stages.

We further established a 3D cell culture system of BE like cells of the cardia (Pastuła et al., 2016). Organoids from cells of the small intestine or stomach have been established in previous studies. (Sato et al., 2009) (Stange et al., 2013) Here it was possible for the first time to culture cardia tissue from a 12 months pL2-IL-1β mouse with BE and dysplasia for at least 12 months in this 3D system, whereas it was not possible to culture tissue from a pL2-IL-1β/FXR$^{-/-}$ mice under the same conditions. We also tried to culture BE tissue from different pL2-IL-1β/FXR$^{-/-}$ mice of different ages (9, 12 or 15 months) but the crypts died after one week in culture indicating that the knockout correlated with reduced ability of self renewal or stem cell expansion. FXR$^{-/-}$ mice show a disrupted glucose and lipid homeostasis, and a higher bile concentration in the body as WT mice (Modica et al., 2010). Since bile acids are known to cause DNA breaks (Huo et al., 2011), we hypothesized that this leads to reduced self renewal capacities in vitro. In a culture medium enriched with more nutrients and supplements might keep the cells alive for a longer time. The different data from the in vitro and in vivo data suggest that disrupted FXR expression in BE tissue in vivo might result in increased proliferation of stem and progenitor cells which likely do not express differentiation marker such as FXR. Only late in the process of carcinogenesis we observed decreasing proliferation and less tumor growth and therefore a similar situation as observed in vitro. In vitro cell survival was decreased in all FXR$^{-/-}$ cell populations and therefore the organoids could not grow lacking epithelial niche cells as required for stem cell proliferation in vitro. However, further experiments are necessary to precisely identify the reasons for the failure of culturing pL2-IL-1β/FXR$^{-/-}$ cardia tissue.

As discussed, one possible reason for the accelerated development of cancer in FXR$^{-/-}$ mice could be the emergence of DNA double strand breaks (DSBs), that are known to support cancer development (Khanna & Jackson, 2001) (C. Bernstein et al., 2013). DNA breaks activate the apoptosis pathway which results in an increase of proliferation of tumor initiating stem cells (Lgr5). Increased proliferation correlates with reduced differentiation rates of tissues and promotes carcinogenesis (Khanna & Jackson, 2001). Our pL2-IL-1β/FXR$^{-/-}$ mice showed increased proliferation and less differentiation. An evidence for DSBs is the occurrence of gamma-H2AX+, that originates from the phosphorylation of H2AX on serine 139 (Turinetto & Giachino, 2015). Gamma-H2AX+cells were only found in pL2-IL-1β/FXR$^{-/-}$ mice. The number of positive cells rose with the age of the mice. With an age of 15 months about 16 % of cells in the cardia had DSBs. DNA breaks could lead to earlier cancer initiation

in FXR knockout mice but cancer progression was only supported at early age. At an age of 12 moths the cancer did no longer benefit from DSBs. Finally, with an age of 15 months the number of DSBs was very high. Consequently, we hypothesize that the cancer promoting effect of the DSBs was turned to the opposite and the difference between the phenotypes of pL2-IL-1β and pL2-IL-1β/FXR$^{-/-}$ mice was completely attenuated. The DNA strand break repair is important mechanism in tissue homogeneity after DSBs in nomal tissue as well as in cancer tissue. With our data we hypothesize that potentially repair mechanism might be lost during accelerated development of dysplasia in our model resulting in even higher high number of DNA breaks with lead to the loss of the promoting effect of DSBs. Inhibition of DNA strand break repair mechanisms are already tested in clinical cancer therapies trails inducing a cancer cell crisis. The repair mechanisms are directly inhibited, during cell cycle check points or with specific small molecule inhibitors for novel oncology treatments (O'Connor, Martin, & Smith, 2007).

In this context, one possible mechanism could be that in the early stages of BE development, signal transducers and activators of transcriptions (STATs) upregulate the expression of FXR, maybe as a protective defense against irritation from bile in order to maintain and protect the differentiation state. FXR expression might inhibit inflammation and tissue damage and therefore attract immune system and recruits cardia stem cells towards to the lower esophagus. In the tumor-stage the pro-differentiation and anti-inflammatory properties are not longer of benefit for the rapid growth of the tumor anymore. Therefore, FXR expression is silenced through unknown mechanism such as methylation. These mechanisms need to be further analyzed, but our model demonstrates that a loss of FXR during early carcinogenesis accelerates the phenotype in the pL2-IL-1β mouse model of BE and EAC.

Taken together our data suggest a protective role of FXR in the Barrett´s Esophagus acting against the progression to cancer. The nuclear expression level of FXR is highest in BE and almost lost in cancer. Therefore, expression levels of FXR should be tested for a use as biomarkers for the progression from BE and EAC and to support the diagnosis of patients with BE or EAC. Additionally, FXR agonists could be used as a potential target for new therapeutic approaches. Of particular interest is Obeticholic acid (OCA), a synthetic derivative of CDCA, a natural bile acid with the strongest affinity for FXR. OCA is currently in long-term Phase III trials for primary biliary cirrhosis and a NIH sponsored Phase II trial was stopped early due to OCA being highly efficacious in treating nonalcoholic steatohepatitis /fatty liver disease. However, despite our data of FXR's role in esophageal tumorigenesis, we have not yet performed studies to assess the chemopreventive potential of FXR agonists, such as OCA for BE. In future studies the interesting and potentially critical aspect of FXR activation in the BE will be analyzed, setting is the role of FXR as a modulator of immune

health in the intestinal tract and activity to repress NF-κB response elements in the IL-1 promoter and resultant suppression of pro-inflammatory cytokines. Substantiation of dual effects of OCA on bile acid and inflammation in BE would produce an ideal therapeutic for preventing BE to EAC etiopathogenesis based on our current understanding of the mechanism of disease. Development of a safe and well-tolerated drug therapy for BE would have substantial impact on the management of BE patients. A similar stabilization (i.e. reduced proliferation, reversal of neoplastic phenotype) of the dysplastic BE lesion as shown by genetic knock out in our work, with a chemopreventive agent could easily be envisioned as a "first-line" therapy, reserving endoscopic treatment for cases with continued progression, or in combination with endoscopic therapies prove useful in reducing or preventing subsequent recurrences

12 Literature

Abdelkarim, M., Caron, S., Duhem, C., Prawitt, J., Dumont, J., Lucas, A., et al. (2010). The Farnesoid X Receptor Regulates Adipocyte Differentiation and Function by Promoting Peroxisome Proliferator-activated Receptor- and Interfering with the Wnt/ -Catenin Pathways. *Journal of Biological Chemistry*, *285*(47), 36759–36767. http://doi.org/10.1074/jbc.M110.166231

Araya, Z., & Wikvall, K. (1999). 6alpha-hydroxylation of taurochenodeoxycholic acid and lithocholic acid by CYP3A4 in human liver microsomes. *Biochimica Et Biophysica Acta*, *1438*(1), 47–54.

Armstrong, D., Marshall, J. K., Chiba, N., Enns, R., Fallone, C. A., Fass, R., et al. (2005). Canadian Consensus Conference on the management of gastroesophageal reflux disease in adults - update 2004. (Vol. 19, pp. 15–35). Presented at the Canadian journal of gastroenterology = Journal canadien de gastroenterologie.

Baptissart, M., Vega, A., Maqdasy, S., Caira, F., Baron, S., Lobaccaro, J.-M. A., & Volle, D. H. (2013). Bile acids: From digestion to cancers. *Biochimie*, *95*(3), 504–517. http://doi.org/10.1016/j.biochi.2012.06.022

Barbera, M., & Fitzgerald, R. C. (2010). Cellular origin of Barrett's metaplasia and oesophageal stem cells. *Biochemical Society Transactions*, *38*(2), 370. http://doi.org/10.1042/BST0380370

Barone, M., Francavilla, A., Polimeno, L., Ierardi, E., Romanelli, D., Berloco, P., et al. (1996). Modulation of rat hepatocyte proliferation by bile salts: in vitro and in vivo studies. *Hepatology*, *23*(5), 1159–1166. http://doi.org/10.1053/jhep.1996.v23.pm0008621149

Bernstein, C., R, A., Nfonsam, V., & Bernstei, H. (2013). DNA Damage, DNA Repair and Cancer. InTech. http://doi.org/10.5772/53919

Bernstein, H., Payne, C. M., Bernstein, C., Schneider, J., Beard, S. E., & Crowley, C. L. (1999). Activation of the promoters of genes associated with DNA damage, oxidative stress, ER stress and protein malfolding by the bile salt, deoxycholate. *Toxicology Letters*, *108*(1), 37–46.

Bhat, S., Coleman, H. G., Yousef, F., Johnston, B. T., McManus, D. T., Gavin, A. T., & Murray, L. J. (2011). Risk of Malignant Progression in Barrett's Esophagus Patients: Results from a Large Population-Based Study. *JNCI Journal of the National Cancer Institute*, *103*(13), 1049–1057. http://doi.org/10.1093/jnci/djr203

Bodin, K., Lindbom, U., & Diczfalusy, U. (2005). Novel pathways of bile acid metabolism involving CYP3A4. *Biochimica Et Biophysica Acta*, *1687*(1-3), 84–93. http://doi.org/10.1016/j.bbalip.2004.11.003

Boufker, H. I., Lagneaux, L., Fayyad-Kazan, H., Badran, B., Najar, M., Wiedig, M., et al. (2011). Role of farnesoid X receptor (FXR) in the process of differentiation of bone marrow stromal cells into osteoblasts. *Bone*, *49*(6), 1219–1231. http://doi.org/10.1016/j.bone.2011.08.013

Burke, Z. D., & Tosh, D. (2012). Barrett's metaplasia as a paradigm for understanding the development of cancer. *Current Opinion in Genetics & Development*, *22*(5), 494–499. http://doi.org/10.1016/j.gde.2012.08.001

Capello, A., Moons, L. M. G., Van de Winkel, A., Siersema, P. D., van Dekken, H., Kuipers, E. J., & Kusters, J. G. (2008). Bile Acid-Stimulated Expression of the Farnesoid X Receptor Enhances the Immune Response in Barrett Esophagus. *The American Journal of Gastroenterology*, *103*(6), 1510–1516. http://doi.org/10.1111/j.1572-0241.2008.01908.x

Carlson, N., Lechago, J., Richter, J., Sampliner, R. E., Peterson, L., Santella, R. M., et al. (2002). Acid suppression therapy may not alter malignant progression in Barrett's metaplasia showing p53 protein accumulation. *The American Journal of Gastroenterology*, *97*(6), 1340–1345. http://doi.org/10.1016/S0002-9270(02)04126-6

Chen, X., Ding, Y. W., Yang, G. Y., Bondoc, F., Lee, M. J., & Yang, C. S. (2000). Oxidative damage in an esophageal adenocarcinoma model with rats. *Carcinogenesis*, *21*(2), 257–263.

Chiang, J. Y. L. (2002). Bile Acid Regulation of Gene Expression: Roles of Nuclear Hormone Receptors. *Endocrine Reviews*, *23*(4), 443–463. http://doi.org/10.1210/er.2000-0035

Coenraad, M., Masclee, A. A., Straathof, J. W., Ganesh, S., Griffioen, G., & Lamers, C. B. (1998). Is Barrett's esophagus characterized by more pronounced acid reflux than severe esophagitis? *The American Journal of Gastroenterology*, *93*(7), 1068–1072. http://doi.org/10.1111/j.1572-0241.1998.00331.x

Corley, D. A., Kubo, A., Levin, T. R., Block, G., Habel, L., Rumore, G., et al. (2009). Race, ethnicity, sex and temporal differences in Barrett's oesophagus diagnosis: a large community-based study, 1994-2006. *Gut*, *58*(2), 182–188. http://doi.org/10.1136/gut.2008.163360

Corley, D. A., Kubo, A., Levin, T. R., Block, G., Habel, L., Zhao, W., et al. (2007). Abdominal Obesity and Body Mass Index as Risk Factors for Barrett's Esophagus. *Gastroenterology*, *133*(1), 34–41. http://doi.org/10.1053/j.gastro.2007.04.046

Dawson, P. A., Haywood, J., Craddock, A. L., Wilson, M., Tietjen, M., Kluckman, K., et al. (2003). Targeted deletion of the ileal bile acid transporter eliminates enterohepatic cycling of bile acids in mice. *The Journal of Biological Chemistry*, *278*(36), 33920–33927. http://doi.org/10.1074/jbc.M306370200

Dawson, P. A., Hubbert, M., Haywood, J., Craddock, A. L., Zerangue, N., Christian, W. V., & Ballatori, N. (2005). The heteromeric organic solute transporter alpha-beta, Ostalpha-Ostbeta, is an ileal basolateral bile acid transporter. *The Journal of Biological Chemistry*, *280*(8), 6960–6968. http://doi.org/10.1074/jbc.M412752200

De Gottardi, A., Dumonceau, J.-M., Bruttin, F., Vonlaufen, A., Morard, I., Spahr, L., et al. (2006). Expression of the bile acid receptor FXR in Barrett's esophagus and enhancement of apoptosis by guggulsterone in vitro. *Molecular Cancer*, *5*, 48. http://doi.org/10.1186/1476-4598-5-48

de Vries, D. R., van Herwaarden, M. A., Smout, A. J. P. M., & Samsom, M. (2008). Gastroesophageal Pressure Gradients in Gastroesophageal Reflux Disease: Relations With Hiatal Hernia, Body Mass Index, and Esophageal Acid Exposure. *The American Journal of Gastroenterology*, *103*(6), 1349–1354. http://doi.org/10.1111/j.1572-0241.2008.01909.x

DeVault, K. R., & Castell, D. O. (2005). Updated Guidelines for the Diagnosis and Treatment of Gastroesophageal Reflux Disease. *The American Journal of Gastroenterology*, *100*(1), 190–200. http://doi.org/10.1111/j.1572-0241.2005.41217.x

Dvorak, K., Fass, R., Dekel, R., Payne, C. M., Chavarria, M., Dvorakova, B., et al. (2006). Esophageal acid exposure at pH < or = 2 is more common in Barrett's esophagus patients and is associated with oxidative stress. *Diseases of the Esophagus*, *19*(5), 366–372. http://doi.org/10.1111/j.1442-2050.2006.00596.x

Everhart, J. E., & Ruhl, C. E. (2009). Mini-Reviews and Perspectives. *Ygast*, *136*(2), 376–386. http://doi.org/10.1053/j.gastro.2008.12.015

Falany, C. N., Johnson, M. R., Barnes, S., & Diasio, R. B. (1994). Glycine and taurine conjugation of bile acids by a single enzyme. Molecular cloning and expression of human liver bile acid CoA:amino acid N-acyltransferase. *The Journal of Biological Chemistry*, *269*(30), 19375–19379.

Fein, M., Peters, J. H., Chandrasoma, P., Ireland, A. P., Oberg, S., Ritter, M. P., et al. (1998). Duodenoesophageal reflux induces esophageal adenocarcinoma without exogenous carcinogen. *Journal of Gastrointestinal Surgery*, *2*(3), 260–268.

Ferguson, H. R., Wild, C. P., Anderson, L. A., Murphy, S. J., Johnston, B. T., Murray, L. J., et al. (2008). Cyclooxygenase-2 and Inducible Nitric Oxide Synthase Gene Polymorphisms and Risk of Reflux Esophagitis, Barrett's Esophagus, and Esophageal Adenocarcinoma. *Cancer Epidemiology Biomarkers & Prevention*, *17*(3), 727–731. http://doi.org/10.1158/1055-9965.EPI-07-2570

Finks, J. F., Wei, Y., & Birkmeyer, J. D. (2006). The rise and fall of antireflux surgery in the United States. *Surgical Endoscopy*, *20*(11), 1698–1701. http://doi.org/10.1007/s00464-006-0042-3

Fiorucci, S., Mencarelli, A., Cipriani, S., Renga, B., Palladino, G., Santucci, L., & Distrutti, E. (2011). Activation of the farnesoid-X receptor protects against gastrointestinal injury caused by non-steroidal anti-inflammatory drugs in mice. *British Journal of Pharmacology*, *164*(8), 1929–1938. http://doi.org/10.1111/j.1476-5381.2011.01481.x

Fitzgerald, R. C., Abdalla, S., Onwuegbusi, B. A., Sirieix, P., Saeed, I. T., Burnham, W. R., & Farthing, M. (2002). Inflammatory gradient in Barrett's oesophagus: implications for disease complications. *Gut*, *51*(3), 316–322.

Gadaleta, R. M., van Erpecum, K. J., Oldenburg, B., Willemsen, E. C. L., Renooij, W., Murzilli, S., et al. (2011). Farnesoid X receptor activation inhibits inflammation and preserves the intestinal barrier in inflammatory bowel disease. *Gut*, *60*(4), 463–472. http://doi.org/10.1136/gut.2010.212159

Gong, Y. Z., Everett, E. T., Schwartz, D. A., Norris, J. S., & Wilson, F. A. (1994). Molecular cloning, tissue distribution, and expression of a 14-kDa bile acid-binding protein from rat ileal cytosol. *Proceedings of the National Academy of Sciences of the United States of America*, *91*(11), 4741–4745.

Goodwin, B., Jones, S. A., Price, R. R., Watson, M. A., McKee, D. D., Moore, L. B., et al. (2000). A regulatory cascade of the nuclear receptors FXR, SHP-1, and LRH-1 represses bile acid biosynthesis. *Molecular Cell*, *6*(3), 517–526.

Grivennikov, S., & Karin, M. (2008). Autocrine IL-6 signaling: a key event in tumorigenesis? *Cancer Cell*, *13*(1), 7–9.

Guan, B., Li, H., Yang, Z., Hoque, A., & Xu, X. (2012). Inhibition of farnesoid X receptor controls esophageal cancer cell growth in vitro and in nude mouse xenografts. *Cancer*, n/a–n/a. http://doi.org/10.1002/cncr.27910

Hanahan, D., & Weinberg, R. A. (2000). The hallmarks of cancer. *Cell*, *100*(1), 57–70.

Hanahan, D., & Weinberg, R. A. (2011). Hallmarks of Cancer: The Next Generation. *Cell*, *144*(5), 646–674. http://doi.org/10.1016/j.cell.2011.02.013

Henning, S. J. (1986). Cambridge Journals Online - Proceedings of the Nutrition Society - Abstract - Development of the gastrointestinal tract. Presented at the Proceedings of the Nutrition Society.

Huber, R. M., Murphy, K., Miao, B., Link, J. R., Cunningham, M. R., Rupar, M. J., et al. (2002). Generation of multiple farnesoid-X-receptor isoforms through the use of alternative promoters. *Gene*, *290*(1-2), 35–43.

Huo, X., Juergens, S., Zhang, X., Rezaei, D., Yu, C., Strauch, E. D., et al. (2011). Deoxycholic acid causes DNA damage while inducing apoptotic resistance through NF-B activation in benign Barrett's epithelial cells. *AJP: Gastrointestinal and Liver Physiology*, *301*(2), G278–G286. http://doi.org/10.1152/ajpgi.00092.2011

Hvid-Jensen, F., Pedersen, L., Drewes, A. M., Sørensen, H. T., & Funch-Jensen, P. (2011). Incidence of adenocarcinoma among patients with Barrett's esophagus. *The New England Journal of Medicine*, *365*(15), 1375–1383. http://doi.org/10.1056/NEJMoa1103042

Inagaki, T., Moschetta, A., Lee, Y.-K., Peng, L., Zhao, G., Downes, M., et al. (2006). Regulation of antibacterial defense in the small intestine by the nuclear bile acid receptor. *Proceedings of the National Academy of Sciences of the United States of America*, *103*(10), 3920–3925. http://doi.org/10.1073/pnas.0509592103

Increased Frequency of Transient Lower Esophageal Sphincter Relaxation Induced by Gastric Distention in Reflux Patients With Hiatal Hernia. (2015). Increased Frequency of Transient Lower Esophageal Sphincter Relaxation Induced by Gastric Distention in Reflux Patients With Hiatal Hernia, 1–8. http://doi.org/10.1053/gg.2000.5950

Joyce, S. A., & Gahan, C. G. M. (2015). Bile Acid Modifications at the Microbe-Host Interface: Potential for Nutraceutical and Pharmaceutical Interventions in Host Health. *Annual Review of Food Science and Technology*, *7*(1), annurev–food–041715–033159. http://doi.org/10.1146/annurev-food-041715-033159

Kahrilas, P. J. (2008). Clinical practice. Gastroesophageal reflux disease. *The New England Journal of Medicine*, *359*(16), 1700–1707. http://doi.org/10.1056/NEJMcp0804684

Kahrilas, P. J., Shaheen, N. J., & Vaezi, M. F. (2008a). American Gastroenterological Association Institute Technical Review on the Management of Gastroesophageal Reflux Disease. *Gastroenterology*, *135*(4), 1392–1413.e5. http://doi.org/10.1053/j.gastro.2008.08.044

Kahrilas, P. J., Shaheen, N. J., & Vaezi, M. F. (2008b). American Gastroenterological Association Medical Position Statement on the Management of Gastroesophageal Reflux Disease. *Gastroenterology*, *135*(4), 1383–1391.e5. http://doi.org/10.1053/j.gastro.2008.08.045

Kalabis, J., Wong, G. S., Vega, M. E., Natsuizaka, M., Robertson, E. S., Herlyn, M., et al. (2012). Isolation and characterization of mouse and human esophageal epithelial cells in 3D organotypic culture. *Nature Protocols*, *7*(2), 235–246. http://doi.org/10.1038/nprot.2011.437

Karin, M., Lawrence, T., & Nizet, V. (2006). Innate immunity gone awry: linking microbial infections to chronic inflammation and cancer. *Cell*, *124*(4), 823–835. http://doi.org/10.1016/j.cell.2006.02.016

Khanna, K. K., & Jackson, S. P. (2001). DNA double-strand breaks: signaling, repair and the cancer connection. *Nature Genetics*, *27*(3), 247–254. http://doi.org/10.1038/85798

Kim, I., Ahn, S. H., Inagaki, T., Choi, M., Ito, S., Guo, G. L., et al. (2007a). Differential regulation of bile acid homeostasis by the farnesoid X receptor in liver and intestine. *The Journal of Lipid Research*, *48*(12), 2664–2672. http://doi.org/10.1194/jlr.M700330-JLR200

Kim, I., Morimura, K., Shah, Y., Yang, Q., Ward, J. M., & Gonzalez, F. J. (2007b). Spontaneous hepatocarcinogenesis in farnesoid X receptor-null mice. *Carcinogenesis*, *28*(5), 940–946. http://doi.org/10.1093/carcin/bgl249

Kuo, L. J., & Yang, L.-X. (2008). Gamma-H2AX - a novel biomarker for DNA double-strand breaks. *In Vivo (Athens, Greece)*, *22*(3), 305–309.

Lechner, S., Müller-Ladner, U., Schlottmann, K., Jung, B., McClelland, M., Rüschoff, J., et al. (2002). Bile acids mimic oxidative stress induced upregulation of thioredoxin reductase in colon cancer cell lines. *Carcinogenesis*, *23*(8), 1281–1288.

Lee, Y.-K., & Moore, D. D. (2008). Liver receptor homolog-1, an emerging metabolic modulator. *Frontiers in Bioscience : a Journal and Virtual Library*, *13*, 5950–5958.

Leedham, S. J., Preston, S. L., McDonald, S. A. C., Elia, G., Bhandari, P., Poller, D., et al. (2008). Individual crypt genetic heterogeneity and the origin of metaplastic glandular epithelium in human Barrett's oesophagus. *Gut*, *57*(8), 1041–1048. http://doi.org/10.1136/gut.2007.143339

Li, F., Jiang, C., Krausz, K. W., Li, Y., Albert, I., Hao, H., et al. (2013). Microbiome remodelling leads to inhibitionof intestinal farnesoid X receptor signallingand decreased obesity. *Nature Communications*, *4*, 1–10. http://doi.org/10.1038/ncomms3384

Lian, F., Xing, X., Yuan, G., Schäfer, C., Rauser, S., Walch, A., et al. (2011). Farnesoid X receptor protects human and murine gastric epithelial cells against inflammation-induced damage. *Biochemical Journal*, *438*(2), 315–323. http://doi.org/10.1042/BJ20102096

Love, M. W., & Dawson, P. A. (1998). New insights into bile acid transport. *Current Opinion in Lipidology*, *9*(3), 225–229.

Lu, T. T., Makishima, M., Repa, J. J., Schoonjans, K., Kerr, T. A., Auwerx, J., & Mangelsdorf, D. J. (2000). Molecular basis for feedback regulation of bile acid synthesis by nuclear receptors. *Molecular Cell*, *6*(3), 507–515.

Makishima, M. (1999). Identification of a Nuclear Receptor for Bile Acids. *Science*, *284*(5418), 1362–1365. http://doi.org/10.1126/science.284.5418.1362

Mantovani, A., Allavena, P., Sica, A., & Balkwill, F. (2008). Cancer-related inflammation. *Nature*, *454*(7203), 436–444. http://doi.org/10.1038/nature07205

Maran, R. R. M., Thomas, A., Roth, M., Sheng, Z., Esterly, N., Pinson, D., et al. (2009). Farnesoid X Receptor Deficiency in Mice Leads to Increased Intestinal Epithelial Cell Proliferation and Tumor Development. *Journal of Pharmacology and Experimental Therapeutics*, *328*(2), 469–477. http://doi.org/10.1124/jpet.108.145409

Matsuzaki, J., Suzuki, H., Tsugawa, H., Watanabe, M., Hossain, S., Arai, E., et al. (2013). Bile Acids Increase Levels of MicroRNAs 221 and 222, Leading to Degradation of CDX2 During Esophageal Carcinogenesis. *Ygast*, *145*(6), 1300–1311. http://doi.org/10.1053/j.gastro.2013.08.008

May, R., Riehl, T. E., Hunt, C., Sureban, S. M., Anant, S., & Houchen, C. W. (2008). Identification of a Novel Putative Gastrointestinal Stem Cell and Adenoma Stem Cell Marker, Doublecortin and CaM Kinase-Like-1, Following Radiation Injury and in Adenomatous Polyposis Coli/Multiple Intestinal Neoplasia Mice. *Stem Cells*, *26*(3), 630–637. http://doi.org/10.1634/stemcells.2007-0621

May, R., Sureban, S. M., Hoang, N., Riehl, T. E., Lightfoot, S. A., Ramanujam, R., et al. (2009). Doublecortin and CaM Kinase-like-1 and Leucine-Rich-Repeat-Containing G-Protein-Coupled Receptor Mark Quiescent and Cycling Intestinal Stem Cells, Respectively. *Stem Cells*, *27*(10), 2571–2579. http://doi.org/10.1002/stem.193

Menke, V., van Es, J. H., de Lau, W., van den Born, M., Kuipers, E. J., Siersema, P. D., et al. (2010). Conversion of metaplastic Barrett's epithelium into post-mitotic goblet cells by -secretase inhibition. *Disease Models & Mechanisms*, *3*(1-2), 104–110. http://doi.org/10.1242/dmm.003012

Modica, S., Bellafante, E., & Moschetta, A. (2009). Master regulation of bile acid and xenobiotic metabolism via the FXR, PXR and CAR trio. *Frontiers in Bioscience (Landmark Edition)*, *14*, 4719–4745.

Modica, S., Gadaleta, R. M., & Moschetta, A. (2010). Deciphering the nuclear bile acid receptor FXR paradigm. *Nuclear Receptor Signaling*, *8*, e005. http://doi.org/10.1621/nrs.08005

Modica, S., Murzilli, S., Salvatore, L., Schmidt, D. R., & Moschetta, A. (2008). Nuclear Bile Acid Receptor FXR Protects against Intestinal Tumorigenesis. *Cancer Research*, *68*(23), 9589–9594. http://doi.org/10.1158/0008-5472.CAN-08-1791

Nakanishi, Y., Seno, H., Fukuoka, A., Ueo, T., Yamaga, Y., Maruno, T., et al. (2012). Dclk1 distinguishes between tumor and normal stem cells in the intestine. *Nature Genetics*. http://doi.org/10.1038/ng.2481

Naugler, W. E., Sakurai, T., Kim, S., Maeda, S., Kim, K., Elsharkawy, A. M., & Karin, M. (2007). Gender Disparity in Liver Cancer Due to Sex Differences in MyD88-Dependent IL-6 Production. *Science*, *317*(5834), 121–124. http://doi.org/10.1126/science.1140485

Nehra, D., Howell, P., Williams, C. P., Pye, J. K., & Beynon, J. (1999). Toxic bile acids in gastro-oesophageal reflux disease: influence of gastric acidity. *Gut*, *44*(5), 598–602.

O'Connor, M. J., Martin, N. M. B., & Smith, G. C. M. (2007). Targeted cancer therapies based on the inhibition of DNA strand break repair. *Oncogene*, *26*(56), 7816–7824. http://doi.org/10.1038/sj.onc.1210879

Oelkers, P., Kirby, L. C., Heubi, J. E., & Dawson, P. A. (1997). Primary bile acid malabsorption caused by mutations in the ileal sodium-dependent bile acid transporter gene (SLC10A2). *The Journal of Clinical Investigation*, *99*(8), 1880–1887. http://doi.org/10.1172/JCI119355

Oh, T. Y., Lee, J. S., Ahn, B. O., Cho, H., Kim, W. B., Kim, Y. B., et al. (2001). Oxidative stress is more important than acid in the pathogenesis of reflux oesophagitis in rats. *Gut*, *49*(3), 364–371.

Olliver, J. R., Wild, C. P., Sahay, P., Dexter, S., & Hardie, L. J. (2003). Chromoendoscopy with methylene blue and associated DNA damage in Barrett's oesophagus. *Lancet*, *362*(9381), 373–374.

Parks, D. J., Blanchard, S. G., Bledsoe, R. K., Chandra, G., Consler, T. G., Kliewer, S. A., et al. (1999). Bile acids: natural ligands for an orphan nuclear receptor. *Science*, *284*(5418), 1365–1368.

Pastuła, A., Middelhoff, M., Brandtner, A., Tobiasch, M., Höhl, B., Nuber, A. H., et al. (2016). Three-Dimensional Gastrointestinal Organoid Culture in Combination with Nerves or Fibroblasts: A Method to Characterize the Gastrointestinal Stem Cell Niche. *Stem Cells International*, *2016*(10), 1–16. http://doi.org/10.1002/ijc.27500

Paull, A., Trier, J. S., Dalton, M. D., Camp, R. C., Loeb, P., & Goyal, R. K. (1976). The histologic spectrum of Barrett's esophagus. *The New England Journal of Medicine*, *295*(9), 476–480. http://doi.org/10.1056/NEJM197608262950904

Portincasa, P., Moschetta, A., & Palasciano, G. (2006). Cholesterol gallstone disease. *Lancet*, *368*(9531), 230–239. http://doi.org/10.1016/S0140-6736(06)69044-2

Prade, E., Tobiasch, M., Hitkova, I., Schaffer, I., Lian, F., Xing, X., et al. (2012). Bile Acids Down-Regulate Caveolin-1 in Esophageal Epithelial Cells through Sterol Responsive Element-Binding Protein. *Molecular Endocrinology*, *26*(5), 819–832. http://doi.org/10.1210/me.2011-1140

Quante, M., Abrams, J. A., Lee, Y., & Wang, T. C. (2012a). Barrett esophagus: What a mouse model can teach us about human disease. *Cell Cycle (Georgetown, Tex.)*, *11*(23). http://doi.org/10.4161/cc.22485

Quante, M., Bhagat, G., Abrams, J. A., Marache, F., Good, P., Lee, M. D., et al. (2012b). Bile Acid and Inflammation Activate Gastric Cardia Stem Cells in a Mouse Model of Barrett-Like Metaplasia. *Cancer Cell*, *21*(1), 36–51. http://doi.org/10.1016/j.ccr.2011.12.004

Renga, B., Mencarelli, A., Cipriani, S., D'Amore, C., Carino, A., Bruno, A., et al. (2013). The Bile Acid Sensor FXR Is Required for Immune-Regulatory Activities of TLR-9 in Intestinal Inflammation. *PLoS ONE*, *8*(1), e54472. http://doi.org/10.1371/journal.pone.0054472.s002

Sasso, Lo, G., Petruzzelli, M., & Moschetta, A. (2008). A translational view on the biliary lipid secretory network. *Biochimica Et Biophysica Acta (BBA) - Molecular and Cell Biology of Lipids*, *1781*(3), 79–96. http://doi.org/10.1016/j.bbalip.2007.12.002

Sato, T., Vries, R. G., Snippert, H. J., van de Wetering, M., Barker, N., Stange, D. E., et al. (2009). Single Lgr5 stem cells build crypt-villus structures in vitro without a mesenchymal niche. *Nature*, *459*(7244), 262–265. http://doi.org/10.1038/nature07935

Schünke, M., Schulte, E., & Schumacher, U. (2012). PROMETHEUS Kopf, Hals und Neuroanatomie: LernAtlas Anatomie. Thieme.

Shaheen, N. J., Crosby, M. A., Bozymski, E. M., & Sandler, R. S. (2000). Is there publication bias in the reporting of cancer risk in Barrett's esophagus? *Gastroenterology*, *119*(2), 333–338. http://doi.org/10.1053/gast.2000.9302

Sihvo, E. I. T., Salminen, J. T., Rantanen, T. K., R m, O. J., Ahotupa, M., F rkkil, M., et al. (2002). Oxidative stress has a role in malignant transformation in Barrett's oesophagus. *International Journal of Cancer*, *102*(6), 551–555. http://doi.org/10.1002/ijc.10755

Sinal, C. J. C., Tohkin, M. M., Miyata, M. M., Ward, J. M. J., Lambert, G. G., & Gonzalez, F. J. F. (2000). Targeted Disruption of the Nuclear Receptor FXR/BAR Impairs Bile Acid and Lipid Homeostasis. *Cell*, *102*(6), 14–14. http://doi.org/10.1016/S0092-8674(00)00062-3

Smith, D. L. H., Keshavan, P., Avissar, U., Ahmed, K., & Zucker, S. D. (2010). Sodium taurocholate inhibits intestinal adenoma formation in APCMin/+ mice, potentially through activation of the farnesoid X receptor. *Carcinogenesis*, *31*(6), 1100–1109. http://doi.org/10.1093/carcin/bgq050

Solaas, K., Ulvestad, A., Söreide, O., & Kase, B. F. (2000). Subcellular organization of bile acid amidation in human liver: a key issue in regulating the biosynthesis of bile salts. *The Journal of Lipid Research*, *41*(7), 1154–1162.

Song, C. S., Echchgadda, I., Baek, B. S., Ahn, S. C., Oh, T., Roy, A. K., & Chatterjee, B. (2001). Dehydroepiandrosterone sulfotransferase gene induction by bile acid activated farnesoid X receptor. *The Journal of Biological Chemistry*, *276*(45), 42549–42556. http://doi.org/10.1074/jbc.M107557200

Sontag, S. J. (1999). Defining GERD. *Yale Journal of Biology and Medicine*, *72*(2-3), 69–80.

Spechler, S. J., & Souza, R. F. (2014). Barrett's Esophagus. *The New England Journal of Medicine*, *371*(9), 836–845. http://doi.org/10.1056/NEJMra1314704

Spechler, S. J., Fitzgerald, R. C., Prasad, G. A., & Wang, K. K. (2010). History, Molecular Mechanisms, and Endoscopic Treatment of Barrett's Esophagus. *Ygast*, *138*(3), 854–869. http://doi.org/10.1053/j.gastro.2010.01.002

Stange, D. E., Koo, B.-K., Huch, M., Sibbel, G., Basak, O., Lyubimova, A., et al. (2013). Differentiated Troy+ Chief Cells Act as Reserve Stem Cells to Generate All Lineages of the Stomach Epithelium. *Cell*, *155*(2), 357–368. http://doi.org/10.1016/j.cell.2013.09.008

Tochtrop, G. P., DeKoster, G. T., Covey, D. F., & Cistola, D. P. (2004). A single hydroxyl group governs ligand site selectivity in human ileal bile acid binding protein. *Journal of the American Chemical Society*, *126*(35), 11024–11029. http://doi.org/10.1021/ja047589c

Toke, O., Monsey, J. D., DeKoster, G. T., Tochtrop, G. P., Tang, C., & Cistola, D. P. (2006). Determinants of cooperativity and site selectivity in human ileal bile acid binding protein. *Biochemistry*, *45*(3), 727–737. http://doi.org/10.1021/bi051781p

Turinetto, V., & Giachino, C. (2015). Multiple facets of histone variant H2AX: a DNA double-strand-break marker with several biological functions. *Nucleic Acids Research*, *43*(5), 2489–2498. http://doi.org/10.1093/nar/gkv061

Ueda, J., Chijiiwa, K., Nakano, K., Zhao, G., & Tanaka, M. (2002). Lack of intestinal bile results in delayed liver regeneration of normal rat liver after hepatectomy accompanied by impaired cyclin E–associated kinase activity. *Surgery*, *131*(5), 564–573. http://doi.org/10.1067/msy.2002.123008

Vakil, N., van Zanten, S. V., Kahrilas, P., Dent, J., Jones, R., the Global Consensus Group. (2006). The Montreal Definition and Classification of Gastroesophageal Reflux Disease: A Global Evidence-Based Consensus. *The American Journal of Gastroenterology*, *101*(8), 1900–1920. http://doi.org/10.1111/j.1572-0241.2006.00630.x

Van de Winkel, A., van Zoest, K. P. M., van Dekken, H., Moons, L. M. G., Kuipers, E. J., & van der Laan, L. J. W. (2011). Differential expression of the nuclear receptors farnesoid X receptor (FXR) and pregnane X receptor (PXR) for grading dysplasia in patients with Barrett's oesophagus. *Histopathology*, *58*(2), 246–253. http://doi.org/10.1111/j.1365-2559.2011.03743.x

Wang, H., Chen, J., Hollister, K., Sowers, L. C., & Forman, B. M. (1999). Endogenous bile acids are ligands for the nuclear receptor FXR/BAR. *Molecular Cell*, *3*(5), 543–553.

Westphalen, C. B., Asfaha, S., Hayakawa, Y., Takemoto, Y., Lukin, D. J., Nuber, A. H., et al. (2014). Long-lived intestinal tuft cells serve as colon cancer–initiating cells. *The Journal of Clinical Investigation*. http://doi.org/10.1172/JCI73434DS1

Wetscher, G. J., Hinder, R. A., Klingler, P., Gadenstätter, M., Perdikis, G., & Hinder, P. R. (1997). Reflux esophagitis in humans is a free radical event. *Diseases of the Esophagus*, *10*(1), 29–32– discussion 33.

Wild, C. P., & Hardie, L. J. (2003). Reflux, Barrett's oesophagus and adenocarcinoma: burning questions. *Nature Reviews Cancer*, *3*(9), 676–684. http://doi.org/10.1038/nrc1166

Xu, Y., Watanabe, T., Tanigawa, T., Machida, H., Okazaki, H., Yamagami, H., et al. (2010). Bile acids induce cdx2 expression through the farnesoid x receptor in gastric epithelial cells. *Journal of Clinical Biochemistry and Nutrition*, *46*(1), 81–86. http://doi.org/10.3164/jcbn.09-71

Yang, F., Huang, X., Yi, T., Yen, Y., Moore, D. D., & Huang, W. (2007). Spontaneous Development of Liver Tumors in the Absence of the Bile Acid Receptor Farnesoid X Receptor. *Cancer Research*, *67*(3), 863–867. http://doi.org/10.1158/0008-5472.CAN-06-1078

Zhang, Y. (2002). Natural Structural Variants of the Nuclear Receptor Farnesoid X Receptor Affect Transcriptional Activation. *Journal of Biological Chemistry*, *278*(1), 104–110. http://doi.org/10.1074/jbc.M209505200

13 Appendices

13.1 Selected FXR regulated genes

IL1b FxR v.s IL1b					
Probe	**Symbol**	**Description**	**logFC**	**FC**	**P.Value**
17462149	*Cxcl12/SDF1	chemokine (C-X-C motif) ligand 12	1,6381823407	3,1127340965	0,0007339185
17514515	*Mmp3	matrix metallopeptidase 3	1,5385608823	2,9050457466	0,0000379845
17421074	Hspb7	heat shock protein family, member 7 (cardiovascular)	1,4119072917	2,6608870867	0,0155287735
17254065	Ccl8	chemokine (C-C motif) ligand 8	1,2120352890	2,3166422779	0,0050275480
17254041	Ccl2/MCP-1	chemokine (C-C motif) ligand 2	1,1758268901	2,2592233272	0,0010303546
17367102	*Mrc1	mannose receptor, C type 1	1,1743630334	2,2569321279	0,0031638820
17254053	*Ccl11	chemokine (C-C motif) ligand 11	1,1411397851	2,2055520154	0,0048189691
17503825	Mmp2	matrix metallopeptidase 2	1,0668894907	2,0949117795	0,0013921213
17451816	Hspb8	heat shock protein 8	1,0339036037	2,0475569850	0,0066284426
17351053	Csf1r	colony stimulating factor 1 receptor	0,9384293159	1,9164406443	0,0008473084
17396383	Tnfsf10	tumor necrosis factor (ligand) superfamily, member 10	0,8546475564	1,8083169378	0,0226490573
17400375	Ctss	cathepsin S	0,8208609312	1,7664598165	0,0082489142
17293006	*Cxcl14	chemokine (C-X-C motif) ligand 14	0,7924244407	1,7319826052	0,0055403583
17238558	Mmp19	matrix metallopeptidase 19	0,6955640991	1,6195175466	0,0063940639
17236288	Igf1	insulin-like growth factor 1	0,6935857294	1,6172982220	0,0539141438
17400365	Ctsk	cathepsin K	0,6444553068	1,5631490040	0,0315026094
17356288	*Ctsf	cathepsin F	0,6075146301	1,5236321444	0,0066547030
17250556	Tnfrsf13b	tumor necrosis factor receptor superfamily, member 13b	0,4312080018	1,3483621190	0,0615617969
17344309	*Tnf	tumor necrosis factor	-0,6475646692	0,6383569785	0,0355508679
17341540	Tnfrsf12a	tumor necrosis factor receptor superfamily, member 12a	-0,6517879175	0,6364910277	0,0268411377
17480500	*Wnt11	wingless-type MMTV integration site family, member 11	-0,6763465413	0,6257479041	0,0247798769
17315200	Krt7	keratin 7	-0,8864024514	0,5409613957	0,0150728059
17246091	*Il23a	interleukin 23, alpha subunit p19	-1,0571571523	0,4805781121	0,0024007353
17391554	*Il1a	interleukin 1 alpha	-1,3861380584	0,3825875791	0,0116081533
17322075	Krt4	keratin 4	-1,5052941654	0,3522583560	0,0028536197
17439367	Cxcl13	chemokine (C-X-C motif) ligand 13	0,9895558340	1,9855735934	0,1893152346
17514592	Mmp7	matrix metallopeptidase 7	0,7202957378	1,6475197247	0,1633200081
17408805	*Wnt2b	wingless-type MMTV integration site family, member 2B	0,6431190506	1,5617018508	0,0794466226
17531705	Ccrl2	chemokine (C-C motif) receptor-like 2	0,5202102158	1,4341642055	0,0258712417
17523642	*Cxcr6	chemokine (C-X-C motif) receptor 6	0,4742451865	1,3891912092	0,0421208613
17257157	Wnt3	wingless-type MMTV integration site family, member 3	0,4375751545	1,3543260962	0,0243210099
17514580	Mmp20	matrix metallopeptidase 20 (enamelysin)	0,4082682114	1,3270918373	0,0177119401
17270576	Wnt9b	wingless-type MMTV integration site family, member 9B	0,3965152472	1,3163245561	0,0343174884
17262695	Il13	interleukin 13	-0,3507586526	0,7841716266	0,0293797768
17457892	*Casp2	caspase 2	-0,4771495478	0,7183956165	0,0312361305
17263388	*Wnt3a	wingless-type MMTV integration site family, member 3A	-0,4831328400	0,7154223826	0,0283457099
17462351	*Il17ra	interleukin 17 receptor A	-0,5120628359	0,7012190834	0,0490827012
17317046	*Tnfrsf11b	tumor necrosis factor receptor superfamily, member 11b (osteoprotegerin)	-0,8655106301	0,5488521108	0,0521782583
17214142	*Cxcr2	chemokine (C-X-C motif) receptor 2	-0,6136934701	0,6535214661	0,2507640229

13.2 Selected pL2-IL-1β regulated genes

IL1b v.s. WT					
Probe	Symbol	Description	logFC	FC	P.Value
17487759	Cd177	CD177 antigen	4,2736264162	19,3414817164	0,0000000005
17438955	Cxcl5	chemokine (C-X-C motif) ligand 5	4,4490170600	21,8417577647	0,0000028106
17391565	Il1b	interleukin 1 beta	3,1109470509	8,6394953905	0,0006970441
17506392	Il17c	interleukin 17C	2,8869348943	7,3969724082	0,0000290043
17418485	Csf3r	colony stimulating factor 3 receptor (granulocyte)	2,4411073360	5,4305839381	0,0052604539
17344309	*Tnf	tumor necrosis factor	2,2080078783	4,6203683691	0,0000479837
17367686	Il1rn	interleukin 1 receptor antagonist	2,0819326089	4,2337398086	0,0000220909
17437213	Cd38	CD38 antigen	2,0618907190	4,1753314256	0,0001112190
17514553	Mmp8	matrix metallopeptidase 8	2,0479160603	4,1350823483	0,0329409502
17480500	*Wnt11	wingless-type MMTV integration site family, member 11	2,0099340960	4,0276382088	0,0000044543
17300725	Mcpt2	mast cell protease 2	1,9647333500	3,9034055191	0,0006212635
17246091	*Il23a	interleukin 23, alpha subunit p19	1,9575357029	3,8839798144	0,0002695315
17214857	Ccl20	chemokine (C-C motif) ligand 20	1,7917154058	3,4622632090	0,0018029265
17514541	Mmp10	matrix metallopeptidase 10	1,6829514426	3,2108414845	0,0061784506
17214142	*Cxcr2	chemokine (C-X-C motif) receptor 2	1,5663165756	2,9614763717	0,0095363384
17421981	Tnfrsf9	tumor necrosis factor receptor superfamily, member 9	1,5040989177	2,8364745463	0,0030735283
17391554	*Il1a	interleukin 1 alpha	1,4978730796	2,8242603350	0,0442708393
17266911	Mmp28	matrix metallopeptidase 28 (epilysin)	1,4924842481	2,8137306846	0,0000873300
17211369	Il17a	interleukin 17A	1,3298630891	2,5137881808	0,0066030207
17514435	Casp4	caspase 4, apoptosis-related cysteine peptidase	1,1973337469	2,2931547986	0,0015568810
17523642	*Cxcr6	chemokine (C-X-C motif) receptor 6	1,1933245643	2,2867910742	0,0012874960
17438987	Cxcl1	chemokine (C-X-C motif) ligand 1	1,1853355093	2,2741627583	0,0270093129
17490149	Cd33	CD33 antigen	1,1469315604	2,2144241171	0,0373806212
17480018	Ctsc	cathepsin C	1,1047780070	2,1506578255	0,0009372606
17317046	*Tnfrsf11b	tumor necrosis factor receptor superfamily, member 11b (osteoprotegerin)	1,1039877810	2,1494801405	0,0168768120
17213213	Casp8	caspase 8	1,0700156786	2,0994561831	0,0013167949
17432674	Tnfrsf1b	tumor necrosis factor receptor superfamily, member 1b	1,0693858494	2,0985398354	0,0015031664
17336559	Notch4	notch 4	1,0595290802	2,0842510763	0,0001256785
17212185	Il1r1	interleukin 1 receptor, type I	1,0440032887	2,0619413378	0,0000513164
17268137	Itga3	integrin alpha 3	1,0269219682	2,0376721776	0,0004317558
17457892	*Casp2	caspase 2	1,0186977417	2,0260892709	0,0000539875
17212211	Il1rl1	interleukin 1 receptor-like 1	0,9452382009	1,9255067771	0,0296302946
17265268	Cxcl16	chemokine (C-X-C motif) ligand 16	0,8871277653	1,8494903401	0,0008400036
17504293	Mmp15	matrix metallopeptidase 15	0,8572839458	1,8116244880	0,0252207377
17367652	Il1f9	interleukin 1 family, member 9	0,8380863534	1,7876773240	0,0227301955
17514424	Casp1	caspase 1	0,8297054311	1,7773224323	0,0161595323
17462351	*Il17ra	interleukin 17 receptor A	0,8275031797	1,7746114471	0,0290430375
17448245	Tlr1	toll-like receptor 1	0,8181075650	1,7630917642	0,0257758600
17514515	*Mmp3	matrix metallopeptidase 3	0,7965631097	1,7369582888	0,3704503234
17234803	Cstb	cystatin B	0,7928066968	1,7324415716	0,0044833976
17420154	Wnt4	wingless-type MMTV integration site family, member 4	0,7738572582	1,7098351745	0,0185242858
17258473	Itgb4	integrin beta 4	0,7158564640	1,6424579827	0,0019684857
17360561	Casp7	caspase 7	0,6995361505	1,6239825724	0,0328599991
17329864	Muc20	mucin 20	0,6985344129	1,6228553490	0,0427487053
17520233	Ctsh	cathepsin H	0,6233332866	1,5404301724	0,0144325252
17263388	*Wnt3a	wingless-type MMTV integration site family, member 3A	0,5519044023	1,4660196107	0,0508391772
17379659	Cd40	CD40 antigen	-0,6997252590	0,6156894449	0,0183937028
17329516	Fgf12	fibroblast growth factor 12	-0,8404833522	0,5584564357	0,0047163527
17316780	Angpt1	angiopoietin 1	-1,0903477429	0,4696481584	0,0075545563
17496947	Fgfr2	fibroblast growth factor receptor 2	-1,1381082667	0,4543549600	0,0031632458
17293006	*Cxcl14	chemokine (C-X-C motif) ligand 14	-1,1557609716	0,4488293821	0,0046839309
17408805	*Wnt2b	wingless-type MMTV integration site family, member 2B	-1,3088650722	0,4036382857	0,0009823743
17218449	Angptl1	angiopoietin-like 1	-1,4467346861	0,3668507943	0,0000012007
17367055	Vim	vimentin	-1,4785711928	0,3588440258	0,0014529615
17257235	Itgb3	integrin beta 3	-1,4967546803	0,3543495985	0,0002002910
17257361	Mrc2	mannose receptor, C type 2	-1,5876760871	0,3327069510	0,0002755793
17214106	Igfbp2	insulin-like growth factor binding protein 2	-1,5990569772	0,3300926735	0,0001802853
17514447	Casp12	caspase 12	-1,6620585065	0,3159879599	0,0001682281
17356288	*Ctsf	cathepsin F	-1,6673912287	0,3148221102	0,0000085161
17221014	Cd34	CD34 antigen	-1,7922542681	0,2887205560	0,0012165739
17441453	Nos1	nitric oxide synthase 1, neuronal	-1,8414670933	0,2790378833	0,0014563232
17367102	*Mrc1	mannose receptor, C type 1	-2,0153115602	0,2473607390	0,0023076403
17410275	Egf	epidermal growth factor	-2,0996601039	0,2333132095	0,0000321277
17462149	*Cxcl12	chemokine (C-X-C motif) ligand 12	-2,5204534100	0,1742881744	0,0000374689
17370043	Angptl2	angiopoietin-like 2	-2,8087474049	0,1427193243	0,0001129597
17269358	Krt15	keratin 15	-2,5781044414	0,1674608268	0,0001397452
17307433	Tnfrsf19	tumor necrosis factor receptor superfamily, member 19	-2,4797926421	0,1792701706	0,0000500093
17296388	Itga1	integrin alpha 1	-2,0027351478	0,2495264840	0,0003848520
17442887	Mmp17	matrix metallopeptidase 17	-1,9592707358	0,2571584142	0,0007518124
17254053	*Ccl11	chemokine (C-C motif) ligand 11	-1,8486579970	0,2776505200	0,0003495832
17239845	Arg1	arginase, liver	0,8549955545	1,8087531816	0,1163471297
17242548	Casp14	caspase 14	0,7113590314	1,6373457849	0,2105301701
17532569	Ccr1	chemokine (C-C motif) receptor 1	0,7072247589	1,6326604263	0,1796551065
17276776	Arg2	arginase type II	0,6995205658	1,6239650295	0,2057141426
17293386	Ctsq	cathepsin Q	0,5468967813	1,4609398508	0,0373789120
17305988	Tep1	telomerase associated protein 1	0,5292294842	1,4431582264	0,0018187396
17498099	Ctsd	cathepsin D	0,3816545645	1,3028351642	0,0313431582
17314666	Wnt1	wingless-type MMTV integration site family, member 1	-0,3938824670	0,7610786912	0,0438093866
17359716	Hif1an	hypoxia-inducible factor 1, alpha subunit inhibitor	-0,5027490054	0,7057606966	0,0156707190

13.3 Gene function of the selected genes

Symbol	gene function
*Casp2	The encoded protein may function in stress-induced cell death pathways, cell cycle maintenance, and the suppression of tumorigenesis
*Ccl11	This chemokine displays chemotactic activity for eosinophils, but not mononuclear cells or neutrophils.
*Ctsf	Represent a major component of the lysosomal proteolytic system
*Cxcl12/SDF1	Plays a role in many diverse cellular functions, including embryogenesis, immune surveillance, inflammation response, tissue homeostasis, and tumor growth and metastasis.
*Cxcl14	CXCL14 deficiency in mice attenuates obesity and inhibits feeding behavior in a novel environment.
*Cxcr2	This receptor mediates neutrophil migration to sites of inflammation
*Cxcr6	unknown
*Il17ra	Interleukin 17A (IL17A) is a proinflammatory cytokine secreted by activated T-lymphocytes. It is a potent inducer of the maturation of CD34-positive hematopoietic precursors into neutrophils.
*Il1a	Involved in various immune responses, inflammatory processes, and hematopoiesis.
*Il23a	This gene encodes a subunit of the heterodimeric cytokine interleukin 23 and can activate the transcription activator STAT4, and stimulate the production of interferon-gamma (IFNG)
*Mmp3	Involved in wound repair, progression of atherosclerosis, and tumor initiation
*Mrc1	Mediates the endocytosis of glycoproteins by macrophages
*Tnf	Involved in the regulation of a wide spectrum of biological processes including cell proliferation, differentiation, apoptosis, lipid metabolism, and coagulation
*Tnfrsf11b	This protein is an osteoblast-secreted decoy receptor that functions as a negative regulator of bone resorption
*Wnt11	unknown
*Wnt2b	unknwon
*Wnt3a	These proteins have been implicated in oncogenesis and in several developmental processes, including regulation of cell fate and patterning during embryogenesis
Angpt1	It plays a critical role in mediating reciprocal interactions between the endothelium and surrounding matrix and mesenchyme and inhibits endothelial permeability
Angptl1	Angiopoietins are members of the vascular endothelial growth factor family and the only known growth factors largely specific for vascular endothelium
Angptl2	Angiopoietins are members of the vascular endothelial growth factor family and the only known growth factors largely specific for vascular endothelium
Arg1	Arginase catalyzes the hydrolysis of arginine to ornithine and urea
Arg2	Arginase catalyzes the hydrolysis of arginine to ornithine and urea
Casp1	Sequential activation of caspases plays a central role in the execution-phase of cell apoptosis
Casp12	unknown
Casp14	Sequential activation of caspases plays a central role in the execution-phase of cell apoptosis
Casp4	Plays important roles in apoptosis, cell migration and the inflammatory response
Casp7	plays a central role in the execution-phase of cell apoptosis.
Casp8	This protein is involved in the programmed cell death induced by Fas and various apoptotic stimuli
Ccl2/MCP-1	This cytokine displays chemotactic activity for monocytes and basophils but not for neutrophils or eosinophils
Ccl20	he protein encoded by this gene displays chemotactic activity for lymphocytes and can repress proliferation of myeloid progenitors
Ccl8	This cytokine displays chemotactic activity for monocytes, lymphocytes, basophils and eosinophils
Ccr1	The ligands of this receptor include macrophage inflammatory protein 1 alpha (MIP-1 alpha), regulated on activation normal T expressed and secreted protein (RANTES)
Ccrl2	unknown
Cd177	Plays a role in neutrophil activation
Cd33	unknown
Cd34	Plays a role in the attachment of stem cells to the bone marrow extracellular matrix or to stromal cells
Cd38	Synthesizes and hydrolyzes cyclic adenosine 5'-diphosphate-ribose, an intracellular calcium ion mobilizing messenger
Cd40	The encoded protein is a receptor on antigen-presenting cells of the immune system and is essential for mediating
Csf1r	The protein encoded by this gene is the receptor for colony stimulating factor 1, a cytokine which controls the production, differentiation, and function of macrophages
Csf3r	Controls the production, differentiation, and function of granulocytes.
Cstb	This gene encodes a stefin that functions as an intracellular thiol protease inhibitor.
Ctsc	This enzyme requires chloride ions for activity and can degrade glucagon
Ctsd	This gene encodes a member of the A1 family of peptidase.
Ctsh	The protein encoded by this gene is a lysosomal cysteine proteinase important in the overall degradation of lysosomal proteins.
Ctsk	Involved in bone remodeling and resorption
Ctsq	unknown
Ctss	The encoded protein can function as an elastase over a broad pH range in alveolar macrophages
Cxcl1	This protein plays a role in inflammation and as a chemoattractant for neutrophils
Cxcl13	B lymphocyte chemoattractant, it preferentially promotes the migration of B lymphocytes, apparently by stimulating calcium influx into, and chemotaxis of, cells expressing Burkitt's lymphoma receptor 1 (BLR-1).
Cxcl5	Recruit neutrophils, to promote angiogenesis and to remodel connective tissue
Egf	This protein acts a potent mitogenic factor that plays an important role in the growth, proliferation and differentiation of numerous cell types.
Fgf12	his growth factor lacks the N-terminal signal sequence present in most of the FGF family members, but it contains clusters of basic residues that have been demonstrated to act as a nuclear localization signal.
Fgfr2	his particular family member is a high-affinity receptor for acidic, basic and/or keratinocyte growth factor, depending on the isoform.
Hif1an	unknown
Hspb7	unknown
Hspb8	This gene appears to be involved in regulation of cell proliferation, apoptosis, and carcinogenesis
Igf1	Involved in mediating growth and development
Igfbp2	High expression levels of this protein promote the growth of several types of tumors and may be predictive of the chances of recovery of the patient
Il13	This cytokine down-regulates macrophage activity, thereby inhibits the production of pro-inflammatory cytokines and chemokines.
Il17a	This cytokine regulates the activities of NF-kappaB and mitogen-activated protein kinases
Il17c	his cytokine was reported to stimulate the release of tumor necrosis factor alpha and interleukin 1 beta from a monocytic cell line
Il1b	This cytokine is an important mediator of the inflammatory response, and is involved in a variety of cellular activities, including cell proliferation, differentiation, and apoptosis.
Il1rn	This protein inhibits the activities of interleukin 1, alpha (IL1A) and interleukin 1, beta (IL1B), and modulates a variety of interleukin 1 related immune and inflammatory responses.
Itga1	The heterodimeric receptor is involved in cell-cell adhesion and may play a role in inflammation and fibrosis
Itga3	Cell surface adhesion molecules.
Itgb3	Integrins are known to participate in cell adhesion as well as cell-surface mediated signalling
Itgb4	This gene encodes the integrin beta 4 subunit, a receptor for the laminins. It plays a pivotal role in the biology of invasive carcinoma
Krt15	he keratins are intermediate filament proteins responsible for the structural integrity of epithelial cells and are subdivided into cytokeratins and hair keratins
Krt4	Member of the keratin gene family and expressed in differentiated layers of the mucosal and esophageal epithelia with family member KRT13
Krt7	member of the keratin gene family
Mcpt2	unknown
Mmp10	Involved in the breakdown of extracellular matrix in normal physiological processes, such as embryonic development, reproduction, and tissue remodeling, as well as in disease processes, such as arthritis and metastasis.
Mmp17	The protein activates MMP-2 by cleavage
Mmp19	Involved in the breakdown of extracellular matrix in normal physiological processes, such as embryonic development, reproduction, and tissue remodeling, as well as in disease processes, such as arthritis and metastasis.
Mmp2	Involved in multiple pathways including roles in the nervous system, endometrial menstrual breakdown, regulation of vascularization, and metastasis.
Mmp20	It degrades amelogenin, the major protein component of dental enamel matrix, and thus thought to play a role in tooth enamel formation
Mmp28	Involved in the breakdown of extracellular matrix for both normal physiological processes, such as embryonic development, reproduction and tissue remodeling, and disease processes, such as asthma and metastasis
Mmp7	The enzyme is involved in wound healing, and studies in mice suggest that it regulates the activity of defensins in intestinal mucosa.
Mmp8	These proteins are involved in the breakdown of extracellular matrix in embryonic development, reproduction, and tissue remodeling, as well as in disease processes, such as arthritis and metastasis
Mrc2	Plays a role in extracellular matrix remodeling by mediating the internalization and lysosomal degradation of collagen ligands
Muc20	This gene encodes a member of the mucin protein family. Mucins are high molecular weight glycoproteins secreted by many epithelial tissues to form an insoluble mucous barrier
Nos1	The protein encoded by this gene belongs to the family of nitric oxide synthases, which synthesize nitric oxide from L-arginine
Notch4	Plays a role in vascular, renal and hepatic development.
Tep1	This gene product is a component of the ribonucleoprotein complex responsible for telomerase activity which catalyzes the addition of new telomeres on the chromosome ends
Tlr1	Plays a fundamental role in pathogen recognition and activation of innate immunit
Tnfrsf12a	unknown
Tnfrsf13b	Plays a crucial role in humoral immunity by interacting with a TNF ligand.
Tnfrsf19	It has been shown to interact with TRAF family members, and to activate JNK signaling pathway when overexpressed in cells
Tnfrsf9	This receptor contributes to the clonal expansion, survival, and development of T cells.
Tnfsf10	This protein preferentially induces apoptosis in transformed and tumor cells, but does not appear to kill normal cells
Vim	The protein encoded by this gene is responsible for maintaining cell shape, integrity of the cytoplasm, and stabilizing cytoskeletal interactions.
Wnt1	These proteins have been implicated in oncogenesis and in several developmental processes, including regulation of cell fate and patterning during embryogenesis
Wnt3	unknown
Wnt4	These proteins have been implicated in oncogenesis and in several developmental processes, including regulation of cell fate and patterning during embryogenesis
Wnt9b	These proteins have been implicated in oncogenesis and in several developmental processes, including regulation of cell fate and patterning during embryogenesis

13.4 Overview of pathways analysis

NAME	GS follow link to MSigDB	SIZE	ES	NES	NOM p-val	FDR q-val	FWER p-val	RANK AT MAX	LEADING EDGE
BIOCARTA_ECM_PATHWAY	BIOCARTA_ECM_PATHWAY	24	0,5526	1,7523	0,0000	0,3539	0,1940	3536	tags=46%, list=21%, signal=58%
BIOCARTA_CSK_PATHWAY	BIOCARTA_CSK_PATHWAY	20	0,6288	1,7497	0,0000	0,2004	0,2410	3201	tags=55%, list=19%, signal=68%
BIOCARTA_PAR1_PATHWAY	BIOCARTA_PAR1_PATHWAY	35	0,5533	1,7346	0,0000	0,1675	0,2880	3078	tags=43%, list=18%, signal=52%
BIOCARTA_GCR_PATHWAY	BIOCARTA_GCR_PATHWAY	16	0,5132	1,6982	0,0000	0,1511	0,2880	3513	tags=38%, list=21%, signal=47%
BIOCARTA_MYOSIN_PATHWAY	BIOCARTA_MYOSIN_PATHWAY	28	0,5382	1,6847	0,0000	0,1525	0,3330	2698	tags=36%, list=16%, signal=43%
BIOCARTA_SPPA_PATHWAY	BIOCARTA_SPPA_PATHWAY	22	0,5793	1,6821	0,0000	0,1350	0,3330	2969	tags=45%, list=18%, signal=55%
BIOCARTA_TOB1_PATHWAY	BIOCARTA_TOB1_PATHWAY	18	0,6319	1,6536	0,0000	0,1438	0,4210	458	tags=33%, list=3%, signal=34%
BIOCARTA_ALK_PATHWAY	BIOCARTA_ALK_PATHWAY	35	0,4454	1,6117	0,0000	0,2102	0,4670	1138	tags=23%, list=7%, signal=24%
BIOCARTA_CXCR4_PATHWAY	BIOCARTA_CXCR4_PATHWAY	24	0,4554	1,5804	0,0000	0,2331	0,5110	3513	tags=33%, list=21%, signal=42%
BIOCARTA_NO2IL12_PATHWAY	BIOCARTA_NO2IL12_PATHWAY	16	0,5539	1,5791	0,0000	0,2145	0,5110	2461	tags=44%, list=15%, signal=51%
BIOCARTA_IL7_PATHWAY	BIOCARTA_IL7_PATHWAY	16	0,5759	1,5783	0,0000	0,1993	0,5110	4124	tags=63%, list=25%, signal=83%
BIOCARTA_CCR3_PATHWAY	BIOCARTA_CCR3_PATHWAY	23	0,4802	1,5730	0,0000	0,1866	0,5110	2969	tags=26%, list=18%, signal=32%
BIOCARTA_EDG1_PATHWAY	BIOCARTA_EDG1_PATHWAY	27	0,5494	1,5350	0,1155	0,2276	0,5700	3286	tags=44%, list=20%, signal=55%
BIOCARTA_CREB_PATHWAY	BIOCARTA_CREB_PATHWAY	26	0,4377	1,5338	0,0000	0,2203	0,6340	3078	tags=35%, list=18%, signal=42%
BIOCARTA_LONGEVITY_PATHWAY	BIOCARTA_LONGEVITY_PATHWAY	15	0,6411	1,5112	0,0000	0,2433	0,6820	3476	tags=60%, list=21%, signal=76%
BIOCARTA_CTCF_PATHWAY	BIOCARTA_CTCF_PATHWAY	23	0,5493	1,5088	0,0000	0,2344	0,6820	3781	tags=52%, list=23%, signal=67%
BIOCARTA_NFAT_PATHWAY	BIOCARTA_NFAT_PATHWAY	47	0,4217	1,4948	0,0000	0,2461	0,6820	3830	tags=38%, list=23%, signal=50%
BIOCARTA_HDAC_PATHWAY	BIOCARTA_HDAC_PATHWAY	25	0,5085	1,4881	0,0000	0,2438	0,6820	3078	tags=44%, list=18%, signal=54%
BIOCARTA_AGR_PATHWAY	BIOCARTA_AGR_PATHWAY	36	0,3788	1,4760	0,1082	0,2639	0,7510	2086	tags=25%, list=12%, signal=29%
BIOCARTA_IGF1MTOR_PATHWAY	BIOCARTA_IGF1MTOR_PATHWAY	18	0,3900	1,4570	0,0000	0,2767	0,8420	3078	tags=28%, list=18%, signal=34%
BIOCARTA_NO1_PATHWAY	BIOCARTA_NO1_PATHWAY	26	0,5639	1,4261	0,0950	0,3287	0,8920	3192	tags=54%, list=19%, signal=66%
BIOCARTA_INTEGRIN_PATHWAY	BIOCARTA_INTEGRIN_PATHWAY	36	0,3417	1,4228	0,0855	0,3211	0,8920	2969	tags=28%, list=18%, signal=34%
BIOCARTA_SHH_PATHWAY	BIOCARTA_SHH_PATHWAY	15	0,4178	1,4128	0,0961	0,3315	0,8920	5216	tags=60%, list=31%, signal=87%
BIOCARTA_CTLA4_PATHWAY	BIOCARTA_CTLA4_PATHWAY	18	0,5936	1,4127	0,1383	0,3196	0,8920	3078	tags=50%, list=18%, signal=61%
BIOCARTA_STATHMIN_PATHWAY	BIOCARTA_STATHMIN_PATHWAY	16	0,5768	1,4082	0,0000	0,3109	0,8920	2993	tags=56%, list=18%, signal=68%
BIOCARTA_ERK_PATHWAY	BIOCARTA_ERK_PATHWAY	28	0,3901	1,4078	0,0000	0,3031	0,8920	1724	tags=18%, list=10%, signal=20%
BIOCARTA_MTOR_PATHWAY	BIOCARTA_MTOR_PATHWAY	22	0,3895	1,4011	0,0000	0,3055	0,9370	6601	tags=64%, list=40%, signal=105%
BIOCARTA_NOS1_PATHWAY	BIOCARTA_NOS1_PATHWAY	17	0,5722	1,3745	0,0000	0,3118	0,9370	3866	tags=59%, list=23%, signal=76%
BIOCARTA_IGF1_PATHWAY	BIOCARTA_IGF1_PATHWAY	21	0,4086	1,3696	0,3057	0,3109	0,9370	3078	tags=33%, list=18%, signal=41%
BIOCARTA_BAD_PATHWAY	BIOCARTA_BAD_PATHWAY	25	0,4983	1,3691	0,0000	0,3040	0,9370	4156	tags=48%, list=25%, signal=64%
BIOCARTA_NKT_PATHWAY	BIOCARTA_NKT_PATHWAY	29	0,4886	1,3645	0,0000	0,3006	0,9370	2461	tags=41%, list=15%, signal=48%
BIOCARTA_NKCELLS_PATHWAY	BIOCARTA_NKCELLS_PATHWAY	19	0,4411	1,3614	0,0869	0,2927	0,9370	4367	tags=42%, list=26%, signal=57%
BIOCARTA_IGF1R_PATHWAY	BIOCARTA_IGF1R_PATHWAY	22	0,4894	1,3560	0,0000	0,2924	0,9370	3078	tags=41%, list=18%, signal=50%
BIOCARTA_UCALPAIN_PATHWAY	BIOCARTA_UCALPAIN_PATHWAY	17	0,4677	1,3447	0,0911	0,3137	0,9370	2048	tags=29%, list=12%, signal=33%
BIOCARTA_TCR_PATHWAY	BIOCARTA_TCR_PATHWAY	40	0,4144	1,3332	0,0000	0,3279	0,9370	3830	tags=40%, list=23%, signal=52%
BIOCARTA_TFF_PATHWAY	BIOCARTA_TFF_PATHWAY	21	0,3447	1,3272	0,2197	0,3255	0,9370	3237	tags=29%, list=19%, signal=35%
BIOCARTA_IL12_PATHWAY	BIOCARTA_IL12_PATHWAY	20	0,4491	1,3270	0,0000	0,3203	0,9370	2603	tags=35%, list=16%, signal=41%
BIOCARTA_MEF2D_PATHWAY	BIOCARTA_MEF2D_PATHWAY	15	0,4463	1,3247	0,1206	0,3145	0,9370	3684	tags=40%, list=22%, signal=51%
BIOCARTA_TH1TH2_PATHWAY	BIOCARTA_TH1TH2_PATHWAY	19	0,4346	1,3122	0,0791	0,3165	0,9370	3359	tags=37%, list=20%, signal=46%
BIOCARTA_P38MAPK_PATHWAY	BIOCARTA_P38MAPK_PATHWAY	35	0,2934	1,3004	0,0000	0,3202	0,9370	1664	tags=14%, list=10%, signal=16%
BIOCARTA_WNT_PATHWAY	BIOCARTA_WNT_PATHWAY	24	0,3341	1,2826	0,1078	0,3457	0,9370	3201	tags=25%, list=19%, signal=31%
BIOCARTA_BARRESTIN_SRC_PATHWAY	BIOCARTA_BARRESTIN_SRC_PATHWAY	15	0,4107	1,2654	0,2072	0,3683	0,9370	2969	tags=27%, list=18%, signal=32%
BIOCARTA_ETS_PATHWAY	BIOCARTA_ETS_PATHWAY	18	0,3982	1,2602	0,0000	0,3662	0,9370	1934	tags=33%, list=12%, signal=38%
BIOCARTA_GPCR_PATHWAY	BIOCARTA_GPCR_PATHWAY	30	0,3638	1,2548	0,1230	0,3636	0,9370	3830	tags=40%, list=23%, signal=52%
BIOCARTA_VEGF_PATHWAY	BIOCARTA_VEGF_PATHWAY	28	0,3560	1,2507	0,1243	0,3618	0,9370	3078	tags=29%, list=18%, signal=35%
BIOCARTA_FMLP_PATHWAY	BIOCARTA_FMLP_PATHWAY	33	0,3688	1,2256	0,2395	0,4104	0,9370	3830	tags=33%, list=23%, signal=43%
BIOCARTA_CARDIACEGF_PATHWAY	BIOCARTA_CARDIACEGF_PATHWAY	18	0,4177	1,2252	0,0891	0,4026	0,9370	909	tags=22%, list=5%, signal=23%
BIOCARTA_MET_PATHWAY	BIOCARTA_MET_PATHWAY	36	0,3335	1,2223	0,2241	0,3985	0,9370	89	tags=8%, list=1%, signal=8%
BIOCARTA_FCER1_PATHWAY	BIOCARTA_FCER1_PATHWAY	34	0,3772	1,2156	0,1235	0,4005	0,9370	3830	tags=41%, list=23%, signal=53%
BIOCARTA_CALCINEURIN_PATHWAY	BIOCARTA_CALCINEURIN_PATHWAY	15	0,4270	1,2143	0,2510	0,3949	0,9370	4269	tags=47%, list=26%, signal=63%
BIOCARTA_MCALPAIN_PATHWAY	BIOCARTA_MCALPAIN_PATHWAY	23	0,3746	1,2102	0,2195	0,3945	0,9370	2993	tags=30%, list=18%, signal=37%
BIOCARTA_CARM_ER_PATHWAY	BIOCARTA_CARM_ER_PATHWAY	33	0,3178	1,2053	0,0721	0,3942	0,9370	3201	tags=27%, list=19%, signal=34%
BIOCARTA_BCR_PATHWAY	BIOCARTA_BCR_PATHWAY	30	0,3231	1,2020	0,1258	0,3933	0,9370	3830	tags=33%, list=23%, signal=43%
BIOCARTA_BIOPEPTIDES_PATHWAY	BIOCARTA_BIOPEPTIDES_PATHWAY	39	0,3722	1,1984	0,2201	0,3949	0,9370	2969	tags=26%, list=18%, signal=31%
BIOCARTA_LAIR_PATHWAY	BIOCARTA_LAIR_PATHWAY	16	0,5136	1,1950	0,3758	0,3902	0,9370	1628	tags=31%, list=10%, signal=35%
BIOCARTA_RAC1_PATHWAY	BIOCARTA_RAC1_PATHWAY	22	0,4554	1,1890	0,3282	0,3957	0,9370	4373	tags=45%, list=26%, signal=61%
BIOCARTA_PITX2_PATHWAY	BIOCARTA_PITX2_PATHWAY	15	0,3956	1,1830	0,2961	0,4071	1,0000	3201	tags=27%, list=19%, signal=33%
BIOCARTA_GH_PATHWAY	BIOCARTA_GH_PATHWAY	27	0,3825	1,1796	0,2069	0,4024	1,0000	3237	tags=30%, list=19%, signal=37%
BIOCARTA_EIF4_PATHWAY	BIOCARTA_EIF4_PATHWAY	24	0,3613	1,1708	0,4964	0,4050	1,0000	5648	tags=46%, list=34%, signal=69%
BIOCARTA_AT1R_PATHWAY	BIOCARTA_AT1R_PATHWAY	28	0,3314	1,1479	0,2759	0,4276	1,0000	1000	tags=14%, list=6%, signal=15%
BIOCARTA_TGFB_PATHWAY	BIOCARTA_TGFB_PATHWAY	18	0,4123	1,1462	0,1875	0,4232	1,0000	4423	tags=39%, list=26%, signal=53%
BIOCARTA_INTRINSIC_PATHWAY	BIOCARTA_INTRINSIC_PATHWAY	22	0,5879	1,1392	0,3634	0,4237	1,0000	1366	tags=23%, list=8%, signal=25%
BIOCARTA_VIP_PATHWAY	BIOCARTA_VIP_PATHWAY	22	0,3944	1,1389	0,2308	0,4177	1,0000	3855	tags=45%, list=23%, signal=59%
BIOCARTA_CDC42RAC_PATHWAY	BIOCARTA_CDC42RAC_PATHWAY	15	0,3334	1,1340	0,2876	0,4209	1,0000	3078	tags=20%, list=18%, signal=24%
BIOCARTA_GATA3_PATHWAY	BIOCARTA_GATA3_PATHWAY	15	0,3650	1,1206	0,2182	0,4423	1,0000	2993	tags=40%, list=18%, signal=49%
BIOCARTA_AMI_PATHWAY	BIOCARTA_AMI_PATHWAY	19	0,6181	1,1192	0,2628	0,4390	1,0000	1366	tags=26%, list=8%, signal=29%
BIOCARTA_COMP_PATHWAY	BIOCARTA_COMP_PATHWAY	17	0,5764	1,1166	0,3891	0,4337	1,0000	224	tags=24%, list=1%, signal=24%
BIOCARTA_BCELLSURVIVAL_PATHWAY	BIOCARTA_BCELLSURVIVAL_PATHWAY	16	0,4221	1,1099	0,3197	0,4390	1,0000	3078	tags=44%, list=18%, signal=54%
BIOCARTA_SPRY_PATHWAY	BIOCARTA_SPRY_PATHWAY	18	0,3017	1,0829	0,3671	0,4721	1,0000	2969	tags=22%, list=18%, signal=27%
BIOCARTA_ERYTH_PATHWAY	BIOCARTA_ERYTH_PATHWAY	15	0,4135	1,0765	0,1783	0,4794	1,0000	2886	tags=40%, list=17%, signal=48%
BIOCARTA_P53HYPOXIA_PATHWAY	BIOCARTA_P53HYPOXIA_PATHWAY	19	0,3894	1,0563	0,3916	0,5065	1,0000	1194	tags=21%, list=7%, signal=23%
BIOCARTA_PGC1A_PATHWAY	BIOCARTA_PGC1A_PATHWAY	19	0,4417	1,0548	0,3036	0,5066	1,0000	3684	tags=47%, list=22%, signal=61%
BIOCARTA_ACH_PATHWAY	BIOCARTA_ACH_PATHWAY	16	0,3787	1,0417	0,3300	0,5182	1,0000	3078	tags=31%, list=18%, signal=38%
BIOCARTA_DC_PATHWAY	BIOCARTA_DC_PATHWAY	22	0,3261	1,0155	0,3983	0,5623	1,0000	3151	tags=45%, list=19%, signal=56%
BIOCARTA_PTDINS_PATHWAY	BIOCARTA_PTDINS_PATHWAY	21	0,2915	1,0042	0,4959	0,5714	1,0000	2944	tags=19%, list=18%, signal=23%
BIOCARTA_MCM_PATHWAY	BIOCARTA_MCM_PATHWAY	18	0,5565	1,0018	0,4686	0,5676	1,0000	1944	tags=39%, list=12%, signal=44%
BIOCARTA_PTEN_PATHWAY	BIOCARTA_PTEN_PATHWAY	17	0,2999	0,9917	0,4231	0,5789	1,0000	6821	tags=59%, list=41%, signal=99%
BIOCARTA_HCMV_PATHWAY	BIOCARTA_HCMV_PATHWAY	17	0,2617	0,9771	0,4257	0,6044	1,0000	3513	tags=29%, list=21%, signal=37%
BIOCARTA_ERK5_PATHWAY	BIOCARTA_ERK5_PATHWAY	17	0,3054	0,9759	0,5037	0,6008	1,0000	4984	tags=41%, list=30%, signal=59%
BIOCARTA_AKT_PATHWAY	BIOCARTA_AKT_PATHWAY	22	0,2752	0,9679	0,3969	0,6050	1,0000	3513	tags=27%, list=21%, signal=34%
BIOCARTA_ATM_PATHWAY	BIOCARTA_ATM_PATHWAY	19	0,3773	0,9677	0,5210	0,5982	1,0000	4186	tags=47%, list=25%, signal=63%
BIOCARTA_CHEMICAL_PATHWAY	BIOCARTA_CHEMICAL_PATHWAY	22	0,3680	0,9655	0,6026	0,5966	1,0000	1459	tags=18%, list=9%, signal=20%
BIOCARTA_IL2RB_PATHWAY	BIOCARTA_IL2RB_PATHWAY	36	0,3041	0,9535	0,3876	0,6057	1,0000	3078	tags=28%, list=18%, signal=34%
BIOCARTA_ATRBRCA_PATHWAY	BIOCARTA_ATRBRCA_PATHWAY	20	0,3887	0,9534	0,5000	0,5991	1,0000	4186	tags=50%, list=25%, signal=67%
BIOCARTA_INSULIN_PATHWAY	BIOCARTA_INSULIN_PATHWAY	22	0,2787	0,9362	0,5972	0,6120	1,0000	3078	tags=27%, list=18%, signal=33%
BIOCARTA_RHO_PATHWAY	BIOCARTA_RHO_PATHWAY	30	0,2294	0,8775	0,6258	0,6924	1,0000	4373	tags=27%, list=26%, signal=36%
BIOCARTA_NGF_PATHWAY	BIOCARTA_NGF_PATHWAY	18	0,3082	0,8462	0,7344	0,7243	1,0000	3078	tags=33%, list=18%, signal=41%
BIOCARTA_RAS_PATHWAY	BIOCARTA_RAS_PATHWAY	23	0,2439	0,8336	0,6165	0,7300	1,0000	3513	tags=26%, list=21%, signal=33%
BIOCARTA_G2_PATHWAY	BIOCARTA_G2_PATHWAY	22	0,2918	0,8304	0,5445	0,7312	1,0000	2312	tags=23%, list=14%, signal=26%
BIOCARTA_G1_PATHWAY	BIOCARTA_G1_PATHWAY	27	0,3053	0,8233	0,6471	0,7310	1,0000	2794	tags=26%, list=17%, signal=31%
BIOCARTA_PDGF_PATHWAY	BIOCARTA_PDGF_PATHWAY	32	0,2366	0,8183	0,6478	0,7299	1,0000	3078	tags=19%, list=18%, signal=23%
BIOCARTA_HER2_PATHWAY	BIOCARTA_HER2_PATHWAY	22	0,2166	0,8095	0,6803	0,7317	1,0000	3078	tags=23%, list=18%, signal=28%
BIOCARTA_TEL_PATHWAY	BIOCARTA_TEL_PATHWAY	18	0,2151	0,7897	0,7824	0,7480	1,0000	1629	tags=11%, list=10%, signal=12%
BIOCARTA_ARF_PATHWAY	BIOCARTA_ARF_PATHWAY	17	0,2783	0,7853	0,9084	0,7495	1,0000	3078	tags=35%, list=18%, signal=43%
BIOCARTA_ARAP_PATHWAY	BIOCARTA_ARAP_PATHWAY	17	0,2327	0,6981	0,6185	0,8375	1,0000	1100	tags=12%, list=7%, signal=13%
BIOCARTA_DEATH_PATHWAY	BIOCARTA_DEATH_PATHWAY	29	0,2055	0,6847	0,7996	0,8395	1,0000	4225	tags=28%, list=25%, signal=37%
BIOCARTA_STEM_PATHWAY	BIOCARTA_STEM_PATHWAY	15	0,2540	0,6712	0,9031	0,8548	1,0000	3255	tags=33%, list=19%, signal=41%
BIOCARTA_RARRXR_PATHWAY	BIOCARTA_RARRXR_PATHWAY	15	0,2125	0,6493	0,7909	0,8765	1,0000	4054	tags=27%, list=24%, signal=35%
BIOCARTA_IL3_PATHWAY	BIOCARTA_IL3_PATHWAY	15	0,1608	0,4934	0,9006	0,9777	1,0000	822	tags=7%, list=5%, signal=7%

13.5 Regulated genes in top pathways of pL2-IL-1β and pL2-IL-1β/FXR$^{-/-}$

	pL2								
NAME	**SIZE**	**ES**	**NES**	**NOM p-val**	**FDR q-val**	**FWER p-val**	**RANK AT MA**	**LEADING EDGE**	
BIOCARTA_TID_PATHWAY	18	-0,5993145	-1,688181	0	0,31865916	0,292	2040	tags=33%, list=12%, signal=38%	
	PROBE	**GENE SYMBC**	**GENE_TITLE**	**RANK IN GEN**	**RANK METRI**	**RUNNING ES**	**CORE ENRICHMENT**		
	IFNG	IFNG	interferon, gamma	14666	-0,3956835	-0,5221639	Yes		
	TNFRSF1B	TNFRSF1B	tumor necrosis factor receptor superfamily, member 1B	14783	-0,4097824	-0,4492157	Yes		
	RB1	RB1	retinoblastoma 1 (including osteosarcoma)	15162	-0,4578799	-0,3825903	Yes		
	WT1	WT1	Wilms tumor 1	15347	-0,48474	-0,2991019	Yes		
	TNF	TNF	tumor necrosis factor (TNF superfamily, member 2)	16582	-0,9064682	-0,1963078	Yes		
	HSPA1A	HSPA1A	heat shock 70kDa protein 1A	16637	-1,0439953	0,00401511	Yes		
BIOCARTA_STRESS_PATHWAY	23	-0,507197	-1,5851674	0	0,403783	0,519	2688	tags=30%, list=16%, signal=36%	
	PROBE	**GENE SYMBC**	**GENE_TITLE**	**RANK IN GEN**	**RANK METRI**	**RUNNING ES**	**CORE ENRICHMENT**		
	IKBKG	IKBKG	inhibitor of kappa light polypeptide gene enhancer in B-cells, kin	14018	-0,3361594	-0,4519997	Yes		
	TRAF2	TRAF2	TNF receptor-associated factor 2	14255	-0,3562474	-0,4076509	Yes		
	MAP2K3	MAP2K3	mitogen-activated protein kinase kinase 3	15313	-0,4795642	-0,3922683	Yes		
	TRADD	TRADD	TNFRSF1A-associated via death domain	15327	-0,4818202	-0,3139328	Yes		
	CASP2	CASP2	caspase 2, apoptosis-related cysteine peptidase (neural precursc	16355	-0,7183344	-0,2575459	Yes		
	JUN	JUN	jun oncogene	16471	-0,7887036	-0,1349346	Yes		
	TNF	TNF	tumor necrosis factor (TNF superfamily, member 2)	16582	-0,9064682	0,00731333	Yes		
BIOCARTA_CYTOKINE_PATHWAY	21	-0,4966244	-1,5175935	0	0,45406917	0,751	2710	tags=33%, list=16%, signal=40%	
	PROBE	**GENE SYMBC**	**GENE_TITLE**	**RANK IN GEN**	**RANK METRI**	**RUNNING ES**	**CORE ENRICHMENT**		
	IL13	IL13	interleukin 13	13996	-0,3344533	-0,450367	Yes		
	IL2	IL2	interleukin 2	14173	-0,3483146	-0,4127415	Yes		
	IFNG	IFNG	interferon, gamma	14666	-0,3956835	-0,3875047	Yes		
	IL17A	IL17A	interleukin 17A	16347	-0,7138851	-0,3894643	Yes		
	IL1A	IL1A	interleukin 1, alpha	16506	-0,8127547	-0,2865243	Yes		
	TNF	TNF	tumor necrosis factor (TNF superfamily, member 2)	16582	-0,9064682	-0,1656481	Yes		
	IFNA1	IFNA1	interferon, alpha 1	16688	-1,2501161	9,59E-04	Yes		
BIOCARTA_41BB_PATHWAY	16	-0,4627377	-1,4172555	0,09128631	0,69763213	0,843	2533	tags=25%, list=15%, signal=29%	
	PROBE	**GENE SYMBC**	**GENE_TITLE**	**RANK IN GEN**	**RANK METRI**	**RUNNING ES**	**CORE ENRICHMENT**		
	IL2	IL2	interleukin 2	14173	-0,3483146	-0,349479	Yes		
	TRAF2	TRAF2	TNF receptor-associated factor 2	14255	-0,3562474	-0,2384943	Yes		
	IFNG	IFNG	interferon, gamma	14666	-0,3956835	-0,1344	Yes		
	JUN	JUN	jun oncogene	16471	-0,7887036	0,01396142	Yes		
BIOCARTA_TNFR2_PATHWAY	17	-0,4289421	-1,3368915	0,09683795	0,88196063	0,963	2688	tags=29%, list=16%, signal=35%	
	PROBE	**GENE SYMBC**	**GENE_TITLE**	**RANK IN GEN**	**RANK METRI**	**RUNNING ES**	**CORE ENRICHMENT**		
	IKBKG	IKBKG	inhibitor of kappa light polypeptide gene enhancer in B-cells, kin	14018	-0,3361594	-0,350182	Yes		
	TRAF2	TRAF2	TNF receptor-associated factor 2	14255	-0,3562474	-0,2808574	Yes		
	TNFRSF1B	TNFRSF1B	tumor necrosis factor receptor superfamily, member 1B	14783	-0,4097824	-0,2164275	Yes		
	DUSP1	DUSP1	dual specificity phosphatase 1	16286	-0,6910442	-0,144525	Yes		
	TNFAIP3	TNFAIP3	tumor necrosis factor, alpha-induced protein 3	16371	-0,7235067	0,0199545	Yes		
BIOCARTA_TOLL_PATHWAY	35	-0,399609	-1,2434516	0,30669144	1	0,963	1775	tags=29%, list=11%, signal=32%	
	PROBE	**GENE SYMBC**	**GENE_TITLE**	**RANK IN GEN**	**RANK METRI**	**RUNNING ES**	**CORE ENRICHMENT**		
	EIF2AK2	EIF2AK2	eukaryotic translation initiation factor 2-alpha kinase 2	14931	-0,4260379	-0,361214	Yes		
	TLR6	TLR6	toll-like receptor 6	15092	-0,4485113	-0,3303916	Yes		
	MYD88	MYD88	myeloid differentiation primary response gene (88)	15193	-0,4619939	-0,294755	Yes		
	MAP2K3	MAP2K3	mitogen-activated protein kinase kinase 3	15313	-0,4795642	-0,2586746	Yes		
	TLR2	TLR2	toll-like receptor 2	15401	-0,4936694	-0,2194035	Yes		
	LY96	LY96	lymphocyte antigen 96	15443	-0,5001023	-0,1767931	Yes		
	TLR3	TLR3	toll-like receptor 3	15538	-0,5156935	-0,1359571	Yes		
	FOS	FOS	v-fos FBJ murine osteosarcoma viral oncogene homolog	15847	-0,5687721	-0,1031749	Yes		
	JUN	JUN	jun oncogene	16471	-0,7887036	-0,0694685	Yes		
	TIRAP	TIRAP	toll-interleukin 1 receptor (TIR) domain containing adaptor prote	16589	-0,9252604	0,00689856	Yes		
BIOCARTA_NFKB_PATHWAY	22	-0,4899326	-1,2335583	0,18604651	1	0,963	2688	tags=36%, list=16%, signal=43%	
	PROBE	**GENE SYMBC**	**GENE_TITLE**	**RANK IN GEN**	**RANK METRI**	**RUNNING ES**	**CORE ENRICHMENT**		
	IKBKG	IKBKG	inhibitor of kappa light polypeptide gene enhancer in B-cells, kin	14018	-0,3361594	-0,4416757	Yes		
	IL1R1	IL1R1	interleukin 1 receptor, type I	14691	-0,399031	-0,4246739	Yes		
	TNFRSF1B	TNFRSF1B	tumor necrosis factor receptor superfamily, member 1B	14783	-0,4097824	-0,3713029	Yes		
	MYD88	MYD88	myeloid differentiation primary response gene (88)	15193	-0,4619939	-0,329498	Yes		
	TRADD	TRADD	TNFRSF1A-associated via death domain	15327	-0,4818202	-0,2683032	Yes		
	TNFAIP3	TNFAIP3	tumor necrosis factor, alpha-induced protein 3	16371	-0,7235067	-0,22696	Yes		
	IL1A	IL1A	interleukin 1, alpha	16506	-0,8127547	-0,1183183	Yes		
	TNF	TNF	tumor necrosis factor (TNF superfamily, member 2)	16582	-0,9064682	0,00731284	Yes		
BIOCARTA_HIF_PATHWAY	15	-0,3488294	-1,1961348	0,21995927	1	0,963	5639	tags=53%, list=34%, signal=80%	
	PROBE	**GENE SYMBC**	**GENE_TITLE**	**RANK IN GEN**	**RANK METRI**	**RUNNING ES**	**CORE ENRICHMENT**		
	ARNT	ARNT	aryl hydrocarbon receptor nuclear translocator	10479	-0,1049184	-0,3136586	Yes		
	LDHA	LDHA	lactate dehydrogenase A	11067	-0,1366177	-0,3123219	Yes		
	EPO	EPO	erythropoietin	11537	-0,1647358	-0,2964014	Yes		
	CREB1	CREB1	cAMP responsive element binding protein 1	11861	-0,1853335	-0,2662288	Yes		
	EDN1	EDN1	endothelin 1	12174	-0,2046965	-0,2302229	Yes		
	VHL	VHL	von Hippel-Lindau tumor suppressor	13840	-0,3223912	-0,2438328	Yes		
	COPS5	COPS5	COP9 constitutive photomorphogenic homolog subunit 5 (Arabic	14006	-0,3349254	-0,1642191	Yes		
	VEGFA	null	null	14973	-0,4303251	-0,1071051	Yes		
	JUN	JUN	jun oncogene	16471	-0,7887036	0,01396048	Yes		
BIOCARTA_IL1R_PATHWAY	32	-0,3982802	-1,1666739	0,21705426	1	0,963	2457	tags=28%, list=15%, signal=33%	
	PROBE	**GENE SYMBC**	**GENE_TITLE**	**RANK IN GEN**	**RANK METRI**	**RUNNING ES**	**CORE ENRICHMENT**		
	IL1B	IL1B	interleukin 1, beta	14249	-0,3560907	-0,3651373	Yes		
	IL1R1	IL1R1	interleukin 1 receptor, type I	14691	-0,399031	-0,3544477	Yes		
	IL1RN	IL1RN	interleukin 1 receptor antagonist	14713	-0,4012909	-0,3183573	Yes		
	MYD88	MYD88	myeloid differentiation primary response gene (88)	15193	-0,4619939	-0,3040867	Yes		
	MAP2K3	MAP2K3	mitogen-activated protein kinase kinase 3	15313	-0,4795642	-0,2665888	Yes		
	JUN	JUN	jun oncogene	16471	-0,7887036	-0,2625744	Yes		
	IL1A	IL1A	interleukin 1, alpha	16506	-0,8127547	-0,188967	Yes		
	TNF	TNF	tumor necrosis factor (TNF superfamily, member 2)	16582	-0,9064682	-0,1090964	Yes		
	IFNA1	IFNA1	interferon, alpha 1	16688	-1,2501161	9,60E-04	Yes		
BIOCARTA_CDMAC_PATHWAY	16	-0,3590518	-1,1658201	0,34302327	0,991057	0,963	859	tags=19%, list=5%, signal=20%	
	PROBE	**GENE SYMBC**	**GENE_TITLE**	**RANK IN GEN**	**RANK METRI**	**RUNNING ES**	**CORE ENRICHMENT**		
	FOS	FOS	v-fos FBJ murine osteosarcoma viral oncogene homolog	15847	-0,5687721	-0,2559761	Yes		
	JUN	JUN	jun oncogene	16471	-0,7887036	-0,1503734	Yes		
	TNF	TNF	tumor necrosis factor (TNF superfamily, member 2)	16582	-0,9064682	0,00731009	Yes		
BIOCARTA_INFLAM_PATHWAY	29	-0,3266846	-1,1480343	0,18503937	0,94474506	1	200	tags=14%, list=1%, signal=14%	
	PROBE	**GENE SYMBC**	**GENE_TITLE**	**RANK IN GEN**	**RANK METRI**	**RUNNING ES**	**CORE ENRICHMENT**		
	IL13	IL13	interleukin 13	13996	-0,3344533	-0,2752453	Yes		
	IL2	IL2	interleukin 2	14173	-0,3483146	-0,2565648	Yes		
	IFNG	IFNG	interferon, gamma	14666	-0,3956835	-0,2528579	Yes		
	IL7	IL7	interleukin 7	15001	-0,4335869	-0,2364951	Yes		
	IL1A	IL1A	interleukin 1, alpha	16506	-0,8127547	-0,2584688	Yes		
	TNF	TNF	tumor necrosis factor (TNF superfamily, member 2)	16582	-0,9064682	-0,1868849	Yes		
	CSF2	CSF2	colony stimulating factor 2 (granulocyte-macrophage)	16645	-1,0622519	-0,1014463	Yes		
	IFNA1	IFNA1	interferon, alpha 1	16688	-1,2501161	9,59E-04	Yes		
BIOCARTA_TNFR1_PATHWAY	29	-0,4243907	-1,1107829	0,30898875	1	1	3537	tags=34%, list=21%, signal=44%	
	PROBE	**GENE SYMBC**	**GENE_TITLE**	**RANK IN GEN**	**RANK METRI**	**RUNNING ES**	**CORE ENRICHMENT**		
	CASP8	CASP8	caspase 8, apoptosis-related cysteine peptidase	13169	-0,2711428	-0,3910396	Yes		
	LMNB2	LMNB2	lamin B2	13429	-0,2905533	-0,3708322	Yes		
	MADD	MADD	MAP-kinase activating death domain	13447	-0,2919113	-0,3359459	Yes		
	TRAF2	TRAF2	TNF receptor-associated factor 2	14255	-0,3562474	-0,3405196	Yes		
	RB1	RB1	retinoblastoma 1 (including osteosarcoma)	15162	-0,4578799	-0,3385289	Yes		
	TRADD	TRADD	TNFRSF1A-associated via death domain	15327	-0,4818202	-0,2890984	Yes		
	BAG4	BAG4	BCL2-associated athanogene 4	16016	-0,6062149	-0,2557896	Yes		
	CASP2	CASP2	caspase 2, apoptosis-related cysteine peptidase (neural precursc	16355	-0,7183344	-0,1877015	Yes		
	JUN	JUN	jun oncogene	16471	-0,7887036	-0,0975854	Yes		
	TNF	TNF	tumor necrosis factor (TNF superfamily, member 2)	16582	-0,9064682	0,00731584	Yes		
BIOCARTA_KERATINOCYTE_PATHWAY	45	-0,2612467	-1,1052853	0,41210938	0,9580409	1	1393	tags=16%, list=8%, signal=17%	
	PROBE	**GENE SYMBC**	**GENE_TITLE**	**RANK IN GEN**	**RANK METRI**	**RUNNING ES**	**CORE ENRICHMENT**		
	TNFRSF1B	TNFRSF1B	tumor necrosis factor receptor superfamily, member 1B	14783	-0,4097824	-0,2294941	Yes		
	MAP2K3	MAP2K3	mitogen-activated protein kinase kinase 3	15313	-0,4795642	-0,2244272	Yes		
	PRKCG	PRKCG	protein kinase C, gamma	15492	-0,508217	-0,1960919	Yes		
	CEBPA	CEBPA	CCAAT/enhancer binding protein (C/EBP), alpha	15829	-0,5655479	-0,1728388	Yes		
	FOS	FOS	v-fos FBJ murine osteosarcoma viral oncogene homolog	15847	-0,5687721	-0,1301905	Yes		
	MAPK13	MAPK13	mitogen-activated protein kinase 13	16218	-0,6681722	-0,101099	Yes		
	JUN	JUN	jun oncogene	16471	-0,7887036	-0,0556706	Yes		
	TNF	TNF	tumor necrosis factor (TNF superfamily, member 2)	16582	-0,9064682	0,0073229	Yes		
BIOCARTA_RELA_PATHWAY	16	-0,4119994	-1,1035224	0,31346154	0,9067817	1	2688	tags=25%, list=16%, signal=30%	
	PROBE	**GENE SYMBC**	**GENE_TITLE**	**RANK IN GEN**	**RANK METRI**	**RUNNING ES**	**CORE ENRICHMENT**		
	IKBKG	IKBKG	inhibitor of kappa light polypeptide gene enhancer in B-cells, kin	14018	-0,3361594	-0,3217842	Yes		
	TNFRSF1B	TNFRSF1B	tumor necrosis factor receptor superfamily, member 1B	14783	-0,4097824	-0,2575894	Yes		
	TRADD	TRADD	TNFRSF1A-associated via death domain	15327	-0,4818202	-0,1608195	Yes		
	TNF	TNF	tumor necrosis factor (TNF superfamily, member 2)	16582	-0,9064682	0,00731036	Yes		

pL2-FxR									
NAME	**SIZE**	**ES**	**NES**	**NOM p-val**	**FDR q-val**	**FWER p-val**	**RANK AT MAX**		
BIOCARTA_ECM_PATHWAY	24	0,55261093	1,752329	0	0,3538794	0,194	3536	tags=46%, list=21%, signal=58%	
	PROBE	**GENE SYMBOL**	**GENE_TITLE**	**RANK IN GEN**	**RANK METRI**	**RUNNING ES**	**CORE ENRICHMENT**		
	ITGA1	ITGA1	integrin, alpha 1	89	1,15483129	0,1447955	Yes		
	MYLK	MYLK	myosin, light chain kinase	627	0,73274982	0,20786247	Yes		
	TLN1	TLN1	talin 1	662	0,71785349	0,29914692	Yes		
	FYN	FYN	FYN oncogene related to SRC, FGR, YES	985	0,62234318	0,3607497	Yes		
	ITGB1	ITGB1	integrin, beta 1 (fibronectin receptor, beta polypeptide, antigen	1628	0,50129879	0,38743287	Yes		
	PIK3CG	PIK3CG	phosphoinositide-3-kinase, catalytic, gamma polypeptide	2120	0,43503979	0,41455442	Yes		
	ROCK1	ROCK1	Rho-associated, coiled-coil containing protein kinase 1	2452	0,39694124	0,4463148	Yes		
	PIK3CA	PIK3CA	phosphoinositide-3-kinase, catalytic, alpha polypeptide	2895	0,34886792	0,4651713	Yes		
	RAF1	RAF1	v-raf-1 murine leukemia viral oncogene homolog 1	2969	0,34343603	0,50544256	Yes		
	PIK3R1	PIK3R1	phosphoinositide-3-kinase, regulatory subunit 1 (p85 alpha)	3078	0,33263457	0,5422115	Yes		
	ARHGAP5	ARHGAP5	Rho GTPase activating protein 5	3536	0,29073223	0,55261093	Yes		
BIOCARTA_CSK_PATHWAY	20	0,6287503	1,7496916	0	0,20043953	0,241	3201	tags=55%, list=19%, signal=68%	
	PROBE	**GENE SYMBOL**	**GENE_TITLE**	**RANK IN GEN**	**RANK METRI**	**RUNNING ES**	**CORE ENRICHMENT**		
	HLA-DRB1	HLA-DRB1	major histocompatibility complex, class II, DR beta 1	74	1,19280124	0,14407563	Yes		
	CD3G	CD3G	CD3g molecule, gamma (CD3-TCR complex)	78	1,17496181	0,29018548	Yes		
	CD3E	CD3E	CD3e molecule, epsilon (CD3-TCR complex)	456	0,80928016	0,36835048	Yes		
	CD4	CD4	CD4 molecule	996	0,62078625	0,41333753	Yes		
	LCK	LCK	lymphocyte-specific protein tyrosine kinase	1743	0,48539665	0,42906144	Yes		
	PTPRC	PTPRC	protein tyrosine phosphatase, receptor type, C	1766	0,48119435	0,48765442	Yes		
	PRKAR1A	PRKAR1A	protein kinase, cAMP-dependent, regulatory, type I, alpha (tissue	2282	0,4162817	0,5086179	Yes		
	PRKACB	PRKACB	protein kinase, cAMP-dependent, catalytic, beta	2467	0,39545903	0,546827	Yes		
	ADCY1	ADCY1	adenylate cyclase 1 (brain)	2891	0,34916481	0,56494796	Yes		
	PRKAR1B	PRKAR1B	protein kinase, cAMP-dependent, regulatory, type I, beta	2993	0,34157488	0,60142267	Yes		
	CREBBP	CREBBP	CREB binding protein (Rubinstein-Taybi syndrome)	3201	0,31913325	0,6287503	Yes		
BIOCARTA_PAR1_PATHWAY	35	0,5532823	1,7345847	0	0,16754006	0,288	3078	tags=43%, list=18%, signal=52%	
	PROBE	**GENE SYMBOL**	**GENE_TITLE**	**RANK IN GEN**	**RANK METRI**	**RUNNING ES**	**CORE ENRICHMENT**		
	ARHGEF6	ARHGEF6	Rac/Cdc42 guanine nucleotide exchange factor (GEF) 6	24	1,41184831	0,12302113	Yes		
	ARHGEF9	ARHGEF9	Cdc42 guanine nucleotide exchange factor (GEF) 9	485	0,79402071	0,16542318	Yes		
	PLCB1	PLCB1	phospholipase C, beta 1 (phosphoinositide-specific)	620	0,73797518	0,22244066	Yes		
	PRKCB	null	null	909	0,63858575	0,26145834	Yes		
	GNA12	GNA12	guanine nucleotide binding protein (G protein) alpha 12	928	0,63531232	0,31638423	Yes		
	ARHGEF17	ARHGEF17	Rho guanine nucleotide exchange factor (GEF) 17	1211	0,5765965	0,3502972	Yes		
	F2R	F2R	coagulation factor II (thrombin) receptor	1366	0,54429346	0,389041	Yes		
	PIK3CG	PIK3CG	phosphoinositide-3-kinase, catalytic, gamma polypeptide	2120	0,43503979	0,38222077	Yes		
	GNAI1	GNAI1	guanine nucleotide binding protein (G protein), alpha inhibiting a	2262	0,41922241	0,41071883	Yes		
	ROCK1	ROCK1	Rho-associated, coiled-coil containing protein kinase 1	2452	0,39694124	0,43437326	Yes		
	ARHGEF15	ARHGEF15	Rho guanine nucleotide exchange factor (GEF) 15	2687	0,37094793	0,45303681	Yes		
	ARHGEF2	ARHGEF2	rho/rac guanine nucleotide exchange factor (GEF) 2	2698	0,36983743	0,4850398	Yes		
	ADCY1	ADCY1	adenylate cyclase 1 (brain)	2891	0,34916481	0,50430256	Yes		
	PIK3CA	PIK3CA	phosphoinositide-3-kinase, catalytic, alpha polypeptide	2895	0,34886792	0,5348769	Yes		
	PIK3R1	PIK3R1	phosphoinositide-3-kinase, regulatory subunit 1 (p85 alpha)	3078	0,33263457	0,5532823	Yes		
BIOCARTA_GCR_PATHWAY	16	0,51322913	1,6982104	0	0,15109038	0,288	3513	tags=38%, list=21%, signal=47%	
	PROBE	**GENE SYMBOL**	**GENE_TITLE**	**RANK IN GEN**	**RANK METRI**	**RUNNING ES**	**CORE ENRICHMENT**		
	NR3C1	NR3C1	nuclear receptor subfamily 3, group C, member 1 (glucocorticoid	820	0,66800022	0,13829003	Yes		
	NOS3	NOS3	nitric oxide synthase 3 (endothelial cell)	1626	0,50136584	0,23072542	Yes		
	PIK3CG	PIK3CG	phosphoinositide-3-kinase, catalytic, gamma polypeptide	2120	0,43503979	0,3232463	Yes		
	PIK3CA	PIK3CA	phosphoinositide-3-kinase, catalytic, alpha polypeptide	2895	0,34886792	0,37475207	Yes		
	PIK3R1	PIK3R1	phosphoinositide-3-kinase, regulatory subunit 1 (p85 alpha)	3078	0,33263457	0,45717567	Yes		
	NFKB1	NFKB1	nuclear factor of kappa light polypeptide gene enhancer in B-cell	3513	0,29246593	0,51322913	Yes		
BIOCARTA_MYOSIN_PATHWAY	28	0,538225	1,684739	0	0,15254751	0,333	2698	tags=36%, list=16%, signal=43%	
	PROBE	**GENE SYMBOL**	**GENE_TITLE**	**RANK IN GEN**	**RANK METRI**	**RUNNING ES**	**CORE ENRICHMENT**		
	ARHGEF6	ARHGEF6	Rac/Cdc42 guanine nucleotide exchange factor (GEF) 6	24	1,41184831	0,1467328	Yes		
	ARHGEF9	ARHGEF9	Cdc42 guanine nucleotide exchange factor (GEF) 9	485	0,79402071	0,20248151	Yes		
	PLCB1	PLCB1	phospholipase C, beta 1 (phosphoinositide-specific)	620	0,73797518	0,27189618	Yes		
	MYLK	MYLK	myosin, light chain kinase	627	0,73274982	0,34843767	Yes		
	PRKCB	null	null	909	0,63858575	0,398607	Yes		
	GNA12	GNA12	guanine nucleotide binding protein (G protein) alpha 12	928	0,63531232	0,464203	Yes		
	ARHGEF17	ARHGEF17	Rho guanine nucleotide exchange factor (GEF) 17	1211	0,5765965	0,50780666	Yes		
	ROCK1	ROCK1	Rho-associated, coiled-coil containing protein kinase 1	2452	0,39694124	0,47511128	Yes		
	ARHGEF15	ARHGEF15	Rho guanine nucleotide exchange factor (GEF) 15	2687	0,37094793	0,50001055	Yes		
	ARHGEF2	ARHGEF2	rho/rac guanine nucleotide exchange factor (GEF) 2	2698	0,36983743	0,538225	Yes		
BIOCARTA_SPPA_PATHWAY	22	0,57931536	1,6821463	0	0,13495614	0,333	2969	tags=45%, list=18%, signal=55%	
	PROBE	**GENE SYMBOL**	**GENE_TITLE**	**RANK IN GEN**	**RANK METRI**	**RUNNING ES**	**CORE ENRICHMENT**		
	ITGA1	ITGA1	integrin, alpha 1	89	1,15483129	0,1396516	Yes		
	PLCB1	PLCB1	phospholipase C, beta 1 (phosphoinositide-specific)	620	0,73797518	0,20053378	Yes		
	PRKCB	null	null	909	0,63858575	0,26344365	Yes		
	PTGS1	PTGS1	prostaglandin-endoperoxide synthase 1 (prostaglandin G/H synth	1068	0,60403943	0,32980865	Yes		
	TBXAS1	TBXAS1	thromboxane A synthase 1 (platelet, cytochrome P450, family 5,	1167	0,58440703	0,39730534	Yes		
	F2R	F2R	coagulation factor II (thrombin) receptor	1366	0,54429346	0,45377177	Yes		
	ITGB1	ITGB1	integrin, beta 1 (fibronectin receptor, beta polypeptide, antigen	1628	0,50129879	0,501064	Yes		
	PLA2G4A	PLA2G4A	phospholipase A2, group IVA (cytosolic, calcium-dependent)	1645	0,49943432	0,56280774	Yes		
	GNAI1	GNAI1	guanine nucleotide binding protein (G protein), alpha inhibiting a	2262	0,41922241	0,5785163	Yes		
	RAF1	RAF1	v-raf-1 murine leukemia viral oncogene homolog 1	2969	0,34343603	0,57931536	Yes		
BIOCARTA_TOB1_PATHWAY	18	0,6318799	1,6536334	0	0,14378718	0,421	458	tags=33%, list=3%, signal=34%	
	PROBE	**GENE SYMBOL**	**GENE_TITLE**	**RANK IN GEN**	**RANK METRI**	**RUNNING ES**	**CORE ENRICHMENT**		
	CD3G	CD3G	CD3g molecule, gamma (CD3-TCR complex)	78	1,17496181	0,13693702	Yes		
	TGFBR3	TGFBR3	transforming growth factor, beta receptor III (betaglycan, 300kD	252	0,93322808	0,23904623	Yes		
	CD28	CD28	CD28 molecule	262	0,92362076	0,34982553	Yes		
	TGFB3	TGFB3	transforming growth factor, beta 3	436	0,81809056	0,43805787	Yes		
	CD3E	CD3E	CD3e molecule, epsilon (CD3-TCR complex)	456	0,80928016	0,5344571	Yes		
	TGFB2	TGFB2	transforming growth factor, beta 2	458	0,80882329	0,6318799	Yes		
BIOCARTA_ALK_PATHWAY	35	0,44540772	1,6116911	0	0,21021622	0,467	1138	tags=23%, list=7%, signal=24%	
	PROBE	**GENE SYMBOL**	**GENE_TITLE**	**RANK IN GEN**	**RANK METRI**	**RUNNING ES**	**CORE ENRICHMENT**		
	TGFBR3	TGFBR3	transforming growth factor, beta receptor III (betaglycan, 300kD	252	0,93322808	0,06407446	Yes		
	BMP5	BMP5	bone morphogenetic protein 5	320	0,88531554	0,13518095	Yes		
	TGFB3	TGFB3	transforming growth factor, beta 3	436	0,81809056	0,19770348	Yes		
	TGFB2	TGFB2	transforming growth factor, beta 2	458	0,80882329	0,26507849	Yes		
	BMP4	BMP4	bone morphogenetic protein 4	636	0,72882849	0,3163072	Yes		
	RFC1	RFC1	replication factor C (activator 1) 1, 145kDa	828	0,6664986	0,36140692	Yes		
	MEF2C	MEF2C	MADS box transcription enhancer factor 2, polypeptide C (myocy	1000	0,61871141	0,4036513	Yes		
	NOG	NOG	noggin	1138	0,58892554	0,44540772	Yes		
BIOCARTA_CXCR4_PATHWAY	24	0,45544925	1,580405	0	0,23309451	0,511	3513	tags=33%, list=21%, signal=42%	
	PROBE	**GENE SYMBOL**	**GENE_TITLE**	**RANK IN GEN**	**RANK METRI**	**RUNNING ES**	**CORE ENRICHMENT**		
	CXCL12	CXCL12	chemokine (C-X-C motif) ligand 12 (stromal cell-derived factor 1)	165	1,01962793	0,16891032	Yes		
	PRKCB	null	null	909	0,63858575	0,23635095	Yes		
	GNAI1	GNAI1	guanine nucleotide binding protein (G protein), alpha inhibiting a	2262	0,41922241	0,22881544	Yes		
	PIK3C2G	PIK3C2G	phosphoinositide-3-kinase, class 2, gamma polypeptide	2416	0,40094528	0,28995305	Yes		
	PIK3CA	PIK3CA	phosphoinositide-3-kinase, catalytic, alpha polypeptide	2895	0,34886792	0,3224751	Yes		
	RAF1	RAF1	v-raf-1 murine leukemia viral oncogene homolog 1	2969	0,34343603	0,3783238	Yes		
	PIK3R1	PIK3R1	phosphoinositide-3-kinase, regulatory subunit 1 (p85 alpha)	3078	0,33263457	0,4301801	Yes		
	NFKB1	NFKB1	nuclear factor of kappa light polypeptide gene enhancer in B-cell	3513	0,29246593	0,45544925	Yes		
BIOCARTA_NO2IL12_PATHWAY	16	0,5539005	1,5790892	0	0,21448487	0,511	2461	tags=44%, list=15%, signal=51%	
	PROBE	**GENE SYMBOL**	**GENE_TITLE**	**RANK IN GEN**	**RANK METRI**	**RUNNING ES**	**CORE ENRICHMENT**		
	CD3G	CD3G	CD3g molecule, gamma (CD3-TCR complex)	78	1,17496181	0,15921725	Yes		
	CCR5	CCR5	chemokine (C-C motif) receptor 5	345	0,87336552	0,26510108	Yes		
	CD3E	CD3E	CD3e molecule, epsilon (CD3-TCR complex)	456	0,80928016	0,37139332	Yes		
	IL12RB1	IL12RB1	interleukin 12 receptor, beta 1	840	0,66274577	0,440888	Yes		
	CD4	CD4	CD4 molecule	996	0,62078625	0,5181916	Yes		
	CD2	CD2	CD2 molecule	1718	0,48865518	0,5431501	Yes		
	IL12RB2	IL12RB2	interleukin 12 receptor, beta 2	2461	0,3958151	0,5539005	Yes		
BIOCARTA_IL7_PATHWAY	16	0,5759391	1,5783471	0	0,19925888	0,511	4124	tags=63%, list=25%, signal=83%	
	PROBE	**GENE SYMBOL**	**GENE_TITLE**	**RANK IN GEN**	**RANK METRI**	**RUNNING ES**	**CORE ENRICHMENT**		
	IL7R	IL7R	interleukin 7 receptor	650	0,72727772	0,09685537	Yes		
	FYN	FYN	FYN oncogene related to SRC, FGR, YES	985	0,62234318	0,19378275	Yes		
	IL2RG	IL2RG	interleukin 2 receptor, gamma (severe combined immunodeficie	1001	0,61834711	0,30907366	Yes		
	LCK	LCK	lymphocyte-specific protein tyrosine kinase	1743	0,48539665	0,35588095	Yes		
	PIK3CG	PIK3CG	phosphoinositide-3-kinase, catalytic, gamma polypeptide	2120	0,43503979	0,4150967	Yes		
	PIK3CA	PIK3CA	phosphoinositide-3-kinase, catalytic, alpha polypeptide	2895	0,34886792	0,4342724	Yes		
	PIK3R1	PIK3R1	phosphoinositide-3-kinase, regulatory subunit 1 (p85 alpha)	3078	0,33263457	0,4858703	Yes		
	CREBBP	CREBBP	CREB binding protein (Rubinstein-Taybi syndrome)	3201	0,31913325	0,5385264	Yes		
	NMI	NMI	N-myc (and STAT) interactor	4090	0,24758705	0,5318402	Yes		
	BCL2	BCL2	B-cell CLL/lymphoma 2	4124	0,2452123	0,5759391	Yes		
BIOCARTA_CCR3_PATHWAY	23	0,48015335	1,5729922	0	0,18657067	0,511	2969	tags=26%, list=18%, signal=32%	
	PROBE	**GENE SYMBOL**	**GENE_TITLE**	**RANK IN GEN**	**RANK METRI**	**RUNNING ES**	**CORE ENRICHMENT**		
	CCL11	CCL11	chemokine (C-C motif) ligand 11	236	0,9455449	0,15361808	Yes		
	PLCB1	PLCB1	phospholipase C, beta 1 (phosphoinositide-specific)	620	0,73797518	0,26159582	Yes		
	CCR3	CCR3	chemokine (C-C motif) receptor 3	904	0,64112443	0,35838413	Yes		
	PRKCB	null	null	909	0,63858575	0,4714466	Yes		
	PIK3C2G	PIK3C2G	phosphoinositide-3-kinase, class 2, gamma polypeptide	2416	0,40094528	0,45230815	Yes		
	RAF1	RAF1	v-raf-1 murine leukemia viral oncogene homolog 1	2969	0,34343603	0,48015335	Yes		
BIOCARTA_EDG1_PATHWAY	27	0,5493875	1,5350312	0,11553031	0,22759323	0,57	3286	tags=44%, list=20%, signal=55%	
BIOCARTA_CREB_PATHWAY	26	0,43770424	1,5337777	0	0,22028114	0,634	3078	tags=35%, list=18%, signal=42%	
BIOCARTA_LONGEVITY_PATHWAY	15	0,64110494	1,5111605	0	0,24333002	0,682	3476	tags=60%, list=21%, signal=76%	
BIOCARTA_CTCF_PATHWAY	23	0,5492772	1,5088023	0	0,23437023	0,682	3781	tags=52%, list=23%, signal=67%	
BIOCARTA_NFAT_PATHWAY	47	0,42171153	1,4948221	0	0,24614617	0,682	3830	tags=38%, list=23%, signal=50%	
BIOCARTA_HDAC_PATHWAY	25	0,5084559	1,4880879	0	0,24382173	0,682	3078	tags=44%, list=18%, signal=54%	
BIOCARTA_AGR_PATHWAY	36	0,37882224	1,4760349	0,10816777	0,26389533	0,751	2086	tags=25%, list=12%, signal=29%	
BIOCARTA_IGF1MTOR_PATHWAY	18	0,3899519	1,4570287	0	0,27672324	0,842	3078	tags=28%, list=18%, signal=34%	

Acknowledgment / Danksagung

Zu besonderem Dank bin ich meinen Professoren verpflichtet. Als erster Gutachter hat mich Herr Professor Dr. Roland Schmid stets mit seinen Anregungen unterstützt. Doch auch Herrn Professor Dr. Michael Pfaffl bin ich für sein zweites Gutachten zu Dank verpflichtet. Ohne seinen wertvollen akademischen Rat wäre diese Arbeit nicht entstanden.

Ich bedanke mich herzlich bei PD Dr. Michael Quante der für die die Überlassung des interessanten Themas, die Unterstützung und die Möglichkeit, diese Dissertation in seiner Arbeitsgruppe anfertigen zu dürfen. Außerdem möchte ich mich besonders herzlich für die sehr gute und motivierende Betreuung bedanken. Am meisten ist ihm für seine verständnisvolle Unterstützung und sein Vertrauen zu danken.

Herzlichen Dank auch an alle die weitere Daten und Auswertungen sowie thematisch zu dieser Doktorarbeit beigesteuert haben, wie Hsin-Yu Fang, Elke Burgermeister und Katja Steiger.

Ebenso geht mein Dank an meine ehemaligen Mitarbeiter, die mich in den vergangenen Jahren mit bereichernden Tipps und Diskussionsbeiträgen wiederholt in neue thematische Bahnen gelenkt haben. Hier möchte ich besonders Marina Lotter und Steffi Neupert hervorheben. Mein Dank gilt auch Marc Tänzer, Jonas Ingermann, Anna Brandtner, Moritz Tobiasch, Julia Horstmann, Carlo Maurer, Natasha Stephans, Bettina Höhl und Agnieszka Pastula.

Zum Besonderen Dank bin ich auch Tobias Leibfritz verpflicht. Er war stets eine große Hilfe fachlich wie persönlich.

Herzlichen Dank auch allen Unterstützern am Rechts der Isar, wie der Apotheke, der Personalverwaltung, dem Sekretariat der 2. Medizinischen Klinik, den Tierpflegern und allen anderen.

Arne Brandt und Olivia Hesse gebührt ein besonderer Dank für ihr hilfreiches Korrekturlesen.

List of puplications

Long-lived intestinal tuft cells serve as colon cancer-initiating cells.
Westphalen CB, Asfaha S, Hayakawa Y, Takemoto Y, Lukin DJ, **Nuber AH**, Brandtner A, Setlik W, Remotti H, Muley A, Chen X, May R, Houchen CW, Fox JG, Gershon MD, Quante M, Wang TC.
J Clin Invest. 2014 Feb 3

Three dimensional gastrointestinal organoid culture in combination with nerves or fibroblasts – A method to characterize the gastrointestinal stem cell niche.
Pastuła A, Middelhoff M, Brandtner A, Tobiasch M, Höhl B, **Nuber AH**, Demir IE, Neupert S, Kollmann P, Mazzuoli-Weber G, Quante M.
Stem Cells International 2015 July 9

List of tables

List of figures

Zusammenfassung

Refluxösophagitis, bei der Säure vom Magen und Gallensäure vom Darm in die Speiseröhre gelangt, verursacht Barrett`s Ösophagus. Dies ist eine Erkrankung der Speiseröhre bei der das vorhandene Plattenepithel durch Zylinderepithel ersetzt wird. Vor allem die Gallensäure aktiviert NfkB und bewirkt DNS-Strangbrüche, welche wahrscheinlich dieas Veranschreiten von Barrett`s Ösophagus zu Ösophaguskarzinom fördert. Für diese Entwicklung könnte der Gallenrezeptor Farnesoid X Rezeptor sein. Dieser Rezeptor ist verantwortlich für die Aufrechterhaltung der Gallensäure-, Glukose- und Lipidhomeostatse.

In dieser Arbeit wurden Mäuse mit einem humanen L2-IL1beta Transgen mit FXR k.o Mäusen gekreuzt. Das Transgen bewirkt eine Überexpression von IL-1beta im Ösophagus und Vormagen der Maus wodurch eine chronische Entzündung imitiert wird. Das Model zeigt Ösophagitis und die Entwicklung von Barrett-Metaplasie bis hin zum Karzinom. Der Gallensäurerezeptor FXR agiert als schützender Faktor im Magen-Darm-Trakt.

Unsere Hypothese ist, dass durch die Kreuzung der beiden Mauslinien die Entzündung im Magen gefördert wird, welche eine schnellere Entwicklung zum Barrett`s Ösophagus zur Folge hat und somit auch eine schnellere Entstehung des Karzinoms bewirkt. Dafür wurden mindestens vier Tiere mit dem Alter von 6, 9, 12 und 15 Monate verwendet um einen histopathologischen Score zu ermitteln. Dazu wurden Tumore in der Kardiaregion gezählt und ausgewertet. Des weiteren wurden die Marker Ki67 für Proliferation und Dclk1 für Stammzellen immunhistochemisch evaluiert. Für die Differenzierung wurde PAS verwendet. Mittels Microarray wurde die veränderten Genexpressionen bei den Tieren mit 12 Monaten ermittelt.

Es zeigte sich, dass Tiere mit pL2-IL-1β ab 9 Monaten Metaplasien, Neoplasien, Dysplasien und Tumore entwickeln. FXR k.o Mäuse zeigen eine gestörte Gallenhomeostase, vermehrte Proliferation in der Speiseröhre, Ösophagitis, Hyperkeratosis und eine verstärkte Karzinogenese. pL2-IL-1β/FXR$^{-/-}$ Tiere zeigen dies lokalisierter und, besonders in 6 Monate alten Mäusen tendenziell etwas stärker ausgeprägt. Mit 9 Monaten zeigt sich eine stärker ausgeprägte Meta-/Dysplasie im Vergleich zu Tieren mit FXR Wildtyp Allel. Mit 15 Monaten ist kaum noch ein Unterschied zwischen den Tieren zu erkennen. Wir zeigten auch, dass pL2-IL-1β/FXR$^{-/-}$ Tiere im Vergleich zu pL2-IL-1β Tieren eine höhre Proliferation und geringere Differenzierung hatten. Die Anzahl der Stammzellen war ähnlich. Nur pL2-IL-1β/FXR$^{-/-}$ Mäuse konnten erfolgreich immunhistochemisch auf gH2AX getestet werden. Bei der Analyse der Microarray Daten ergab sich kein signifikanter Unterschied in der Genexpression der Mäuse. In Zellkulturexperimenten zeigte Gallensäure keinen Einfluss auf

nicht entzündetes Epithel und Gewebe. Weiterhin konnte durch Gallensäure auch kein Einfluss auf die Migration von Tumorzellen festgestellt werden.

Die FXR Expression ist bei BE Patienten und in Mäusen mit Barrett-Phänotyp am höchsten. Im Tumor ist eine Expression von FXR nicht mehr feststellbar. Daher könnte FXR als möglicher Biomarker bei Diagnosen bei Patienten behilflich sein. Diese Arbeit lässt vermuten, dass FXR einen Schutz gegen die Entwicklung zum Krebs bei Barrett`s Ösophagus bietet.